Effects of Metal Cations on Steels Corrosion in Chloride Aqueous Solution

Md. Saiful Islam

Graduate School of Engineering

Hokkaido University

2019

Acknowledgements

I am deeply grateful to Dr. Masatoshi Sakairi, Associate Professor, Divisions of Materials Science and Engineering, Graduate School of Engineering, Faculty of Engineering, Hokkaido University, who has guided and advised me as a supervisor throughout the study and in preparing this thesis.

I would like to express my gratitude to Professor Tetsu Yonezawa, Assistant Professor Yoshihei Ishida and Assistant Professor Nguyen Mai Thanh, Divisions of Materials Science and Engineering, Graduate School of Engineering, Faculty of Engineering, Hokkaido University, for their valuable advice and cooperation.

I would like to express my heartfelt thanks to Professor Kazuhisa Azumi and Associate Professor Koshi Fushimi, Department of Materials Science, Graduate School of Engineering, Hokkaido University for their appreciated suggestions.

I would like to express cordial thanks to Professor Seiichi Watanabe, Center for Advanced Research of Energy and Materials, Faculty of Engineering, Hokkaido University and Professor Mikito Ueda, Department of Materials Science, Graduate School of Engineering, Faculty of Engineering, Hokkaido University for their valued suggestions.

I would like to express my gratefulness to Mr. Keita Suzuki, technical staff, XPS laboratory at the Graduate School of Engineering and Research, Hokkaido University, for providing valuable advice and technical support for the research.

I would like to express my thankfulness to many of my friends and laboratory members who have supported me to carried out the research. I am very much grateful to Japanese Government for giving me the financial support (MEXT scholarship) to carry out the research and reside in Japan. I am also grateful to e^3 program and Hokkaido University for providing me the opportunity to carry out the research.

Finally, I am grateful to my beloved wife, Mst. Nila Khatun for giving me great support to carry out this research.

Md. Saiful Islam

September 2019

Lists of Abbreviations

Symbol/Abbreviation	Unit	Elaboration
AFM	-	Atomic force microscope
AES	-	Auger electron spectroscope
SEM	-	Scanning electron microscope
XPS	-	X-ray photoelectron spectroscope
EDS	-	Energy dispersive X-ray spectroscope
EIS	-	Electrochemical impedance spectroscope
OCP	[V]	Open circuit potential
Z	[Ωcm^2]	Impedance
E	[V]	Potential
j	[Acm^{-2}]	Current density
SSE	-	Silver/Silver chloride electrode (Ag/AgCl)
R_{sol}	[Ωcm^2]	Resistance of electrolyte/solution
R_{ct}	[Ωcm^2]	Charge transfer resistance
R_c	[Ωcm^2]	Corrosion resistance
R_d	[Ωcm^2]	Resistance of defect in the protective film
Q	[$\mu s^n \Omega^{-1} cm^{-2}$]	Constant phase element (CPE)
Q_f	[$\mu s^n \Omega^{-1} cm^{-2}$]	Constant phase element of protective film
C_{dl}	[F]	Capacitance of double layer
f	[Hz]	Frequency
ω	[Hz]	Angular frequency ($\omega = 2\pi f$)
n	-	CPE parameter, Varies from 0 to 1
X	-	Hardness of metal cation
I_n	[eV]	Ionization potential of metal atom at oxidized state, n
X^0_M	-	Electronegativity of metal atom
D	[gcm^3]	Density of specimen
ΔM_a	[mg]	Mass change
S	[cm^2]	Surface area of specimen
t	[s]	Time
pH_{int}	-	Initial pH
pH_{corr}	-	pH after corrosion (after immersion tests)

pH_{adj}	-	pH after adjustment
ΔpH	-	pH difference
R_a	[nm]	Average surface roughness
C_R	[μmy^{-1}]	Corrosion rate
η_i	[%]	Corrosion inhibition efficiency based on immersion
η_e	[%]	Corrosion inhibition efficiency based on EIS
Na_{sol}	-	Na^+ containing solution
Mg_{sol}	-	Mg^{2+} containing solution
Zn_{sol}	-	Zn^{2+} containing solution
Al_{sol}	-	Al^{3+} containing solution
Zr_{sol}	-	Zr^{4+} containing solution

Contents

Chapter 1: Introduction

1.1 Corrosion of Metals

Metals are very common materials that are used abundantly and play a major role in our daily and industrial life [1-5]. It is a basic attitude that all metals are chemically unstable in an ordinary environment except noble ones. When metal contacts with environments, chemical reactions are started, and generally metal oxide is formed [6]. For this reason, all non-noble metals tend to form a layer of metal oxide, although this layer is thin (5-10 nm). The oxide layer of metals works as a barrier against the surrounding environment [6]. The stability of oxide films depends on the composition and environmental conditions. Fig. 1.1 shows the composition and structure of oxide films in different metals [7-9]. The oxide layer of mild steel (Fig. 1.1 a)) has a poor protection ability, and the layer is damaged, metal dissolution is initiated. Stainless steel contains chromium which provides a unique self-healing property. In case the surface is scratched or damaged, the thin oxide layer formed on the surface (Fig. 1.1 b)), which is only a few nm thick (1~3 nm), immediately rebuilds the layer (oxide film) with the assistance of oxygen from air or water. This is the reason why stainless steel shows excellent corrosion resistance property compare to the other steels. Therefore, the oxide films on the metal surface play an important role in the properties of metals and have a great influence against corrosion. Aluminum alloy also shows good corrosion resistance due to the stable oxide layer (Fig. 1.1 c)) on the surface.

Corrosion of metals is a natural phenomenon in which two chemical reactions are always involved [9], one is oxidation reaction (anodic reaction) and another is a reduction reaction (cathodic reaction). Depending on the nature of the environment, reactions are as follows:

$$M \rightarrow M^{n+} + ne^- \quad \text{(anodic reaction)} \tag{1.1}$$

$$1/2O_2 + H_2O + 2e^- \rightarrow 2OH^- \quad \text{(cathodic reaction in neutral medium)} \tag{1.2}$$

$$2H^+ + 2e^- \rightarrow H_2 \quad \text{(cathodic reaction in acidic medium)} \tag{1.3}$$

Since the reactions of the Eqs. (1.1) and (1.2) occur simultaneously in the neutral solutions containing oxygen at the surface of the metal, the produced M^{n+} reacts with OH^- to form metal hydroxide as shown in Eq. (1.4).

$$M^{n+} + nOH^- \rightarrow M(OH)_n \tag{1.4}$$

If the amount of hydroxide produced exceeds the solubility, the surface of the metal is covered with the precipitation of hydroxide, and the hydroxide may undergo a dehydration reaction as in the Eq. (1.5), oxides are formed.

$$M(OH)_n \rightarrow MO_{n/2} + n/2\ H_2O \tag{1.5}$$

Therefore, the metal surface is covered with hydroxide or oxide in aqueous solutions. Depending on the type of metallic material, oxide films are formed on the metal in the atmosphere or hydroxides are formed in the solution may become a highly protective film. This is generally called oxide films (passive films), and the reason why aluminum, titanium, stainless steel has high corrosion resistance is attributable to these oxide films. Once the oxide films are destroyed [9], corrosion starts with the chemical reactions as mentioned in Eqs. (1.1) and (1.2). Deterioration of the entire exposed surface of a metal by uniform corrosion attack is mentioned as general corrosion. General corrosion accounts for the greatest amount of metal destruction by corrosion but is considered as a safe form of corrosion, due to the fact that it is predictable, manageable and often preventable. Destruction of surface oxide films in a small area by the corrosive anion is defined as a defect, and the hole of the micro-order generated as the defect grows due to severe local corrosion is mentioned as pitting corrosion. Another type of corrosion which is similar to pitting, but occurs at a specific location and often associated with a stagnant micro-environment, like those found under gaskets, washers, and clamps is mentioned as crevice corrosion. Acidic conditions or a depletion of oxygen in a crevice can lead to crevice corrosion.

1.1.1 Corrosion rate of metal

Corrosion rates determine the life span of metal-based structures. This reality dictates the choice of metals used for different purposes, and in different environments. It also determines the maintenance requirements for structures. The rate of corrosion is the speed at which any given metal deteriorates in a specific environment. The rate or speed is dependent upon environmental conditions as well as the type, and condition of the metal. The corrosion rate (C_R) is calculated based on the mass change assuming uniform corrosion over the entire exposed surface of the metal using the following Eq. (1.6).

$$\text{Corrosion rate, } C_R = \frac{M_1 - M_2}{D \times S \times t} \tag{1.6}$$

Here, M_1 is the mass of specimen before immersion; M_2 is the mass of specimen after immersion; D is the density of specimen; S is the surface area of specimen and t is the time of immersion.

Generally, the corrosion rate is calculated in micrometer per day (μm/d) or micrometer per year (μm/y), corrosion rate in the US is normally calculated using mils per year (mpy). To convert the corrosion rate between the mils per year (mpy) and the metric equivalent millimeter per year (mm/y), the following relation is used:

$$1 \text{ mpy} = 0.0254 \text{ mm/y} = 25.4 \text{ } \mu\text{m/y} \quad (1.7)$$

1.2 Factors of corrosion

Corrosion of metal is a process of destroying metal objects in which chemical reactions occur on the surface under the action of the environment. Corrosion process of metals is influenced by a number of internal and external factors [10]. Internal factors of corrosions include compositions of metal, the way of processing, structures, surface conditions, properties of surface films, etc [10]. External factors of corrosions include dissolved oxygen concentration, anion concentration such as chloride ion, pH, temperature [10]. Both factors are responsible for proceeding the corrosion process. Overall, the corrosion process can be controlled by altering or modifying the external factors. Here we will discuss the external (environmental) factors of metal corrosion.

1.2.1 Dissolved oxygen

Dissolved oxygen plays a very important and complicated role in the corrosion of metals. Oxygens take part in the cathodic reaction in neutral, alkaline, and acidic medium. Corrosion rate on the steel surface generally increases due to an increase in dissolved oxygen concentration in the solution [11]. Since the dissolved oxygen in the vicinity of the surface is consumed in the cathodic reaction, the cathodic reaction is limited by the diffusion rate of oxygen from the bulk solution to the steel surface. The maximum current obtained in this situation is known as the limiting current. The limiting current of cathodic reaction is greatly influenced by the oxygen concentration at a certain level in the bulk solution. Fig. 1.2 shows the effect of oxygen concentration on the limiting current. On the other hand, the corrosion product layer generated by the corrosion reaction on the steel surface reduces the diffusion rate of oxygen from the bulk solution to the metal surface. Therefore, it has the effect of lowering the corrosion rate. It is reported that the corrosion rate of metals in aqueous solution decreases when dissolved oxygen concentration exceeds a certain level [12, 13]. In view of this excessive oxygen corrosion inhibiting effect, a method of reducing steel pipe corrosion by increasing the concentration of dissolved oxygen in a condensate water supply system of a boiling water nuclear power plant has been studied [14]. Ishii et al. [15] reported that the corrosion rate of aluminum increases with increasing dissolved oxygen concentration in the concentration range of 0.1 ppm to 22.7 ppm. Goto et al. [16] explained that when the dissolved oxygen concentration in the corrosive solution exceeds about 140 ppm, the corrosion on the whole surface becomes severe as the oxygen concentration increases and porous corrosion products

are formed on the sample surface. Pijanowski et al. [17] reported that the corrosion rates of stainless steel 304 and 316 are greatly increased and the corrosion rates of mild steel are decreased significantly by the removal of oxygen from their environment. They [17] also reported that the removal of oxygen from their environments slightly reduces the corrosion rate of nickel, monel, brass, and inconel. They [17] further explained that the effect of oxygen concentration in the environment of stainless steels 304 and 316 is to have a greater influence on corrosion rates than the temperature in the range of 20°C to 80°C. Cohen [18] reported that the corrosion rate in the presence of oxygen is 65 times higher the rate in the absence of oxygen. Whitman [19] stated that the corrosion rate increased at higher velocity due to an increase in oxygen diffusion and breaking down of the protective films on the metal surfaces. Frese [20] showed that iron tends to become passive with a high concentration of oxygen. From the above discussions, it can be said that the corrosion rate of metals correlates with the dissolved oxygen concentration in the solutions.

1.2.2 Temperature

From the perspective of reaction kinetics, it is well known that the rate of reaction is increased with increasing the temperature. The corrosion of metal is directly related to the electrochemical reactions mentioned in the Eqs. 1.1 and 1.2. Therefore, once the temperature is increased then the rate of electrochemical reactions is also increased, and the metal dissolution rate is increased as well. This is due to the increasing temperature also increases the kinetic energy of the particles so that the possibility of collisions effective in the greater redox reactions. In an open vessel, allowing dissolved oxygen to escape, corrosion rate increases with an increase in temperature to about 80 °C and then falls to a very low value at the boiling point. The lower corrosion rate above 80°C is related to a marked decrease of oxygen solubility in water as the temperature is raised and this effect eventually overshadows the accelerating effect of temperature alone [10, 21, 22]. In a closed system, on the other hand, oxygen cannot escape, and the corrosion rate continues to increase with temperature until all the oxygen is consumed [21, 22].

It has been reported that the corrosion rate of metal increases with increasing the temperature below 80°C. [10, 23]. It has been also reported that the corrosion rate of aluminum increases as the temperature rises from 20°C to 40°C. [24]. On the other hand, the corrosion rate of all metallic materials does not increase as the temperature rises, because the corrosive environment changes the concentration of external factors depending on the temperature change. For example, when the temperature exceeds a certain level, the concentration of

dissolved oxygen in the solution decreases, the cathodic reaction is suppressed and the corrosion rate decreases. Pijanowski et al. [17] reported that the corrosion rates of nickel and monel can be accelerated by increasing temperature, and the corrosion rates of brass and inconel are relatively unaffected by temperature changes between 20°C and 80°C. Obi-Egbedi et al. [25] reported that the corrosion rates of mild steel are increased with increasing the temperature in sulphuric acid solutions. Qi et al. [26] reported that the corrosion of carbon steel in hydrogen sulfide environments is increased up to 40°C, and then gradually decreased obviously with temperature due to the rapid increase of corrosion film resistance. Overall, temperature plays a significant role in the corrosion of metals.

1.2.3 pH

Surface films of metal play a major role against corrosion in aqueous solution, and the stability of the surface films is mostly depended on the pH of the solution. Therefore, pH has a great influence on the corrosion of metals in aqueous solutions. In general, the rate of corrosion is higher in acid than in neutral and alkaline medium. In the case of iron, at very high pH, protective coating of iron oxide is formed which prevents corrosion whereas low pH severe corrosion takes place. For metals like zinc, iron, magnesium etc., hydrogen evolution is thermodynamically favored cathodic reaction [27]. Corrosion of each metal in acidic medium is therefore highly pH dependent. The decrease in pH facilitates the rate of hydrogen evolution and hence increases the corrosion rate of metals. In the case where a protective film is formed on the metal surface, change in solution pH may affect the solubility of the film and therefore affect the corrosion process. Prawoto et al. [5] reported that the corrosion of duplex stainless steel is decreased with increasing the pH of the solution. pH is one of the most important control factor in many chemical treatment systems to prevent scale and corrosion. For example, the pH of boiler water is usually controlled at a minimum value of 10.5. This is high enough to prevent corrosion and at the same time allows precipitation of the various scale-forming salts [28]. S. Basu explained that boiler feed water pH is controlled above 9.0 to avoid the formation of carbonic acid [29]. The pH of the boiler feed water should be maintained between 8.5 and 9.5 for system corrosion protection [30]. E. J. Bonner reported that the boiler feed water pH is maintained at a figure higher than 8.5 to minimize boiler corrosion [31]. Pure water readily absorbs carbon dioxide (CO_2) when exposed to the atmosphere, which forms carbonic acid. Carbonic acid is a weak acid and an effective source of acidity, and accelerate the corrosion of metals. Carbonic acid dissociates into bicarbonate that is in equilibrium with carbonate [32]. Reactions are as follows:

$$CO_2 + H_2O \rightleftarrows H_2CO_3 \quad (1.7)$$

$$H_2CO_3 + H_2O \rightleftarrows H_3O^+ + HCO_3^- \quad (pKa = 6.35) \quad (1.8)$$

$$HCO_3 + H_2O \rightleftarrows H_3O^+ + CO_3^{2-} \quad (pKa = 10.33) \quad (1.9)$$

To avoid the formation of species (HCO_3^-), the pH of boiler feed water is maintained higher than 9.5. Matsunami et al. [27] demonstrated that the corrosion rate of carbon steel is gradually decreased at temperatures between 25 and 90°C with increasing the pH in sulfide and ammonium containing solutions. Zaid et al. [33] reported that corrosion resistance on the aluminum alloy surface obtained by electrochemical measurements is halved in the neutral region compared to the other pH regions. Corrosion of metal is closely related to its potential and the potential of a metal greatly depends on pH [34]. From the point of view, it is obvious that pH has an important role in the corrosion of metals.

1.2.4 Chloride ions

It is well known that chloride ions destroy the surface films and initiate the metal dissolution. As the concentration of chloride ions increases in the solution, the rate of surface films destruction is also increased. It is considered that, once the surface films are destroyed, metal dissolution proceeds. Therefore, the chloride ion concentration is directly related to the corrosion rate of metals in the aqueous solutions. Fig. 1.3 shows the surface films of metal destruction by the chloride ions. A corrosion test was carried out by changing the chloride ion concentration in the solution from 0.001 M to 1 M, the corrosion rate of the metal was increased with increasing chloride ion concentration [33, 35]. McCafferty et al. [36] and Han et al. [37] have shown that the corrosion rate of metal increases with increasing the concentrations of chloride ions. Prawoto et al. [5] reported that the corrosion of duplex stainless steel is increased with increasing chloride ion concentration. Therefore, from the above reports, it can be said that the corrosion rate of metals increases with increasing chloride ion concentration.

1.3 Effect of metal cations on corrosion

As described above (section 1.2), metal corrosions are greatly affected by the external factors in aqueous solutions. Solutions containing cations and anions influence the corrosion of metals significantly. Several researchers [38-49] have shown that corrosion of metals affected by metal cations, and some metal cations suppress the corrosion of metals in aqueous solutions appreciably. Goldie et al. [38] introduced first the application of rare earth salts as a corrosion inhibitor. They showed that, with the addition of 0.001 M of $Ce(NO_3)$ and $La(NO_3)$ to

3.5% NaCl solution, the inhibition efficiencies were 91 and 82% for carbon steel. Amadeh et al. [39] reported that a mixture of rare earth cations (Ce and La) can be used as a corrosion inhibitor for carbon steel in NaCl containing solutions. Drazic *et al*. [40] explained that Cd^{2+}, Mn^{2+}, and Zn^{2+} inhibited the corrosion of iron in 0.25 M H_2SO_4 solutions. Leidheiser Jr. *et al*. [41, 42] reported that Sn^{2+} and Pb^{2+} effectively inhibited the corrosion of iron and steel in acid solutions, and Co^{2+} and Ni^{2+} inhibited the corrosion of galvanized steel in 3% NaCl solutions. Khedr *et al*. [43, 44] reported the effect of some metal cations (K^+, Mg^{2+}, Cu^{2+}, Zn^{2+}, Hg^{2+}, Cd^{2+}, Co^{2+}, and Ni^{2+}) on the corrosion of aluminum in neutral and acid Cl^- solutions. Felhosi *et al*. [45] described that the addition of Ca^{2+} and Zn^{2+} ions to 1-hydroxyethane-1, 1-diphosphonic acid solution increased the corrosion inhibition efficiency on carbon steel. Telegdi *et al*. [46] explained that the corrosion inhibition effect of amino phosphoric acid on iron was increased with the addition of bivalent metal cations (Ba^{2+}, Sr^{2+}, Ca^{2+}, and Zn^{2+}). Zhang *et al*. [47] reported about the inhibition effect of metal cations (Na^+, Ca^{2+}, Mn^{2+}, and Zn^{2+}) to intergranular stress corrosion cracking of sensitized type-304 stainless steel in 10^{-5} kmol/m^3 sulfate solutions. Sathiyanarayanan *et al*. [48] explained the inhibition performance of Zn^{2+}, Mg^{2+}, and Ce^{4+} (1-10 mM) on corrosion of iron in 0.5 M H_2SO_4 solutions. Prabakaran *et al*. [49] reported that the corrosion inhibition effect of propyl phosphonic acid was enhanced by Zn^{2+} on the corrosion of carbon steel in a neutral aqueous medium. All the above researches were carried out by focusing on the metal cation effects on the corrosion of metal in aqueous solutions, and there is no research quantitatively clarifying the influence of metal cations on the corrosion of metals in chloride aqueous solutions with the consideration of pH and temperatures. Moreover, the mechanisms of effects are not fully elucidated in such case.

1.4 Hardness of metal cation

Incorporation of the metal cations in the surface oxide films would be significant to clarify the influence of metal cations on the corrosion of metals in aqueous solutions. Therefore, the hard and soft acids and bases (HSAB) concept are introduced to elucidate the influence of metal cations in such case. In the HSAB concept, Lewis acids and bases are divided into “hard” and “soft” ones, respectively. Hard acids and hard bases make stable ionic bonds, and soft acids and soft bases make stable covalent bonds. However, the value of the bonding power cannot be shown because the HSAB concept is a qualitative concept. The metal cation hardness is based on the HSAB concept. The hardness of metal cations is denoted by X, and it is expressed as follows [9, 50, 51]:

$$X = [X^0_M + (\Sigma I_n)^{1/2}]^2 / 10 \quad (1.10)$$

Here X^0_M is the electronegativity of the metal atom, and I_n (eV) is the ionization potential from the neutral metal atom to the given oxidized state, n. The hardness of metal cations, X (Eq.1.10) is a quantitative indicator that indicates the bonding power. This X would be the best way to explain the bonding power between metal cations and the surface layer of metals. Based on the HSAB concept, X was introduced to explain the corrosion behavior of metals in freshwater [50]. Table 1 shows a list of metal cation harness, X, and Fig. 1.4 shows the effect of metal cations on the surface film based on the HSAB concept [51]. Previous research showed that X is not a suitable corrosion indicator regarding the corrosion of metals in freshwater [9]. It is still unknown the possibility of X as an indicator for corrosion of metals in chloride aqueous solutions with the consideration of pH and temperatures.

1.5 Corrosion inhibitors

Nowadays, corrosion is the most damaging and challenging problems in several countries particularly in United States, Australia, Kuwait, Germany, Japan, Sweden, China, India and Bangladesh where it causes around 1-5% loss of the Gross National Product (GNP) of each nation as estimated by the National Association of Corrosion Engineers (NACE) in 2002 [52]. This cost of corrosion can be reduced from 15 to 35% by properly applying the existing methods of corrosion prevention [53]. Using inhibitors is one of the very common and convenient methods to minimize the corrosion of metals [54].

The corrosion inhibitor is a substance or a mixture of substances applied to an environment in a small amount that significantly prevents or reduces the corrosion of metals exposed to that environment [55]. Concentrations of corrosion inhibitors can vary from 1 to 15,000 ppm (0.0001 to 1.5 wt %). Corrosion inhibitors help the metal or the alloy maintain its resistance against corrosion via various inhibition mechanisms. In general, inhibitors are classified into two categories as inorganic and organic inhibitors. Inorganic inhibitors that include nitrates, molybdates, sodium chromates, phosphates, hydroxides, and silicates. These compounds mostly act as an anodic inhibitor (also known as passivation inhibitors) by reducing anodic reaction, resulting in a cohesive and insoluble film on the metal surface [56, 57]. Some examples of inorganic cathodic inhibitors are the ions of the magnesium, zinc, and nickel that reacts with the hydroxyl (OH^-) of the water forming the insoluble hydroxides as ($Mg(OH)_2$, $Zn(OH)_2$, $Ni(OH)_2$ which are deposited on the cathodic site of the metal surface, and protect the cathodic reaction on the surface [57]. Also, polyphosphates, phosphonates, tannins, lignins

[58] and calcium salts as examples that present the same reaction mechanism. Zinc ions are used as cathodic inhibitors because of the precipitation of $Zn(OH)_2$ at cathodic sites as a consequence of the localized high pH [59, 60].

Organic inhibitors are generally used occasionally that can act as cathodic and anodic or both inhibitor. These inhibitors build up a protective hydrophobic film adsorbed molecules on the metal surface, which provides a barrier to the dissolution of the metal in the electrolyte [57]. Some examples organic inhibitors are amines, urea, Mercapto benzothiazole (MBT), benzotriazole and toliotriazol, aldehydes, heterocyclic nitrogen compounds, sulfur-containing compounds, and acetylenic compounds and also ascorbic acid, succinic acid, tryptamine, caffeine and extracts of natural substances [57, 61, 62]. Sastri et al. [63] classified the inhibitors based on the corrosive environment such as petroleum wells, gas wells, drinking water, cooling water, acidic aqueous solution, atmospheric corrosion, concrete, etc. Most effective classification of corrosion inhibitors based on the mechanism of action that was proposed by Aramaki et al. [64]. In this classification method, inhibitors can be divided into three types as precipitation type, oxidation type, and adsorption type inhibitors.

1.5.1 Precipitation type inhibitors

Precipitation type inhibitors are compounds that cause the formation of precipitates on the surface of the metal, thereby providing a protective film. Hard water that is high in calcium and magnesium is less corrosive than soft water because of the tendency of the salts in the hard water to precipitate on the surface of the metal and form a protective film. If a film due to dense precipitation is formed on the metal surface and the diffusion or migration of hydrogen ions or oxygen is hindered, the cathode reaction is suppressed. These type inhibitors are capable of suppressing both the anode and cathode reactions.

The most common inhibitors of this category are the silicates and the phosphates. Sodium silicate, for example, is used in many domestic water softeners to prevent the occurrence of rust. In aerated hot water systems, sodium silicate protects steel, copper, and brass. A complexing agent (chelating agent) is mentioned as another example of inhibitor which reacts with metal ions eluted by an anodic reaction to form a precipitated film on the surface. Precipitation occurs when the metal ion and the inhibitor form a complex and become uncharged [65, 66]. Sodium octyl thio-propionate (NaOTP) acts as a precipitating type inhibitor for steel in a neutral solution that reacts with iron ions eluted from the steel and form a precipitated film on the steel surface and exhibits high corrosion inhibiting effect [67, 68].

1.5.2 Oxidation type inhibitors

Many metals used in the real environment form a dense passive film on the surface in neutral solution. It has been reported that Fe_2O_3 exists in the uppermost surface of steel in a neutral solution [69] and Al_2O_3 exists on the surface of aluminum [70]. Although these coatings have the ability to suppress corrosion, they are destroyed by corrosive substances in solution, so it is difficult to prevent corrosion of metals only by these passive films. In the oxidized inhibitor, the inhibitor added on the metal material further forms a passive film to form a layer sufficiently resistant to corrosive substances, thereby suppressing corrosion of the metallic material.

A representative example of an oxidative inhibitor that suppresses the anode reaction of steel is chromate [71]. The chromate ion is added to the solution that forms a coating consisting of γ - Fe_2O_3 in the inner layer and Cr_2O_3 in the outer layer and $Cr(OH)_3$ in the solution interface of the outer layer [63]. From the polarization curves of steel in corrosive solutions containing chromic acid measured in previous studies, it has been reported that chromic acid suppresses the anode reaction but does not suppress the cathode reaction [72]. Apart from the above-mentioned oxidation type inhibitors, molybdate is a typical example of an oxidation type inhibitor that suppresses both anode reaction and cathode reactions [73]. Although the corrosion inhibition mechanism of molybdate is not clarified, it is reported that FeOOH bonded to MoO_3 exists on the surface of steel immersed in a solution containing molybdate [74].

1.5.3 Adsorption type inhibitors

Adsorption is a surface phenomenon exhibited by solids which consist of adhesion in an extremely thin layer of the molecules of gases, liquids and dissolved substances with which they are in contact. The adsorption of ions or neutral molecules on bare metal surfaces immersed in solution is determined by the mutual interactions of all species present at the phase boundary. These include electrostatic and chemical interactions of the adsorbate with the surface, adsorbate-adsorbent, and adsorbate-solvent interactions. There are two types of adsorptions depending on the nature of the forces involved [75, 76]. (a) Chemisorption: In this type of adsorption, a single layer of molecules, atoms or ions is attached to the surface by chemical bonds and is essentially irreversible. (b) Physical adsorption: In this type, the attachment is by the weaker van der Waal's forces, whose energy levels approximate to those of condensation. The factors that influence the adsorption of inhibitor ions on metal surfaces are [77]:

1) The surface charge on the metal
2) The functional groups and structure of the inhibitor
3) The interaction between adsorbed inhibitor species (synergism and antagonism)
4) The reaction of adsorbed inhibitors.

The adsorption type inhibitor contains many organic compounds, and in general, the portion composed of carbon and hydrogen atoms other than the polar group is called a nonpolar group. Therefore, when the adsorbed inhibitor adsorbs to the base metal, the polar group is oriented to the metal side and the inhibitor molecule or ion is oriented like the nonpolar group on the solution side [78].

The adsorbed inhibitor inhibits metal corrosion for the following two reasons. One is that the exposed metal surface has high reactivity, but the polar group of the inhibitor binds to the active exposed metal surface so that the exposed surface is stabilized and the corrosion reaction is suppressed. The other is that the nonpolar group located on the solution side forms a dense structure due to van der Waals forces and therefore prevents corrosive substances such as chloride ions from migrating to the metal base. Most of the organic inhibitors containing nitrogen and sulfur like amines, triazoles, alkythiourea etc. belonging amino ($-NH_2$), carboxyl (-COOH), and phosphonate (PO_3H_2) although other functional groups or atoms can form coordinate bonds with metal surfaces are categorized as adsorption type inhibitors.

1.6 Environmental restrictions and research trend of inhibitors

Metal corrosion in aqueous solutions can be minimized or prevented using inhibitors as described above. However, most of the inhibitors (especially inorganic inhibitors) are costly, and pertain our environment and the human body. Below are the examples of inhibitors that have been adopted so far and their use on the environment has been prohibited [79]. Chromate with high corrosion inhibiting ability was widely used as an inhibitor in circulating water of the circulation cooling system in the 1960's, but hexavalent chromium compounds are toxic and carcinogenic [80]. Therefore, it was forbidden from use in the 1970's. After that, polyphosphate was used as an alternative inhibitor, but its usage was banned as it also causes red tide by seawater eutrophication by releasing it to rivers. Methylene phosphonate was used as a further alternative inhibitor, because it is hard to be naturally purified by microorganisms. It is no longer used because it may lead to the river/marine pollution. Therefore, recent research trend is to find some inhibitors that will have extensive attention due to their properties of environment-friendly, low influence on human body, low cost, easy to handle, and renewability [81-83].

1.7 Purpose of the research

This research aims to clarify the inhibition of steels corrosion in chloride aqueous solutions by metal cations at room temperature and elevated temperatures with the consideration of pH and chloride ions concentration.

Very few research has been carried out focusing on the effect of metal cations on the corrosion of steels in aqueous environments. In the previous research, it was shown that metal cations inhibited the corrosion of metal in freshwater at room temperature. The metal cation hardness, *X* was introduced to clarify the effects of metal cations on the corrosion. It is not fully elucidated the corrosion behavior of different types of steel in chloride aqueous solutions under the comparative conditions. Therefore, it is needed to clarify in details the corrosion behavior of different types of steels in chloride aqueous solutions at room temperature along with elevated temperatures under the consideration of pH and chloride ions concentration. It is also needed to clarify the relation between *X* and corrosion behavior of steels in the chloride aqueous environment. The corrosion inhibition mechanisms of metal cations were not also fully elucidated in chloride aqueous solutions at high temperatures under the consideration of pH. Therefore, it is also needed to clarify in details the corrosion inhibition mechanisms of metal cations under the comparative conditions in the chloride aqueous environment. The clarification of metal cation concentration effect on the corrosion is also needed.

In chapter 2, the corrosion behavior of mild steel in chloride aqueous solution has been explained and the relation between corrosion rate and *X* has been explored. The mechanisms of corrosion inhibition effect of metal cations have been clarified.

In chapter 3, the corrosion behavior of SUS304 in 0.5 M chloride aqueous solution has been discussed. *X* has been introduced to explain the corrosion inhibition effect of metal cations based on the HSAB concept.

It is considered that metal cations significantly inhibited the corrosion of steels in chloride aqueous solutions. It is further needed to clarify the effects of metal cations on steel corrosion in concentrated chloride aqueous solutions. In chapter 4, the role of metal cations on corrosion of coated steel substrate in concentrated chloride aqueous solutions has been elucidated by immersion tests and electrochemical tests. The mechanisms of corrosion inhibition effect have been explained.

Temperature effect on the corrosion inhibition performance of metal cations till now remains unknown and the mechanism also not fully explained. In chapter 5, the effects of metal cations on mild steel corrosion in chloride aqueous solutions have been explored at different temperatures (25, 50 and 80°C). The corrosion inhibition mechanisms of metal cations at different temperatures also have been proposed based on the experimental results.

In the previous chapter, it was suggested that Zn^{2+} effectively inhibited the corrosion of steel in chloride aqueous solutions. Therefore, it is needed to clarify the effects of Zn^{2+} concentration on the steel corrosion in chloride aqueous solutions. In chapter 6, the effects of Zn^{2+} concentration on the mild steel corrosion in chloride aqueous solutions were clarified based on the immersion tests and electrochemical tests. The corrosion inhibition efficiencies were elucidated regarding the Zn^{2+} concentration.

Chapter 7 is the summarization of chapter 2 to chapter 6. This paper reflects the significant inhibition effect of metal cations on steels corrosion in chloride aqueous solutions at room temperature as well as elevated temperatures. As the metal cations are available, easy to handle, environment-friendly and cost effective, the final goal of this research is to establish metal cations as corrosion inhibitors.

Table 1.1 List of metal cation hardness, *X*

Metal cation	Na^{+}	Mg^{2+}	Zn^{2+}	Al^{3+}	Zr^{4+}
X	1.01	3.54	4.64	7.94	10.22

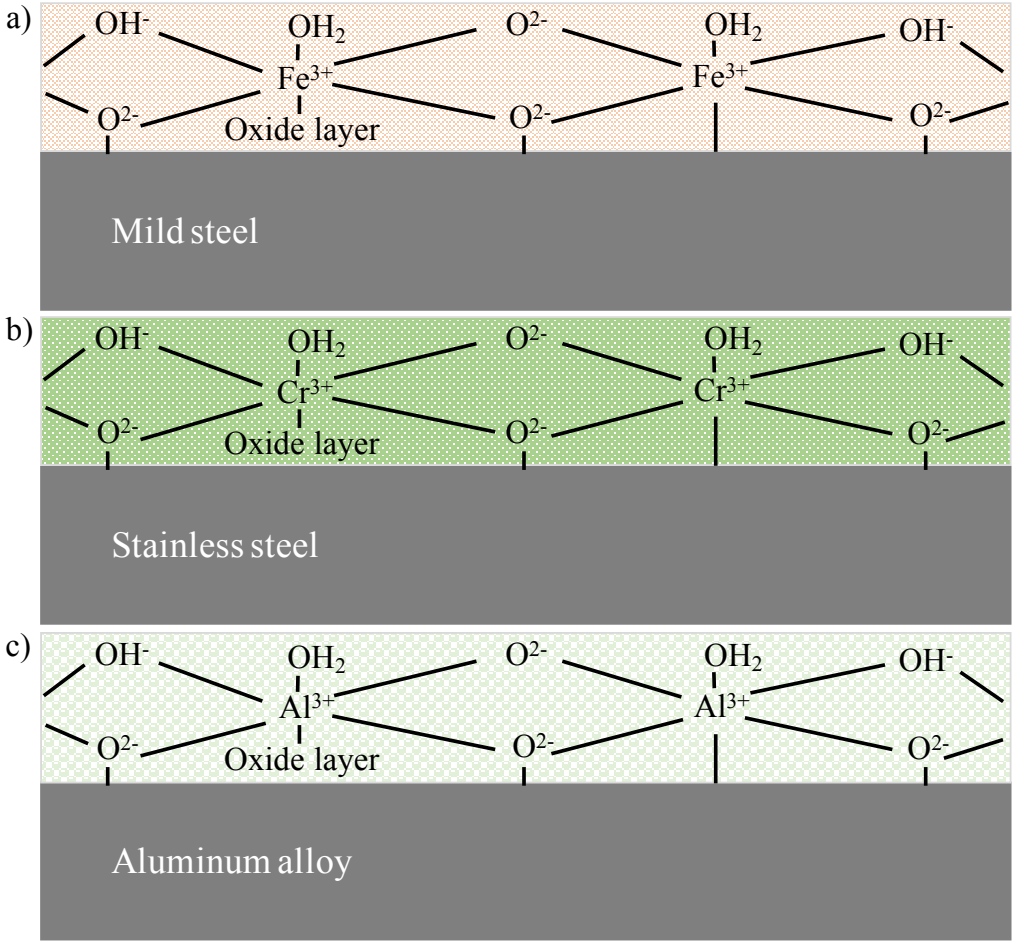

Fig. 1.1 Compositions and structure of oxide layer formed on different metals, a) mild steel, b) stainless steel and c) aluminum alloy

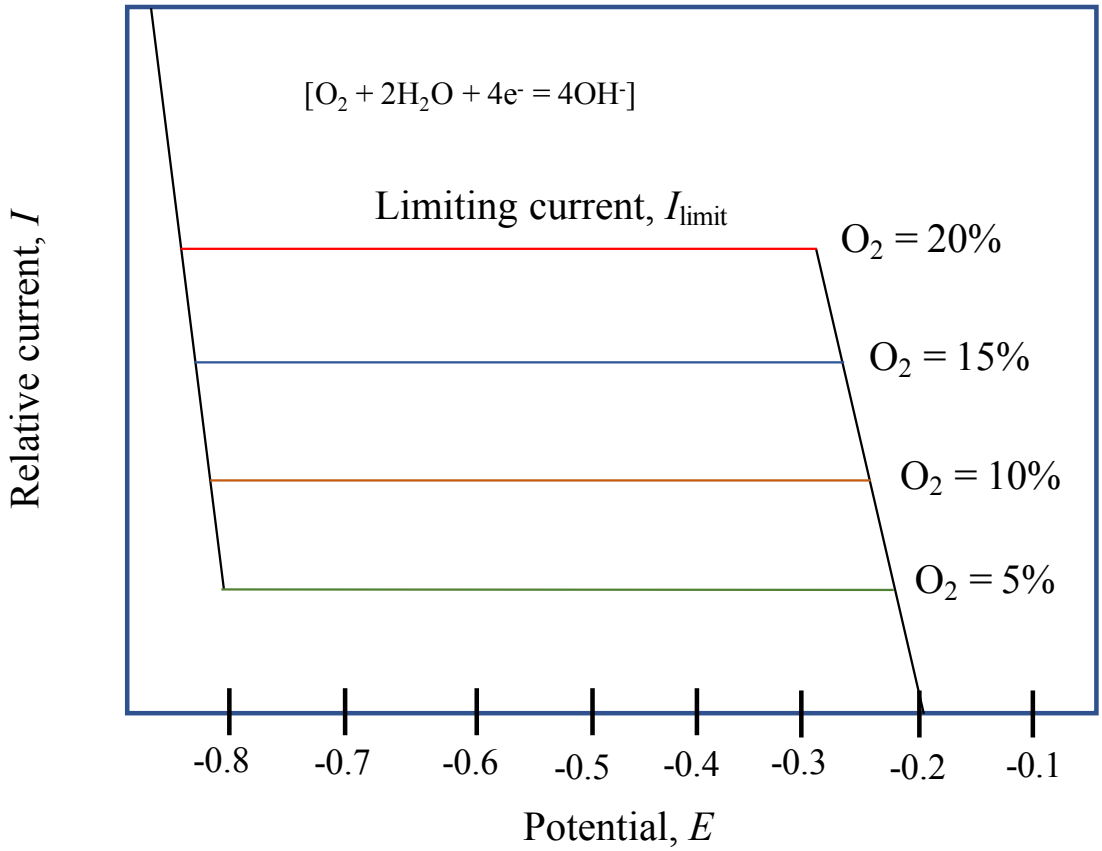

Fig. 1.2 Influence of oxygen concentration on the limiting current

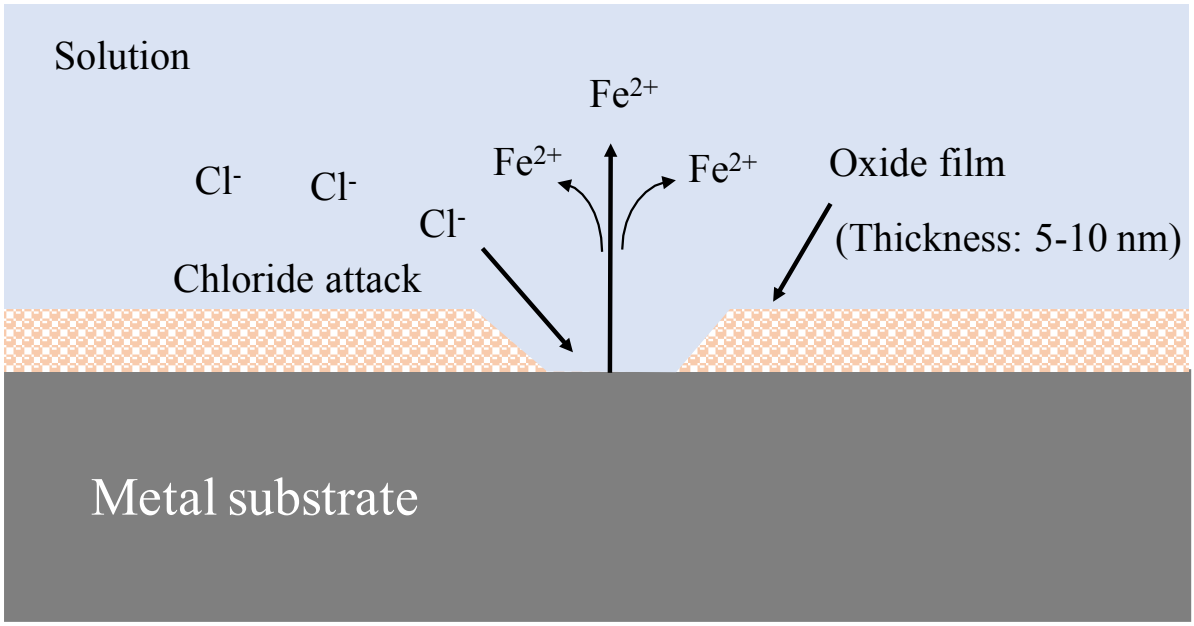

Fig. 1.3 Destruction of oxide layer by chloride attack and initiation of metal dissolution.

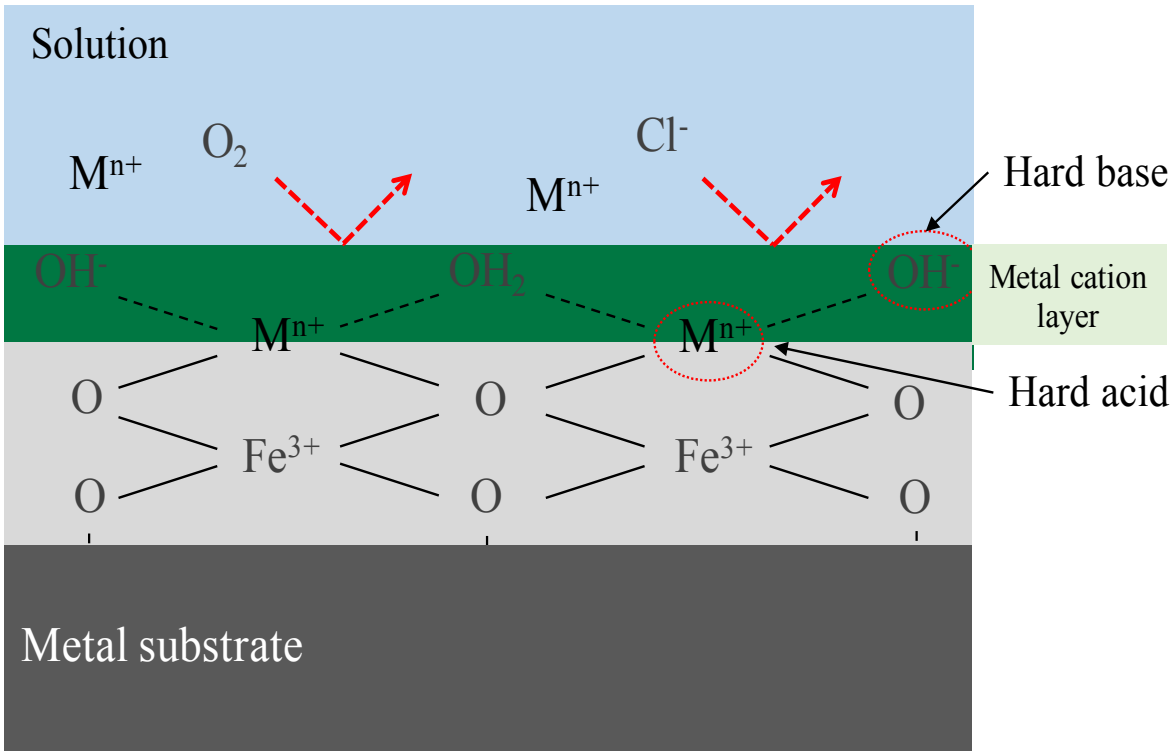

Fig. 1.4 Effects of metal cation hardness and formation of cation layer on the surface film

References

1. I. Santana, A. Pepe, E. Jimenez-Pique, S. pellice, I. Milosev and S. Cere, Surf. Coat. Technol., 265 (2015) 106-116.
2. S. Khara, S. Choudhary, S. Sangal and K. Mondal, Surf. Coat. Technol., 296 (2016) 203-210.
3. M. A. Amin and M. M. Ibrahim, Coross. Sci., 53 (2011) 873-885.
4. E. Tada and H. Kaneko, ISIJ Int., 51 (2011) 1882-1889.
5. Y. Prawoto, K. Ibrahim and W. B. Wan Nik, Arab. J. Sci. Eng., 34 (2009) 115-127.
6. J. Gullman, Factors influencing the corrosion rate of metal objects, Greens villa, Stockholm University, Stockholm, (1991).
7. S. Ningshen, M. Sakairi, K. Suzuki and S. Ukai, Coros. Sci., 78 (2014) 322-334.
8. M. Sakairi, R. Sasaki, A. Kaneko, Y. Seki and D. Nagasawa, Electrochim. Acta, 131 (2014) 123-129.
9. K. Otani and M. Sakairi, Corros. Sci., 111 (2016) 302-312.
10. G. V. Akimov, Corrosion, 15 (1959) 23-36.
11. R. W. Revie and H. H. Uhlig, Corrosion and Corrosion Control: An Introduction to Corrosion Science and Engineering 4th ed., Jhon Wiley & Sons, (2008).
12. P. Sarin, V. L. Snoeyink, J. Bebee, K. K. Jim, M. A. Beckett, W. M. Kriven and J. A. Clement, Water Research, 38 (2004) 1259-1269.
13. H. H. Uhilig, D. Triadis and M. Stern, J. Electrochem. Soc., 102 (1955) 59-66.
14. I. Yasushige, Nuclear Industry, 22 (1976) 70-80.
15. K. Ishii, R. Ozaki, K. Kaneko and M. Masuda, J. Japan Inst. Met., 70 (2006) 845-848.
16. K. Goto, I. Toshiro and S. Yoshihiko, light metal, 20 (1970) 88-89.
17. B. S. Pijanowski and I. Mahmud, A study of the effects on temperature and oxygen content on the corrosion of several metals, Institute of Ocean Science and Engineering, The Catholic University of America, Washington D.C., (1969).
18. M. Cohen, Can. J. Chem., 37 (1959) 286-291.
19. W. G. Whitman, Chem. Rev., 2 (1926) 419-435.
20. F. G. Frese, Int. Eng. Chem., 30 (1938) 83-85.
21. F. N. Speller, Corrosion Causes and Prevention, 3rd ed., MeGraw-Hill, New York, (1951).
22. K. James and P. E. Rice, Consulting Engineer, Drew Principles of industrial Water Treatment, Olney, Maryland, (1977).
23. F. Bentiss, M. Traisnel and M. Lagrenee, J. Appl. Electrochem., 31 (2001) 41-48.
24. G. Itoh, light metal, 31 (1981) 683-696.

25. N. O. Obi-Egbedi, I. B. Obot and A. O. Eseola, Arab. J. Chem., 7 (2014) 197-207.
26. Y. Qi, H. Luo, S. Zheng, C. Chen, Z. Lv and M. Xiong, Int. J. Electrochem. Sci., 9 (2014) 2101-2112.
27. K. Matsunami, T. Kato and K. Sugimoto, Int. J. Pres. Ves. & Piping, 45 (1991) 179-197.
28. L. I. Pincus, Practical boiler water treatment-introducing air-conditioning system, McGraw-Hill Book Company, New York, (1962) 37-38.
29. S. Basu, Boiler chemistry control and treatment of feed water, Elsevier SciTech Connect, (2015).
30. Handbook of Industrial Water Treatment, General Electric Company, (2012).
31. E. J. Bonner, Water treatment for modern boiler plant in the paper industry, Prime Conference Proc. Instn. Mech. Engrs., (1967) 24-33.
32. I. G. Wenten, Khoiruddin, F. Arfianto and Zudiharto, Desalination, 314 (2013) 109-114.
33. B. Zaid, D. Saidi, A. Benzaid and S. Handji, Corros. Sci., 50 (2008) 1841-1847.
34. M. Pourbaix, Atlas of Electrochemical Equilibria in Aqueous Solutions 2nd ed., English, NACE, (1974).
35. M. F. Hurley and J. R. Scully, Corrosion, 62 (2006) 892-904.
36. E. McCafferty and N. Hackerman, J. Electrochem. Soc., 119 (1972) 999-1009.
37. J. Han, J. W. Carey and J. Zhang, J. Appl. Electrochem., 41 (2011) 741-749.
38. Goldie and McCarrol, Corrosion inhibitors, (1984).
39. A. Amadeh, S. R. Allahkaram, S. R. Hosseni, H. Moradi and A. Abdolahosseini, Anti-corrosion methods and materials, 55 (2008) 135-143.
40. D. M. Drazic and L. Z. Vorkapic, Corros. Sci., 18 (1978) 907-910.
41. H. Leidheiser Jr., Corros., 36 (1980) 339-345.
42. H. Leidheiser Jr. and I. Suzuki, J. Electrochem. Soc., 128 (1981) 242-249.
43. M. G. A. Khedr and A. M. S. Lashien, J. Electrochem. Soc., 136 (1989) 968-972.
44. M. G. A. Khedr and A. M. S. Lashien, Corros. Sci., 33 (1992) 137-151.
45. I. Felhosi, Zs. Keresztes, F. H. Karman, M. Mohai, I. Bertoti and E. Kalman, J. Electrochem. Soc., 146 (1999) 961-969.
46. J. Telegdi, M. M. Shaglouf, A. Shaban, F. H. Karman, I. Betroti, M. Mohai and E. Kalman, Electrochim. Acta, 46 (2001) 3791-3799.
47. S. Zhang, T. Shibata and T. Haruna, Corros. Sci., 47 (2005) 1049-1061.
48. S. Sathiyanarayanan, C. Jeyaprabha, S. Muralidharan and G. Venkatachari, App. Surf. Sci., 252 (2006) 8107-8112.

49. M. Prabakaran, M. Venkatesh, S. Ramesh and V. Periasamy, App. Surf. Sci., 276 (2013) 592-603.
50. K. Otani, M. Sakairi, R. Sasaki, A. Kaneko and Y. Seki, J. Solid State Electrochem., 18 (2014) 325-332.
51. M. Misono, E. Ochiai, Y. Saito and Y. Yoneda, J. Inorg. Nucl. Chem., 29 (1967) 2658-2691.
52. NACE Corrosion Cost Study, (2002).
53. NACE Corrosion Cost Study, (2011).
54. C. Verma, E. E. Ebenso and M. A. Quraishi, J. Mol. Liq., 248 (2017) 927-942.
55. I. B. Obot, N. O. Obi-Egbedi and S. A. Umoren, Corros. Sci., 51 (2009) 1868-1875.
56. P. R. Roberge, Handbook of corrosion engineering, Mc Graw Hill Handbook, New York, (1999).
57. V. Gentil, Corrosão, 4th ed., Rio de Janeiro: LTC, (2003).
58. L. V. Ramanathan, Corrosão e seu controle, São Paulo: Hemus, (1988).
59. www.npl.co.uk/upload/pdf/basics_of_corrosion_control.pdf
60. C. G. Dariva and A. F. Galio, Corrosion inhibitors-principles, mechanism and applications, (2014) 365-379.
61. A. C. Dutra and L. D. P. Nunes, Proteção catódica técnicas de combate a corrosão, 5th ed., Rio de Janeiro: interciências, (2011).
62. A. S. Yaro, A. A. Khadom and R. K. Wael, J. Alexandria Eng., 52 (2013) 129-135.
63. V. S. Sastri, Corrosion Inhibitors, Principles and Applications, John Wiley & Sons, (1998).
64. K. Aramaki, Rust prevention & control, 20 (1976) 9-50.
65. H. Yasushi, K. Hiroko and K. Shigeaki, Electrochemistry, 37 (1969) 804-814.
66. K. Aramaki, K. Yoshitomo, Anticorrosion technology, 33 (1984) 583-586.
67. K. Aramaki, A. Yamamoto, Anticorrosion Technology, 33 (1984) 683-688.
68. Y. Yamamoto, H. Nishihara and K. Aramaki, Corrosion, 48 (1992) 641-648.
69. N. Sato, Corros. Sci., 31 (1990) 1-19.
70. R. S. Alwitt, J. Electrochem. Soc., 121 (1974) 1322-1328.
71. I. L. Rosenfeld, Corrosion Inhibitors, McGraw-Hill Inc., (1981).
72. K. Aramaki, Rust prevention & control, 48 (2004) 151-189.
73. V. S. Sastri, R. H. Packwood, J. R. Brown, J. S. Bednar, L. E. Galbraith and V. E. Moore, Br. Corros. J., 24 (1989) 30-35.
74. E. Fujioka, H. Nishihara and K. Aramaki, Corros. Sci., 38 (1996) 1915-1933.
75. C. C. Nathan, Corrosion Inhibitors, NACE, Texas: Houston, USA, (1973).

76. R. G. Kelly, R. Scully, D. W. Shoesmith and R. G. Buchheit, Electrochemical Techniques in Corrosion Science and Engineering, Marcel Dekker press, New York, (2002).
77. J. C. Bailey, F. C. Porter, A. W. Pearson and R. A. Jarman, Aluminum and aluminum alloys, in Corrosion: metal /environment reactions, 3th ed., Springer, London, (1994).
78. K. Aramaki, Rust prevention & control, 48 (2004) 108-117.
79. K. Aramaki, Rust prevention & control, 48 (2004) 23-107.
80. N. I. Sax and R. J. Lewis, Dangerous Properties of Industrial Materials, 7th ed., Van Nostrand Reinhold, (1989).
81. X. Li, S. Deng, X. Xie and H. Fu, Corros. Sci., 87 (2014) 15-26.
82. P. Mourya, S. Banerjee and M. M. Singh, Corros. Sci., 85 (2014) 352-363.
83. L. Li, Corros. Sci., 63 (2012) 82-90.

Chapter 2

Effects of metal cations on mild steel corrosion in Cl^- containing aqueous solutions

2.1 Introduction

The stability of metal, when exposed to the environment depends on a multitude of factors that may vary greatly with the concentration of Cl^- and SO_4^{2-}. Mild steel is very popular and widely used metallic materials, and the corrosion of this steel is a serious problem in water supply pipelines, storage tanks, and industrial equipment etc., and the corrosion behavior has been studied by many researchers [1-3]. The corrosion rate of mild steel can be accelerated by the presence of Cl^- and SO_4^{2-} containing compounds [4-6]. A large number of chlorine compounds (Cl_2, NaOCl, $Ca(OCl)_2$ etc.) are used as disinfectants in the wastewater treatment and bleach for both domestic and industrial purposes. These compounds are also widely used to disinfect drinking water and swimming pool water and to control bacteria and odors in the food industry [7-9]. An enormous amount of chlorine compounds is also used in the laundry to bleach and wash the clothes. Chlorine compounds are listed as a known poison that have an adverse effect on the corrosion of the pipeline of water circulation system and other metallic equipment that exposed in that environment, and these compounds are dissociated into Cl^- and OCl^- in the aqueous solution as following Eqs.:

$$Cl_2 + H_2O \rightarrow H^+ + Cl^- + HOCl \quad (2.1)$$

$$NaOCl + H_2O \rightarrow NaOH + H^+ + OCl^- \quad (2.2)$$

$$Ca(OCl)_2 + H_2O \rightarrow Ca(OH)_2 + H^+ + OCl^- \quad (2.3)$$

The oxide layer (passive film) of the steel is generally destroyed by the penetration of Cl^- in aqueous solution [4, 10-13]. Fig. 2.1 (a) and (b) shows the penetration and film thinning mechanism of Cl^- into the oxide films [14-17]. After the destruction of the passive films, the corrosion process starts with a coupled of electrochemical reactions [1, 2, 18]. Fig. 2.1 (c) shows the anodic reaction of metal dissolution (Eq. (2.4)) and the cathodic reaction of oxygen reduction (Eq. (2.5)).

$$Fe\ (s) \rightarrow Fe^{2+}\ (aq) + 2e^- \quad (2.4)$$

$$1/2O_2 + H_2O + 2e^- \rightarrow 2OH^- \quad (2.5)$$

Otani et al. [18, 19], Kato [20] and Takasaki [21] investigated the corrosion behavior of mild steel by emphasizing the effects of metal cations in model fresh water, and they found that Zn^{2+} and Al^{3+} have the ability to inhibit the corrosion. Mahdavian et al. [22] investigated the

corrosion inhibition of mild steel by some zinc complexes in sodium chloride solution. Prabhu et al. [23] investigated the corrosion behavior of metal surface treated with a new organic chelating inhibitor in acid solution. Jin-xia Xu et al. [24] investigated the steel corrosion in saturated calcium hydroxide solution with metal oxides and nitrates. For this reason, the effect of metal cations on the corrosion of mild steel should be considered in the Cl^- containing aqueous solution. The effect of metal cations on corrosion of mild steel in 10 mM Cl^- aqueous solution is not fully understood. It is needed to clarify the effect of metal cations on the corrosion behavior of mild steel in the solution that contains 10 mM Cl^- at a same pH.

Existence of the metal cations on the passive films would be significant to clarify the influence of metal cations on the corrosion of mild steel in the 10 mM Cl^- aqueous solution. According to the Lewis concept regarding acid and bases, cations and anions act as acids and bases, respectively [25]. Further, acids and bases are categorized into 'hard' and 'soft' [26]. According to the hard and soft acids and bases (HSAB) concept, soft acids react and form strong bonds with soft bases, whereas hard acids react and form strong bonds with hard bases. The metal cation hardness is based on the HSAB concept. The hardness of metal cations, X, is expressed by the Eq. 1.10 (chapter 1) [18, 27, 28]

Hard acids and hard bases can form stable bonds. Hydroxyl groups, which are categorized as hard bases, are located on the outermost layer of the oxide films of mild steel and metal cations with large X, which are categorized as hard acids easily bond with hydroxyl groups on the mild steel. For this reason, the value of X indicates the tendency of formation of a chemical bond between metal cations in the solution and hydroxyl groups on the mild steel surface. For this reason, the HSAB concept is very useful for understanding the incorporation of metal cations in the oxide films [29]. Based on the HSAB concept, the hardness of metal cation, X was introduced to explain the corrosion behavior of metals in freshwater [27]. However, X is not a suitable corrosion indicator regarding the corrosion of metals in freshwater [18]. It is still unknown the possibility of X as an indicator for corrosion of metals in the 10 mM Cl^- aqueous solution. The mechanism of corrosion inhibition of metal cations is also unknown. By considering the corrosion rate of mild steel that depends on the metal cations [18, 19], Cl^- concentration, pH [30, 31], the present research purpose is to find out the effects of metal cations on corrosion of mild steel, and the mechanism of corrosion inhibition in 10 mM Cl^- aqueous solution at an equal level of pH.

In this experiment, comparative conditions were used to study the influence of metal cations on corrosion of mild steel in 10 mM Cl^- aqueous solution. The pH of solutions and the experimental temperature were controlled initially to obtain the effective influence of metal

cations on corrosion. The influence of metal cations on corrosion of mild steel in the mentioned environment was investigated by electrochemical impedance spectroscopy (EIS), immersion tests, surface observation and analysis with a scanning electron microscope (SEM), Energy dispersive X-ray spectroscope (EDS) and X-ray photoelectron spectroscope (XPS).

2.2 Experimental

2.2.1 Specimens

Mild steel sheets (7 × 7 mm in size and 0.7 mm in thickness) were used as specimens. The chemical composition of mild steel is shown in Table 2.1. The methods used to prepare specimens for immersion tests and electrochemical measurements are shown in Fig. 2.2. To make electrical contact, a wire was connected with each specimen to perform the electrochemical measurements. All the specimens were molded in epoxy resin (Struers Ltd., EpoFix Resin). The exposed surface of each molded specimen was grounded (Marumoto Struers S5629, LaboForce-3) with SiC abrasive papers from #400 to #4000 grit size, then finally polished by colloidal silica. Before the immersion tests, the specimens were taken out from the epoxy resin. All the specimens were ultrasonically cleaned (SIBATA ultrasonic cleaner, SU-2T) in ethanol and then in highly purified water. The specimens were kept in a desiccator to avoid any type of contamination and humidity.

2.2.2 Solutions

Five different salt solutions, 10 mM NaCl (Na_{sol}), 0.1 mM $MgCl_2$ (Mg_{sol}), 0.1 mM $ZnCl_2$ (Zn_{sol}), 0.1 mM $AlCl_3$ (Al_{sol}), and 0.1 mM $ZrOCl_2$ (Zr_{sol}) were used as test solutions. The Cl^- concentration was adjusted to 10 mM by NaCl. In this study, Na_{sol} was considered as a standard solution. Water used in this study was highly purified that was distilled twice and then purified by water purifier (MILLIPORE, Simplicity UV). All chemicals used in this study were special analytical grade and obtained from Kanto Chemical Co. Ltd.

Electrochemical reactions are mostly depended on the pH of the aqueous solution [30, 31]. The pH of used solutions was controlled between 5.5 and 6.0 by 0.1 M NaOH (Table 2.2). The pH measurement of the solutions before and after immersion tests was carried out using the pH meter (Eutech Instruments Pte. Ltd., Cyber-Scan 6000).

2.2.3 Immersion tests

Specimens were immersed in the solutions for 3 d at 25°C. The test performing bottles were open to the air during immersion tests. The mass of the specimens was measured using a micro-balance (METTLER TOLEDO MX5, Pro FACT) before and after immersion tests, and the corrosion rates (C_R) were calculated from the mass variation using the Eq. (2.6).

$$C_R\ (\mu m/y) = \frac{(M_1 - M_2)}{D \times S \times t} \times 3650 \quad (2.6)$$

Where M_1 is mass before immersion (mg), M_2 is mass after immersion (mg), D is the density of specimen (g/cm^3), S is the surface area of the specimen (cm^2) and t is immersion time (d).

2.2.4 Electrochemical tests

All the electrochemical measurements were carried out in a three-electrode system using a potentiostat (Pocketstat, IVIUM TECHNOLOGIES). Open-circuit potential (OCP) was measured for 1 h at 25°C and the potentiodynamic measurements were carried out in the cathodic and anodic direction with a scan rate of 1 mV/s. The cathodic and anodic scan was started separately to obtain the individual electrochemical properties of mild steel immersed in the corresponding solutions with a metal cation. A platinum plate of 4 cm^2 and an Ag/AgCl electrode (SSE) immersed in a saturated KCl solution were used as counter and reference electrodes, respectively. The exposed surface area of the working electrode in the solution was 49 mm^2. EIS measurements were carried out in the frequency range from 10 kHz to 1 mHz, and modulation amplitude of 10 mV. Reproducible data were acquired in all electrochemical measurements.

2.2.5 Surface observations and analysis

Surface morphology is the important criteria which reflect the corrosion behavior of the mild steel regarding the solution. Surface observations of the specimen after immersion were carried out to clarify the variance of the specified corrosion behavior of mild steel in the different solutions of metal cation. Before and after the immersion tests, the surfaces of the specimens were observed by a digital camera (Nikon, D80-DSLR), optical microscope (WRAYMER-G500) and Scanning Electron Microscope (SEM) using secondary electrons imaging (SEM, JEOL Ltd., JSL6510-LA). For SEM observation, the acceleration voltage of the electron beam was set at 10 kV in order to be sensitive to the morphology of the surface. EDS analysis was carried out to analyze the surface composition of the specimen after immersion tests.

Surface analysis was carried out to clarify the situation of specimen surface after immersion in the solutions with a different metal cation. The center area of the specimens after immersion was analyzed by X-ray Photoelectron Spectroscope (XPS, JEOL Ltd., JPS-9200) using a monochrome Al Kα X-ray source. Before the analysis, the immersed specimens were cleaned ultrasonically by ethanol and then in highly purified water. After cleaned, specimens were kept in a desiccator to avoid humidity and any type of contamination. The diameter of the specimen analyzed by the XPS was 3 mm.

2.3 Results

2.3.1 Immersion tests

Fig. 2.3 (a) shows the appearance of specimens at the starting of immersion and 3 (b) shows the specimens after immersion in Na_{sol}, Mg_{sol}, Zn_{sol}, Al_{sol} and Zr_{sol} during 3 d at 25°C. In Fig. 2.3 (b), there are many brown color corrosion products are observed on the specimen surface in the case of Na_{sol}, and Mg_{sol}. The amounts of corrosion products in Zn_{sol}, Al_{sol}, and Zr_{sol} are decreased compared with Na_{sol} and Mg_{sol}. Fig. 2.3 (c) shows the surface images of specimens after immersion in the solutions before (upper row) and after (bottom row) ultrasonic cleaning. Brown color corrosion products were deposited on the specimen surface that was observed before ultrasonic cleaning, and the amount was varied depending on the solutions. Less amount of brown color corrosion products is observed in the case of Zn_{sol} as compared to the other solutions. The corrosion rates were calculated from the mass loss after immersion for 3 d in the different solutions. The density of specimen, 7.874 g/cm^3 was used to calculate the corrosion rates [32]. Fig. 2.4 shows the corrosion rate as a function of *X*. The corrosion rate is gradually decreased with increasing the value of *X* up to 5, and over 5, the corrosion rate is not decreased gradually. The correlation coefficient is -0.42 indicating that the corrosion rate is not clearly related to *X*. However, the results of immersion corrosion tests indicate that Zn_{sol} has the better corrosion inhibition effect on mild steel in a high concentration of Cl^- containing aqueous solution.

The pH of the test solutions before and after immersion for 3 d is shown in Table 2.2. Initial pH (pH_{int}) of Al_{sol} and Zr_{sol} showed low value than other solutions of a metal cation and it was adjusted (pH_{adj}) to 5.7 and 5.8. Average pH of the test solutions is around 5.8. The pH was slightly increased after immersion (pH_{corr}) in all solutions due to the formation of OH^- at the metal surface [18, 33].

2.3.2 Electrochemical tests

2.3.2.1 Open-circuit potential (OCP) and potentiodynamic polarization

The open circuit potentials of mild steel measured in the solution of metal cations rapidly reach a stable value at around 3000 s of immersion (Fig. 2.5 (a)). All the measured values are confined in a reduced range of potentials between -0.22 V and -0.45 V. Only slight difference can be noticed in the case of Mg_{sol}, Zn_{sol}, Al_{sol} and Zr_{sol} as compared to Na_{sol}, and Na_{sol} induces the most negative open-circuit potential and Zn_{sol} the most positive one. Open-circuit potentials at 1 s and at 3000 s as a function of *X* are shown in Fig. 2.5 (b). The metal cations which have large *X* show no significant difference. However, Zn_{sol} shows higher average potential than Na_{sol}, and Na_{sol} shows the lowest average potential at 3000 s as compared to the other solutions with metal cations.

Fig. 2.6 (a) shows the cathodic polarization curves and Fig. 2.6 (b) shows the anodic polarization curves. From the Figs. 2.6 (a) and (b) (indicated by arrow), it is found that Zn_{sol} shows lower current density as compared to the Na_{sol} and Na_{sol} shows the highest current density among used solutions both in cathodic and anodic polarization curves. For the other solutions of metal cation, there are no significant influences of cathodic and anodic reactions as well.

2.3.2.2 Electrochemical Impedance Spectroscopy (EIS)

EIS measurements were carried out to elucidate the initial corrosion behavior of the mild steel and the effect of metal cations on the properties of the protective layer. Fig. 2.7 shows the Bode diagram of (a) Impedance plots, (b) phase shift plots and (c) Nyquist plots of the mild steel in the solutions after immersion for 1 h, and impedance spectra depend on the kinds of metal cations. There was no rust formed during EIS measurements. The fitted lines calculated by Randle's equivalent circuit model [34-36] are also shown in Fig. 2.7, and the equivalent circuit model is shown in Fig. 2.7 (d). All the spectra can be well described by the equivalent circuit. This model consists of solution resistance (R_{sol}), charge-transfer resistance (R_{ct}), and constant phase element (CPE), Q. The impedance can be expressed in terms of R_{sol}, R_{ct} and CPE parameters n and Q by Eq. (2.7) [37-40].

$$Z = \mathrm{R_{sol}} + \frac{\mathrm{R_{ct}}}{1+ (j\omega)^n \, \mathrm{QR_{ct}}} \tag{2.7}$$

Here $\omega = 2\pi f$ and *f* is the frequency in units of Hz. The value of CPE parameter, n varies from 0 to 1. When n = 1, the CPE behaves as a pure capacitor, and when n = 0, the CPE behaves as a pure resistor. The CPE parameters are calculated by using the Eq. 2.7. The simulated values

of CPE parameters are shown in Table 2.3.

The magnitude of impedance at low frequencies in the Bode diagram implies the corrosion resistance of mild steel in the solution. Among five experimental solutions, Zn_{sol} shows the larger impedance at low frequency (Fig. 2.7 (a)). The higher phase shift is observed for Zn_{sol} (Fig. 2.7 (b)), and the magnitude of each Nyquist plots are different depending on the solutions (Fig. 2.7 (c)). The larger magnitude of Nyquist plot is observed in the case of Zn_{sol} among other solutions.

The (a) R_{sol}, (b) R_{ct}, and (c) Q as a function of *X* are shown in Fig. 2.8. The R_{sol} is not significantly changed with *X* (Fig. 2.8 (a)). Higher R_{ct} is observed in the case of Zn_{sol} (Fig. 2.8 (b)) than other solutions, and there are no significant influences for the other solutions. High R_{ct} means that mild steel has high corrosion resistance in the solution. This is supposed that Zn_{sol} exposes the high corrosion resistance (R_{ct}) than other solutions. The value of Q is decreasing with increasing the value of *X* up to 5 and then the Q is again increasing with increasing the value of *X* (Fig. 2.8 (c)). Zn_{sol} shows the lowest value of Q than other solutions of the metal cation (Table 2.3). Otani et al. [19] reported that the decrease in Q indicates that Zn^{2+} can decrease the defect in the protective film on mild steel. Therefore, this result indicates that Zn_{sol} has relatively perfect oxide film and narrow metal/solution interface area than other solutions.

The results of EIS and immersion tests showed that the corrosion rate of mild steel decreases with increasing the value of *X* up to 5. In addition, the correlation coefficients of R_{sol} vs *X*, R_{ct} vs *X*, and Q vs *X* are 0.51, 0.15 and -0.01 respectively (Fig. 2.8 (a), (b) and (c)), and these values are too small to regard the corrosion rate with hardness of metal cations, *X*. Therefore, the hardness of metal cations, *X*, is not suitable as a corrosion indicator of mild steel in 10 mM Cl^- aqueous solution. The results obtained from EIS and immersion tests suggest that Zn_{sol} has high corrosion resistance over other metal cations used in this study in 10 mM Cl^- aqueous solution.

2.3.3 Surface observations and analysis

The results of immersion corrosion tests showed that the corrosion rates of the specimens after immersion for 3 d is different in each solution. The changes in the appearance of specimen surfaces were observed to clarify the situation. Specimen surface was first observed by an optical microscope, and grain boundaries were observed. To be more clear about surface morphology changes, the surface observations were carried out by SEM. Fig. 2.9 shows the surface SEM images of specimen and different surface morphologies are observed for the

different solutions. SEM images depict the clear grain boundaries that are observed in the case of Na_{sol}, Mg_{sol}, Al_{sol} and Zr_{sol}. Pits and grain boundaries are observed in the case of Na_{sol}. A few numbers of pits are also observed for Mg_{sol}, Al_{sol} and Zr_{sol}, and some corrosion products are deposited on the surface in the case of Zn_{sol}. Zn^{2+} may form less soluble salts and tend to precipitate in a form of hydroxide, oxide, or hydroxy salts. Severe corrosion is observed for Na_{sol} as compared to the other solutions. The results suggest that corrosion may be affected with corrosion inhibiting effect of the metal cation and Zn^{2+} has the better corrosion inhibition effect on mild steel in the 10 mM Cl^- aqueous solution. An EDS analysis result is shown in Fig. 2.10. The left side of Fig. 2.10 shows the SEM image of the EDS analysis area, and the right side shows the EDS analysis result, and Zn is found on the mild steel surface after immersion in the solution.

The results of the immersion corrosion tests and electrochemical measurements suggest that the protectiveness of passive film may be affected by the metal cations in the solution. For better understanding, the influence of metal cations and also the incorporation of metal cations on the surface film structure, the specimen surfaces after the immersion tests were investigated by XPS. Fig. 2.11 shows the XPS wide spectra of mild steel surface after immersion in the solution with metal cations. This figure clearly shows the peak of Zn2p1/2 and Zn2p3/2 after immersion in the Zn_{sol}. Fig. 2.12 (a) shows the XPS narrow spectra of Na 1s and Fig. 2.12 (b) shows the Mg 1s, Zn 2p3/2, Al 2p3/2 and Zr 3d5/2 spectra in each solution. XPS analysis results show that there is no peak of Na1s on the specimen after immersion in all solution suggesting that Na^+ cannot form any compound on the mild steel in the solution (Fig. 2.12 (a)). The clear peak is observed (Fig. 2.12 (b)) in the case of Zn^{2+} among all experimental metal cations meaning that only Zn^{2+} remains on the mild steel after immersion in the solution. Zn^{2+} may precipitate as oxides or hydroxides [18, 19] and make a chemical bond with the oxide film of mild steel in 10 mM Cl^- aqueous solution and forms a metal cation layer which inhibits the anodic and cathodic reactions, and protects the dissolution of metal [18, 19]. These results correspond with other tests like immersion tests and electrochemical tests.

2.4 Discussions

According to the results in this study, the corrosion properties of mild steel significantly affected by metal cations in the solution. Electrochemical measurements showed that the decrease of corrosion rate of mild steel due to an inhibitory effect of both the anodic reaction of iron oxidation and the cathodic reaction of oxygen reduction. This inhibitory effect might be the consequences of metal cation that was incorporated on the oxide films of the metal

surface and suppress the corrosion rate.

The structure of passive films formed on mild steels in neutral solution has been reported by many researchers through the electron diffraction technique, and the passive films consist of Fe_3O_4 and γ-Fe_2O_3 in neutral solutions [41-44]. The possible corrosion mechanism of metal cations with the passive film of mild steel in the 10 mM Cl^- aqueous solution is shown in Fig. 13. Metal cations (M^{n+} = Na^+, Mg^{2+}, Al^{3+}, and Zr^{4+}) are not able to make (Fig. 2.13 (a)) any compound (precipitate) or unable to make any bond with the oxide film of mild steel (Fig. 2.13 (b)). From the Pourbaix diagram, it is known that Mg^{2+} ([Mg^{2+} = 0.1mM]) and Zr^{4+} ([Zr^{4+} = 0.1mM]) cannot precipitate as oxides or hydroxides at pH lower than 8 [45]. After immersion, the pH of the solution was about 6.5 (Table 2.2). Therefore, Mg^{2+} and Zr^{4+} may not be able to precipitate on the mild steel in this pH. Al^{3+} ([Al^{3+} = 0.1mM]) is able to form oxides or hydroxides on mild steel at pH lower than 6 [45]. However, oxides or hydroxides are not stable [45, 46]. Then Cl^- can arrive on the metal surface through destroying the oxide films and initiate the electrochemical reactions. Consequently, Al_{sol} shows higher corrosion rate than Zn_{sol} (Fig. 2.4) in this experiment due to the instability of the oxides or hydroxides that are formed on mild steel [45, 46].

The possible corrosion mechanism of Zn^{2+} would be different from other metal cations (M^{n+} = Na^+, Mg^{2+}, Al^{3+}, and Zr^{4+}). EDS and XPS analysis results show the clear evidence that Zn^{2+} remains on the mild steel after immersion in the solution among metal cations used in this study. It is expected that Zn^{2+} reacts with the OH^- (reaction (2.5)) to form hydroxides (reaction (2.8)) in the cathodic area due to locally high pH near the surface [33, 45, 47]. From the Pourbaix diagram, it is also known that Zn^{2+} ([Zn^{2+} = 0.1mM]) can precipitate as hydroxides on the mild steel at pH around 6 [45].

$$Zn^{2+} + 2OH^- \rightarrow Zn(OH)_2 \qquad (2.8)$$

The mechanism of corrosion inhibition is as follows:

The produced hydroxides can possibly bind in a chemical bond with the outermost layer of the oxide film of mild steel [45, 48]. Another possibility is that Zn^{2+} directly makes a bond with OH^- of oxide film (oxide film contains so many OH^-) and thus form a metal cation layer on the oxide film (Fig. 2.13 (c)) [18, 19]. Several studies also have shown that metal cations that have large *X* can easily bond with OH^- on the oxide film of mild steel [18, 19, 28, 29]. The anodic area may be smaller than the cathodic area and the Zn^{2+} layer may also cover the anodic area. Therefore, the metal cation layer of Zn^{2+} would have good protective ability against the Cl^- attack in the solution, and the protective layer would prevent the cathodic and anodic reactions

(Fig. 2.13 (d)) on the mild steel [18, 19]. For this reason, the corrosion rate of the mild steel immersed in Zn_{sol} was lower than those in other solutions with metal cations.

2.5 Conclusion

The effects of metal cations on mild steel corrosion in 10 mM Cl^- aqueous solution were investigated by immersion tests followed with SEM, EDS, XPS, and EIS.

- The corrosion behavior of mild steel in the 10 mM Cl- aqueous solution was changed with *X*, while the corrosion rate was not highly correlated with *X*.
- Different surface morphologies were observed by SEM, and it was found that some corrosion products were deposited on the surface after immersion in the Zn_{sol}.
- Among the metal cations used in this study, only Zn^{2+} was detected by XPS on the specimen surface after immersion in the Zn_{sol}.
- Zn^{2+} forms a protective layer with the oxide film of mild steel in the solution, and thus inhibits the electrochemical reactions, and consequently lowers the corrosion rate as well.

Table 2.1 Chemical composition of specimen (mass %)

C	Si	Mn	P	S	Fe
0.02	0.01	0.18	0.01	< 0.01	Bal.

Table 2.2 pH of the solution used for immersion tests, initial value (pH_{int}), after adjust (pH_{adj}) and after immersion of specimens (pH_{corr}).

Test solutions	pH_{int}	pH_{adj}	pH_{corr}
Na_{sol}	5.8	5.8	6.3
Mg_{sol}	5.8	5.8	6.5
Zn_{sol}	5.8	5.8	6.5
Al_{sol}	4.2	5.7	6.5
Zr_{sol}	3.8	5.8	6.5

Table 2.3 The simulated values of CPE parameters of mild steel after immersion in the solutions for 1 h.

Solutions	R_{sol} ($k\Omega cm^2$)	R_{ct} ($k\Omega cm^2$)	Q ($\mu s^n \Omega^{-1} cm^{-2}$)	n
Na_{sol}	0.45	5.83	10.00	0.77
Mg_{sol}	0.43	8.81	4.93	0.77
Zn_{sol}	0.43	25.00	2.04	0.74
Al_{sol}	0.44	9.88	6.60	0.83
Zr_{sol}	0.46	11.73	8.20	0.82

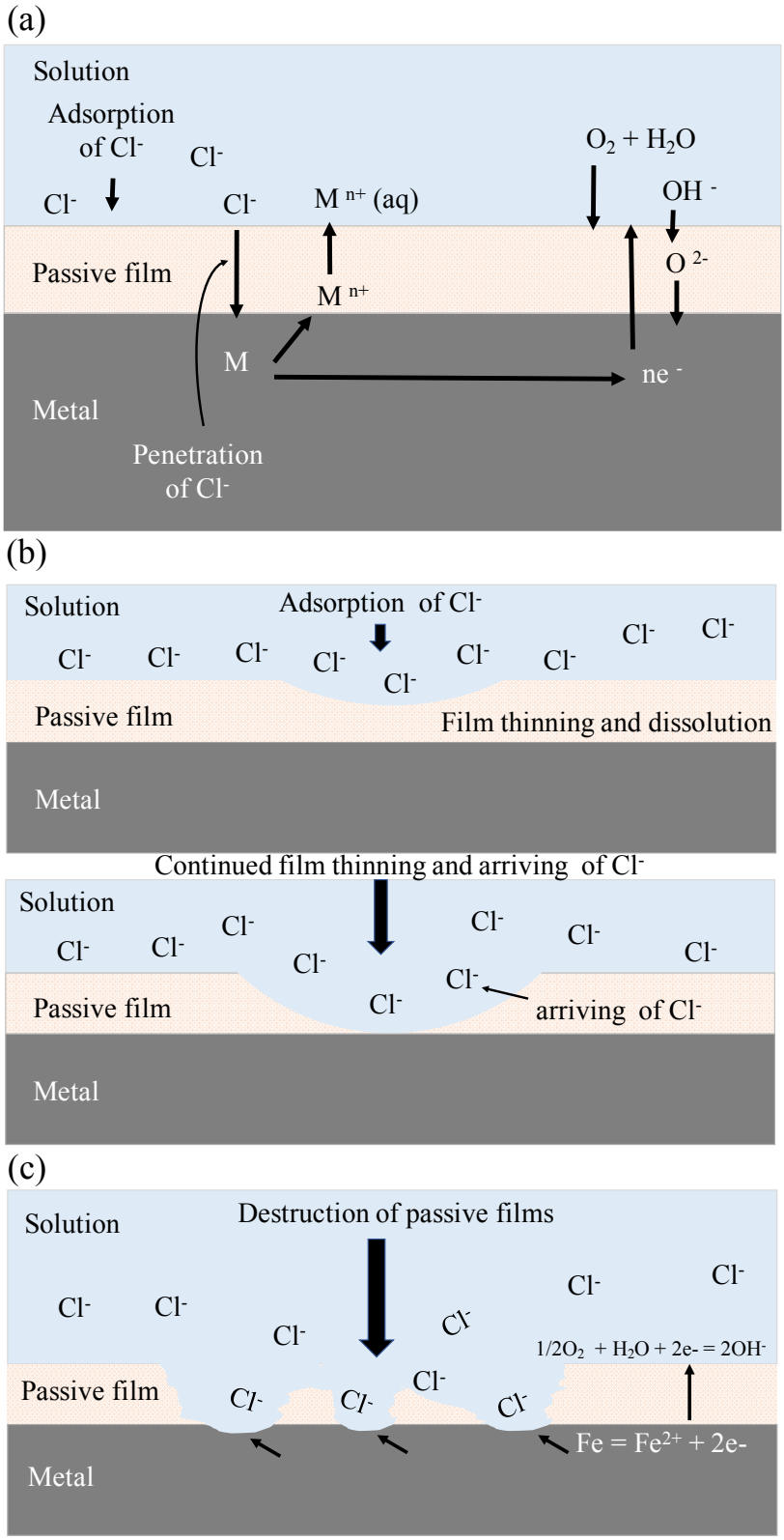

Fig. 2.1 Schematic representation of adsorption of Cl^- on the metal surface by (a) penetration, (b) film thinning, and (c) dissolution with electrochemical reactions on mild steel surface in 10 mM Cl^- aqueous solution.

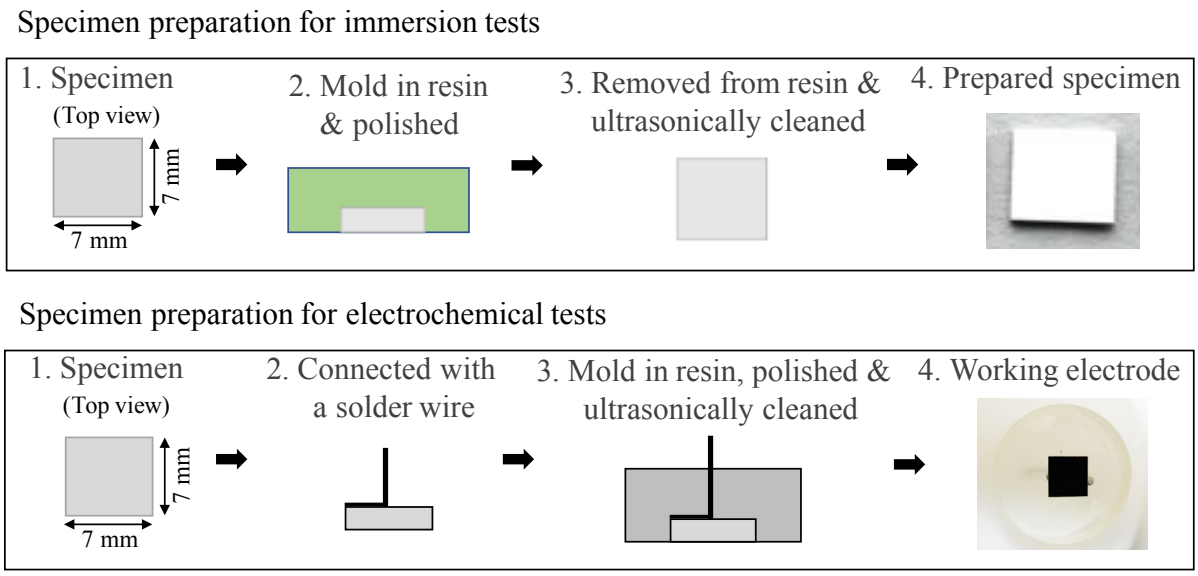

Fig. 2.2 Schematic images of methods used to prepare the specimens for immersion tests and electrochemical tests.

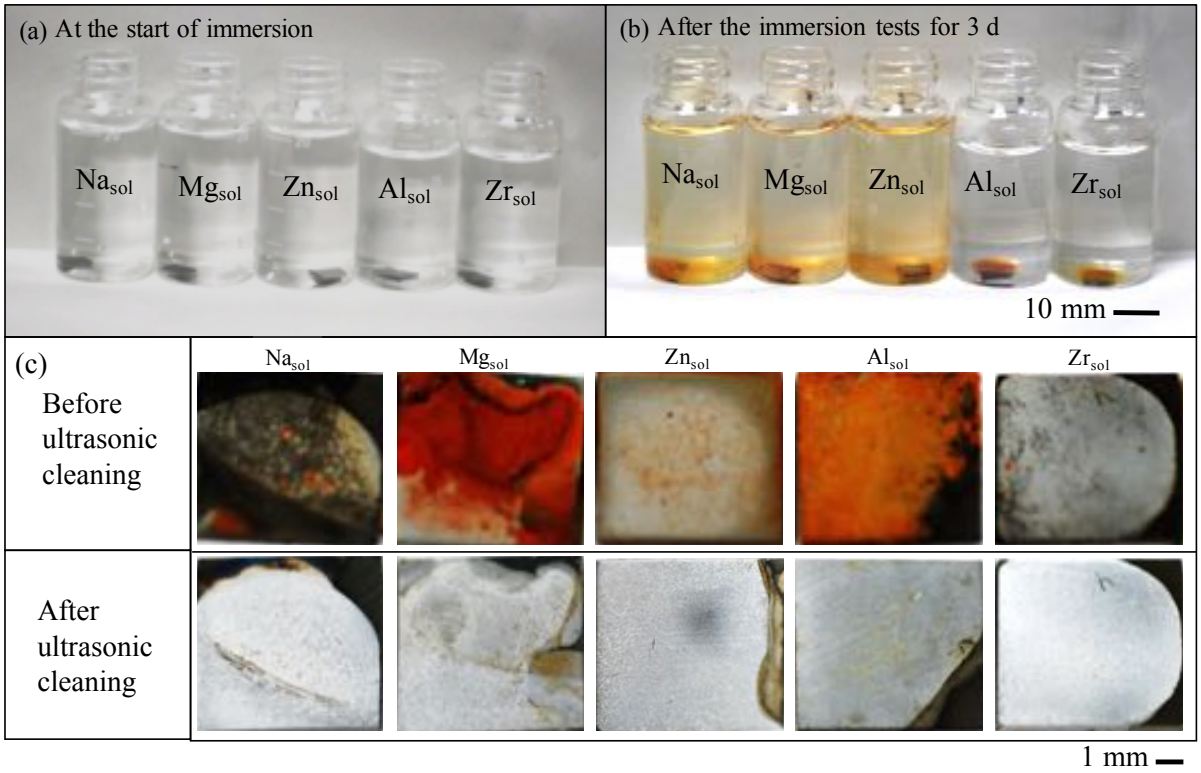

Fig. 2.3 Appearance of specimens after immersion in the solutions of metal cation (a) at the start of immersion, (b) after the immersion tests for 3 d, and (c) surface images of specimens after immersion in the solutions for 3 d (before and after ultrasonic cleaning).

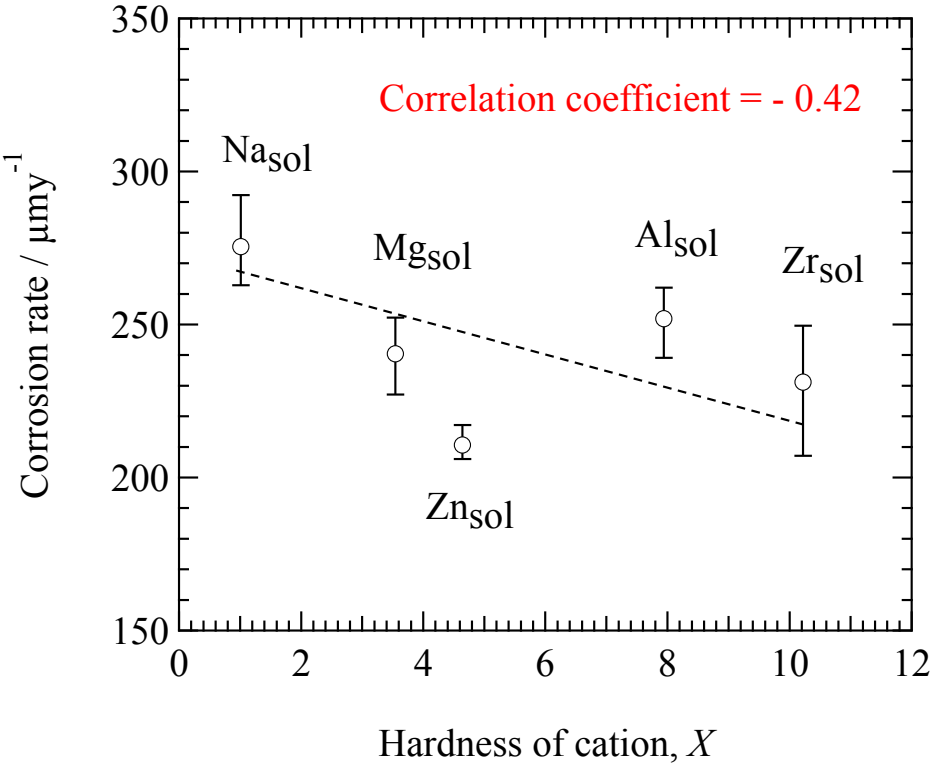

Fig. 2.4 Corrosion rate as a function of hardness of metal cation, X.

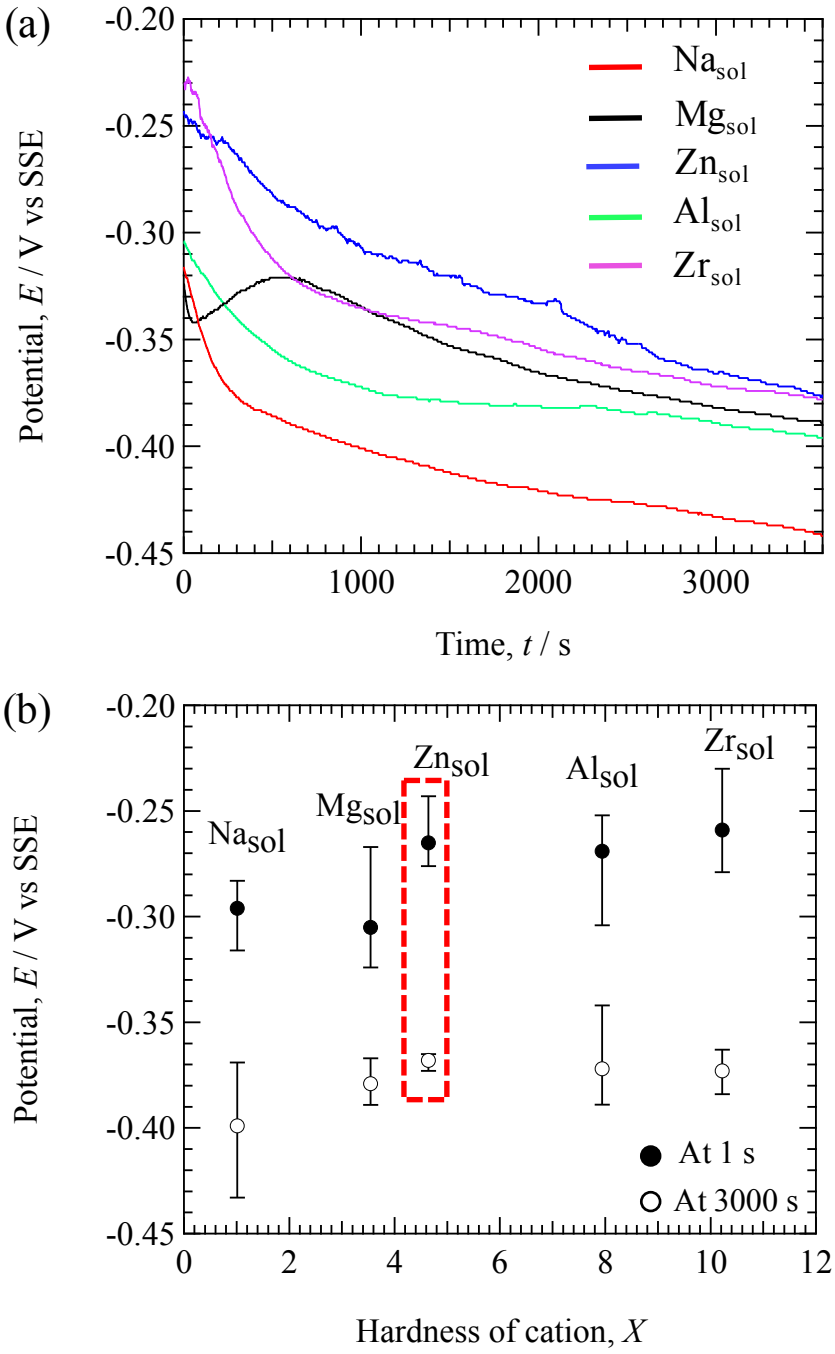

Fig. 2.5 (a) Open-circuit potential during the immersion tests in different solutions and (b) open-circuit potential of specimen during immersion at 1 s and at 3000 s.

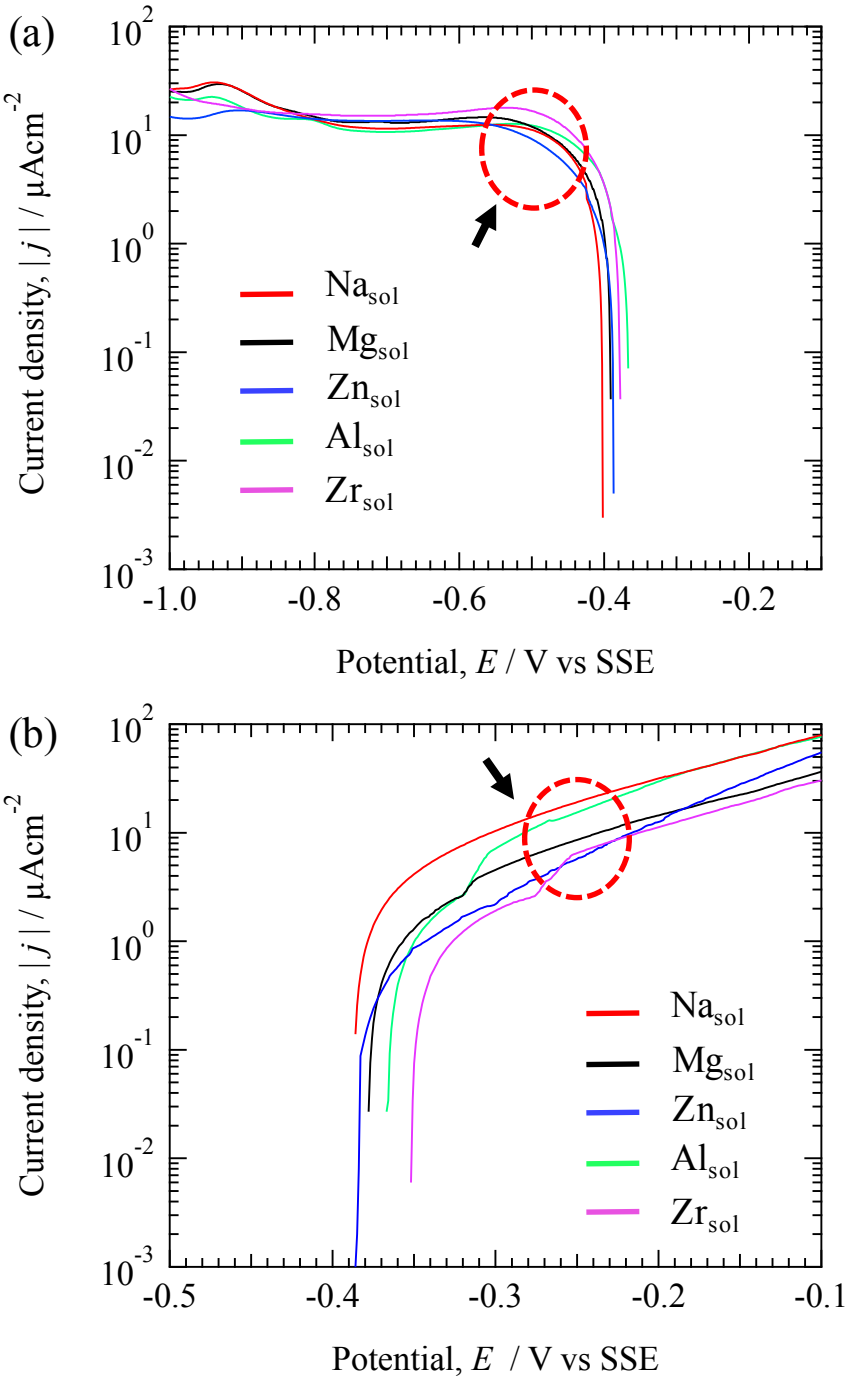

Fig. 2.6 (a) Cathodic and (b) anodic polarization curves of specimen immersed in the different solutions with metal cations.

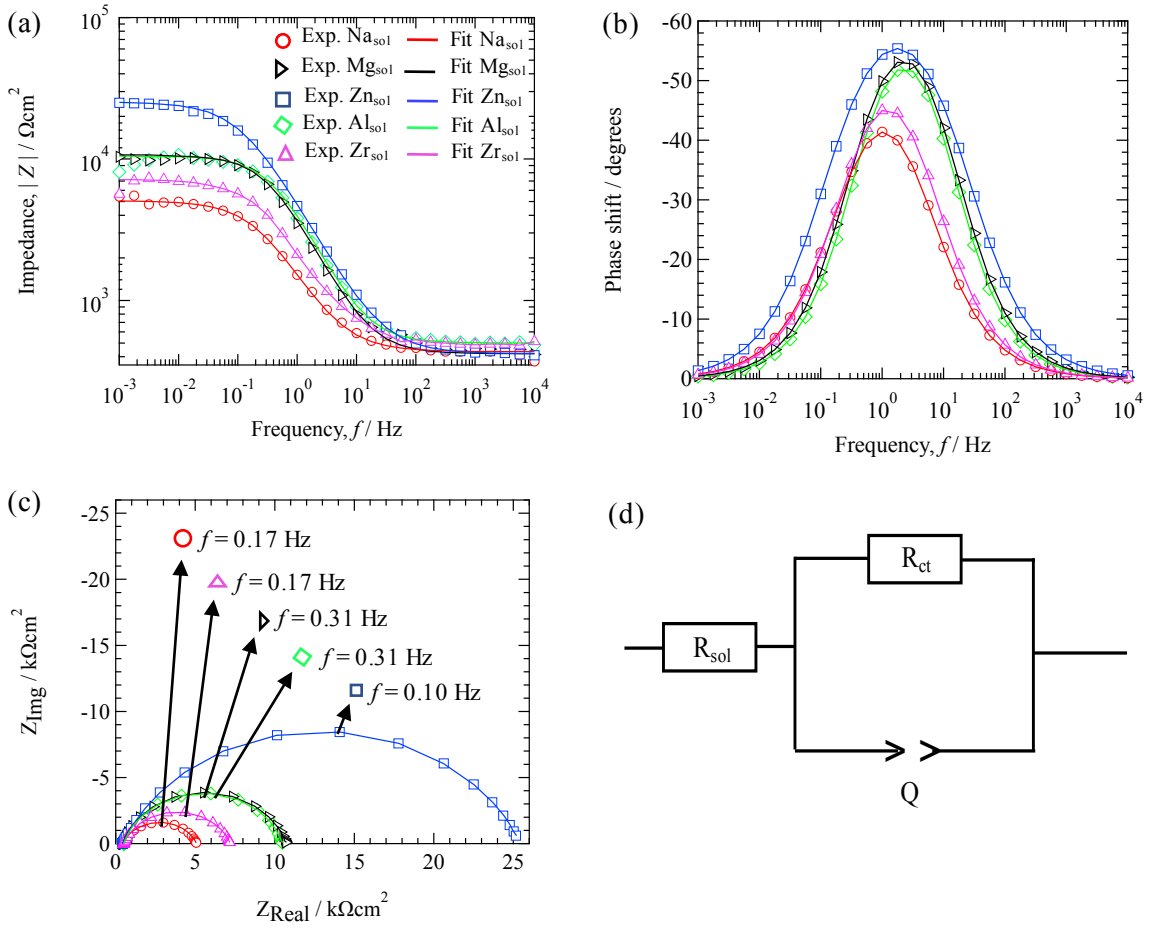

Fig. 2.7 Results of EIS after immersion for 1 h in the solutions with metal cations, Bode diagram of (a) Impedance and (b) phase shift plots, (c) Nyquist plots, and (d) equivalent circuit model used to fit the EIS data.

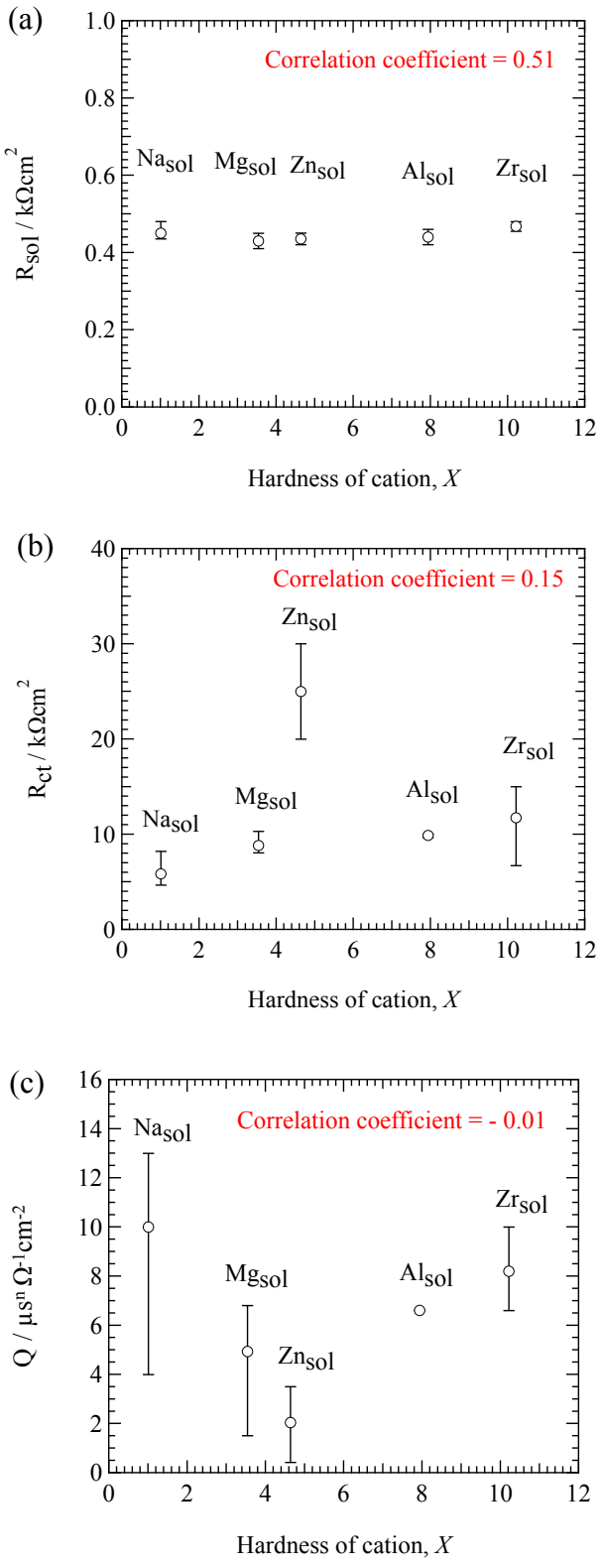

Fig. 2.8 Changes of (a) R_{sol}, (b) R_{ct} and (c) Q with X (hardness of metal cation).

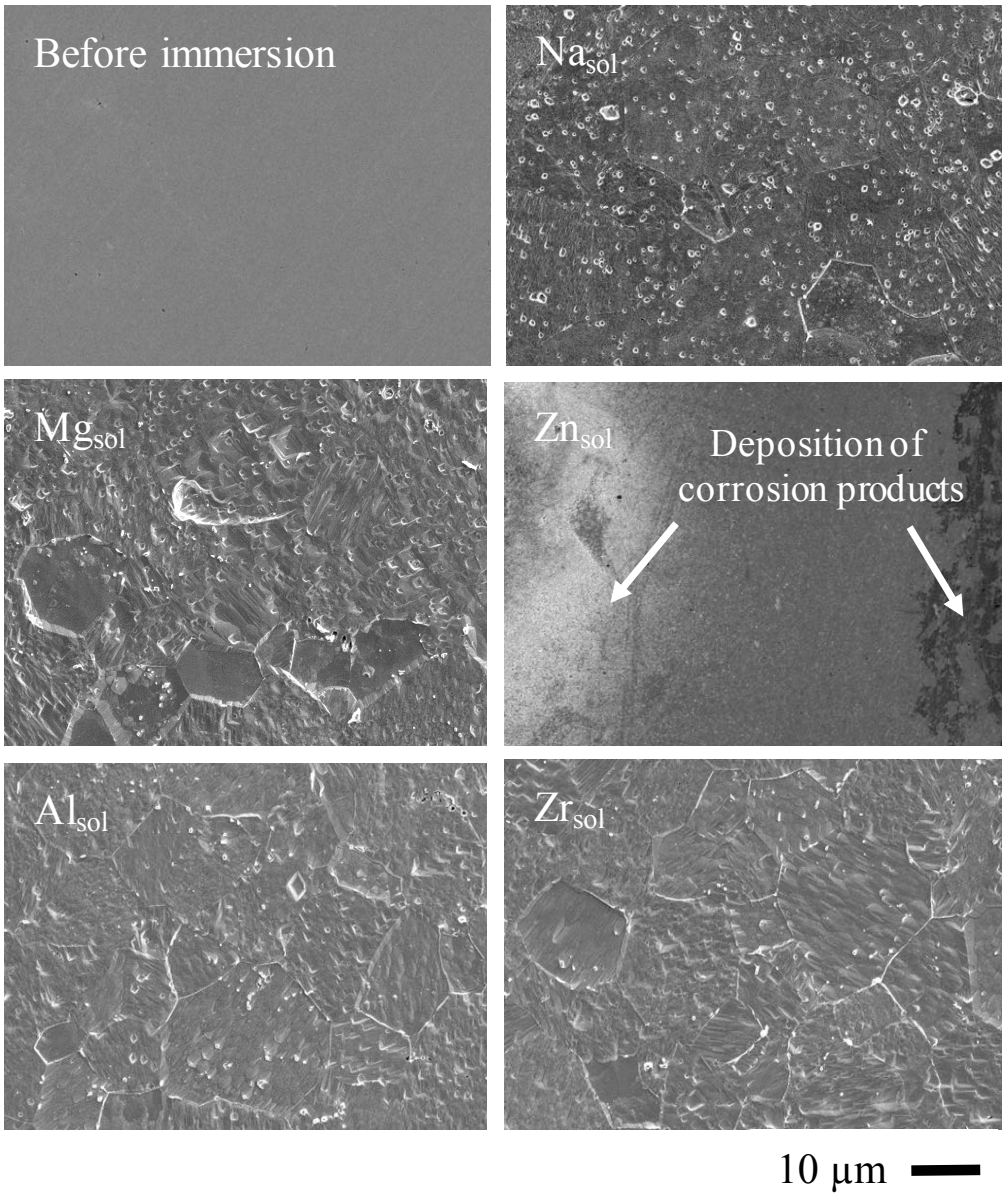

Fig. 2.9 Surface SEM images of specimen after immersion in the solutions for 3 d at 25°C.

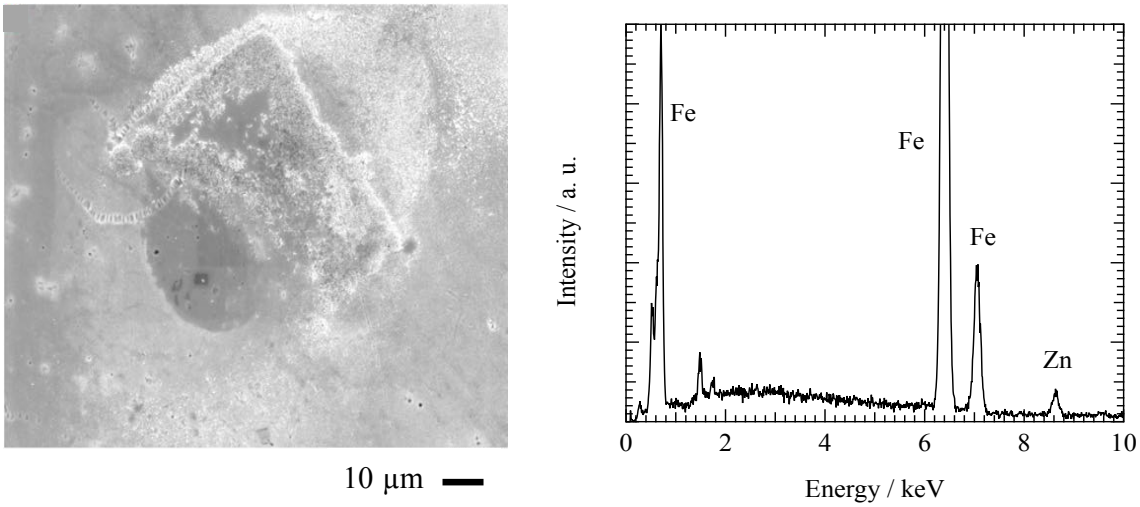

Fig. 2.10 SEM image of analysis area (left) and EDS results (right) of the specimen surface after immersion in the Zn_{sol}.

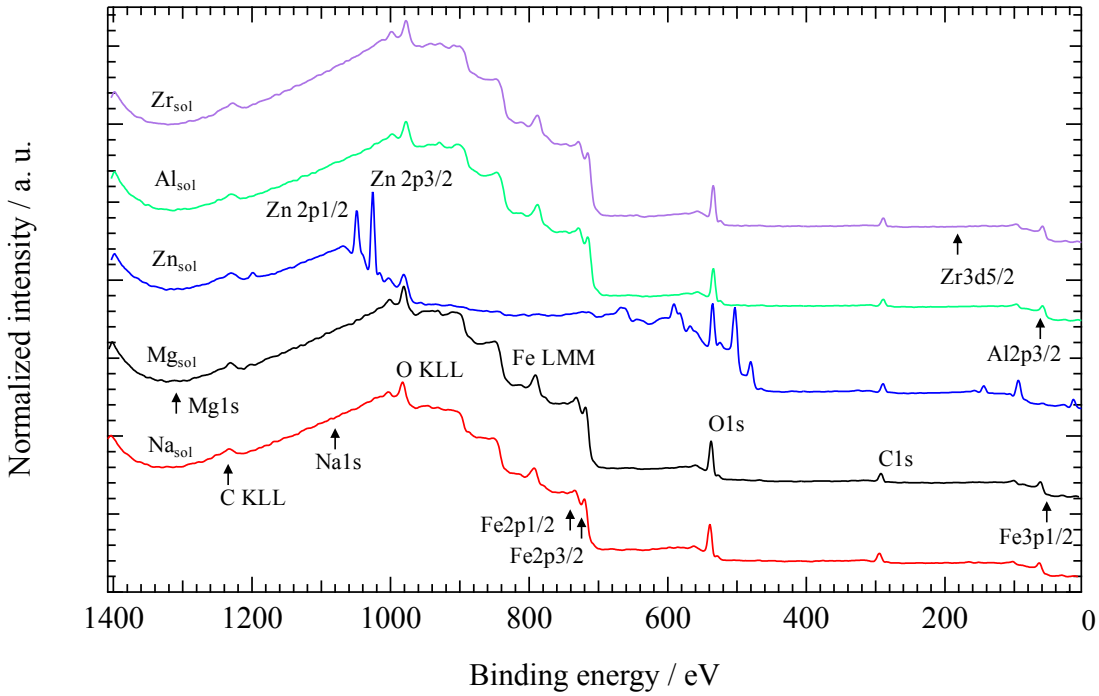

Fig. 2.11 XPS wide spectra of mild steel surface after immersion in the solutions with metal cations.

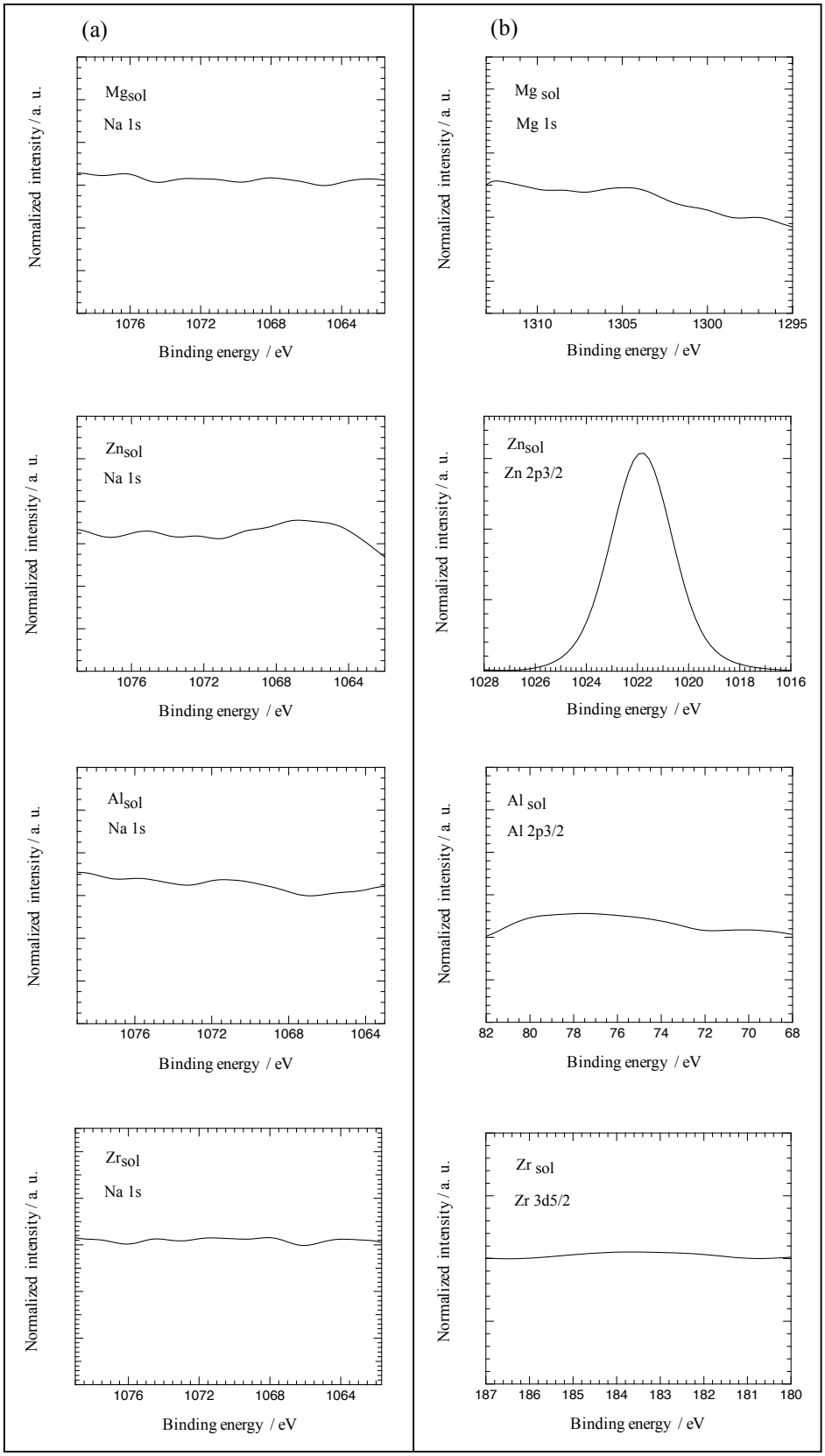

Fig. 2.12 XPS narrow spectra of (a) Na 1s, and (b) Mg 1s, Zn 2p3/2, Al 2p3/2 and Zr 3d5/2 after immersion in the solutions of metal cations.

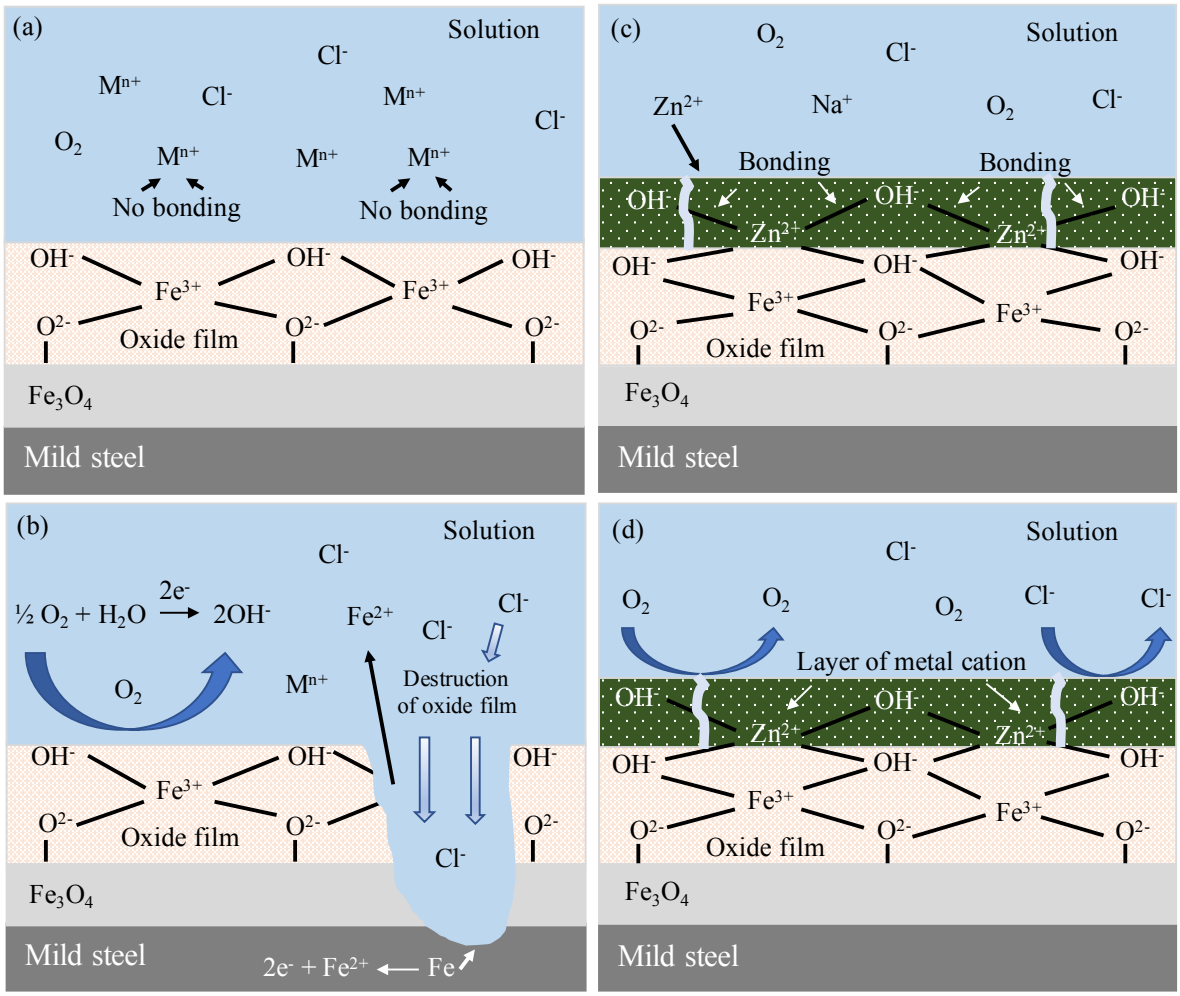

Fig. 2.13 (a) and (b) possible corrosion mechanism of metal cations (M^{n+} = Na^{+}, Mg^{2+}, Al^{3+}, and Zr^{4+}) with the passive film of mild steel in 10 mM Cl^{-} aqueous solution, (c) and (d) possible corrosion inhibition mechanism of Zn^{2+} with the passive film of mild steel in 10 mM Cl^{-} aqueous solution.

References

1. R. E. Melchers, Corros. Sci., 48 (2006) 4174-4201.
2. G. S. Vasyliev, Corros. Sci., 98 (2015) 33-39.
3. C. P. Gardiner and R. E. Melchers, Corros. Sci., 44 (2002) 2665-2673.
4. R. T. Foley, Corrosion, 26 (1970) 58-70.
5. H. Fang, B. Brown and S. Nesic, Corrosion, 67 (2011) 1-12.
6. T. Haruna, K. Domoto and T. Shibata, Japan Soc. Corros. Eng., 51 (2002) 350-355.
7. G. C. White, Current chlorination and dechlorination practices in the treatment of potable water, wastewater and cooling water. In: Jolley RL, ed. Water chlorination: environmental impact and health effects. Ann Arbor, MI, Ann Arbor Sci., 1 (1978) 1-18.
8. G. R. Dychdala, Chlorine and chlorine compounds. In: Black SS, ed. Disinfection, sterilization and preservation, 2nd edi. Philadelphia, PA, Lea and Febiger, (1977) 167-195.
9. Guidelines for drinking water quality, second edition. Health criteria and other supporting information. World Health Organization, Geneva (1996).
10. H. J. Engell and N. D. Stolica, Arch. Eisenhuttenw, 30 (1959) 239-248.
11. L. A. Krebs, J. Kruger, M. B. Ives, J. L. Luo, and J. R. Rodda, The Electrochemical Society, Pennington, NJ (2001) 561-562.
12. D. D. Macdonald, J. Electrochem. Soc., 139, (1992) 3434-3449.
13. E. McCafferty, Introduction to corrosion science, Springer (2010) 283-286.
14. H. J. Engell, Electrochim. Acta, 22 (1977) 987-993.
15. K. G. Weil and D. Menzel, J. Electrochem. Soc., 63 (1959) 669-673.
16. S. Miyake, Sci. Papers Inst. Phys. Chem. Res., 36 (1939) 363-370.
17. E. McCafferty, Corros. Sci., 45 (2003) 1421-1438.
18. K. Otani, M. Sakairi, Corros. Sci., 111 (2016) 302-312.
19. K. Otani, M. S. Islam and M. Sakairi, J. Electrochem. Soci., 164 (2017) C498-C504.
20. M. Kato, Boshoku Gijutsu, 31 (1982) 27-33.
21. S. Takasaki, Zairyo-to-Kankyo, 64 (2015) 114-120.
22. M. Mahdavian and R. Naderi, Corros. Sci., 53 (2011) 1194-1200.
23. R. A. Prabhu, T. V. Venkatesha and B. M. Praveen, International scholarly research network, ISRN Metallurgy, (2012) 1-7.
24. J. Xu, L. Jiang, W. Wang, L. Tang and L. Cui, Water Sci. and Eng., 6 (2013) 354-363.
25. G. N. Lewis, Valence and the structure of atoms and molecules, The Chemical Catalog Co., New York (1923).
26. R. G. Pearson, Hard and soft acids and bases, J. Am. Chem. Soc., 85 (1963) 3533-3539.

27. K. Otani, M. Sakairi, R. Sasaki, A. Kaneko, Y. Seki, J. Solid State Electrochem., 18 (2014) 325-332.
28. M. Misono, E. Ochiai, Y. Saito, Y. Yoneda, J. Inorg. Nucl. Chem., 29 (1967) 2658-2691.
29. S. Zhang, T. Shibata, T. Haruna, Corros. Sci., 47 (2005) 1049-1061.
30. K. F. Ankinpelumi, Investigation the effect of pH level on corrosion rate, University of Lagos, Lagos (2012).
31. I. A. Ammar and S. Riad, J. Phys. Chem., 62 (1958) 150-154.
32. The chemical society of Japan, Handbook of chemistry basic, 2nd ed., Maruzen, Tokyo, 2004 (Japanese).
33. J. Han, B. N. Brown, D. Young and S. Nesic, J. Appl. Electrochem., 40 (2010) 683-690.
34. I. Martinez, C. Andrade, Corros. Sci., 50 (2008) 2948-2958.
35. A. Popova, M. Christov, A. Vasilev, Corros. Sci., 49 (2007) 3290-3302.
36. D. A. Lopez, S.N. Simison and S.R. de Sanchez, Corros. Sci., 47 (2005) 735-755.
37. B. Hirschorn, M. E. Orazem, B. Tribollet, V. Vivier, I. Frateur and M. Musiani, Electrochim. Acta, 55 (2010) 6218-6227.
38. M. E. Orazem, I. Frateur, B. Tribollet, V. Vivier, S. Marcelin, J. Electrochem. Soci., 160 (2013) C215-C225.
39. P. C. Torres, T. J. Mesquita and R. P. Nogueira, J. Phys. Chem. 119 (2015) 4136-4147.
40. G. J. Brug, A. L. G. Van Den Eeden, M. S. Rehbach and J. H. Sluyters, J. Electroanal Chem., 176 (1984) 275-295.
41. I. Iitaka, S. Miyake, T. Iimori, Nature, 139 (1937) 156.
42. M. Cohen, J. Phys. Chem., 56 (1952) 451-453.
43. E. McCafferty and J. P. Wightman, Surf. Inter. Anal., 26 (1998) 549–564.
44. A. Valeria and M. A. Christopher Brett, Electrochim. Acta, 47 (2002) 2081-2091.
45. M. Pourbaix, Atlas of electrochemical equilibria in aqueous solutions, National Association of Corrosion Engineers, Huston, Texas (1974).
46. A. Y. Chatalov, Dokl. Akad. Naouk S. S. S. R., 86 (1952) 7-775.
47. E. Tada and H. Kaneko, ISIJ Int., 51 (2011) 1882-1889.
48. O. T. De Rincon, O. Perez, E. Paredes, Y. Caldera, C. Urdaneta and I. Sandoval, Cement and Concrete Composites, 24 (2002) 79-87.

Chapter 2 has been oriented from the following article

[Md. S. Islam, K. Otani and M. Sakairi, Effects of metal cations on mild steel corrosion in 10 mM Cl^- aqueous solution, *Corros. Sci.*, 131 (2018) 17-27.]

Chapter 3

Metal cation effects on corrosion of SUS304 in Cl^- aqueous solutions

3.1 Introduction

SUS304 is very popular and widely used in applications requiring high corrosion resistance. However, corrosion of stainless steel is a serious problem in liquid supply pipes, liquid storage tanks, ships and many other constructions. Corrosion of stainless steel has been investigated by many researchers [1-11]. The corrosion resistance property of stainless steel mostly depends on the stability of the passive films. In the corrosive environments, the re-passivation properties of the passive films provide the key to the high corrosion resistance of stainless steels [12, 13]. Corrosion of stainless steel depends on the various environmental factors. One of the important factors is the presence of anions (Cl^- and SO_4^{2-}) in the aqueous solution. Cl^- plays a major role in corrosion of steel because the passive films are easily destroyed by this anion [14-18]. Corrosion reactions are initiated on the steel surface while the passive films are destroyed by Cl^- in the aqueous solution [14-20]. The passive films stability is decreased with increasing the Cl^- concentration in the aqueous solution. In other words, corrosion of steel is highly correlated with the Cl^- concentration [21-27]. There are reports that metal cations can change the corrosion behavior of steel in aqueous solution [21-29]. Islam et al. [21] studied the inhibiting effects of metal cations on mild steel corrosion in Cl^- containing an aqueous solution. Otani et al. [22, 23] investigated the effects of metal cations on steel corrosion in fresh water and they found that metal cations have an ability to make a layer on the passive films and protect the film from Cl^- attack in the solution. Zhang et al. [24] studied the inhibiting effect of metal cations and reported that some metal cations (Mn^{2+}, Ni^{2+}, and Zn^{2+}) effectively inhibit the intergranular stress corrosion cracking of sensitized type 304 stainless steel in SO_4^{2-} (10^{-5} kmol/m^3) containing an aqueous solution. They also clarified the effects of metal cations with hardness, *X*, which is based on the hard and soft acid and base (HSAB) concept. Khedr et al. [25] studied the role of metal cations in the corrosion and corrosion inhibition of aluminum in aqueous solutions of SO_4^{2-} and NO_3^-. O'dell et al. [28] reported that some metal cations exhibit inhibiting effects to the intergranular stress corrosion cracking of sensitized type 304 stainless steel in Cl^- containing an aqueous solution. Drazic et al. [29] reported that Cd^{2+}, Mn^{2+}, and Zn^{2+} inhibit the corrosion of iron in sulphuric acid solutions. Gatos [30] investigated the effects of metal cations on the corrosion of iron in acids. In some nuclear power reactors, metal cations are added into high temperature water for suppressing corrosion of the reactor component

materials and avoiding the accumulation of radioactive metal element [24, 31]. Therefore, it has been confirmed that metal cations affect the corrosion of stainless steel in aqueous solution [24, 32]. However, the effects of metal cations on corrosion of SUS304 in 0.5 M Cl^- aqueous solution remain unknown and the corrosion inhibition mechanism of metal cations with the passive films are not fully elucidated.

In this study, the effects of metal cations on corrosion of SUS304 in 0.5 M Cl^- aqueous solution were investigated by immersion tests and electrochemical tests. Surface analyses were carried out by scanning electron microscope (SEM), atomic force microscope (AFM) and X-ray photoelectron spectroscope (XPS). The corrosion inhibition mechanism of metal cations with the passive films has also been clarified by the hardness of metal cation, *X*, based on the hard and soft acids and bases (HSAB) concept.

3.2 Experimental

3.2.1 Specimens

SUS304 sheets were cut into small pieces (7 × 7 × 1 mm) and were used as specimens. In the case of electrochemical tests, a conductive wire was connected to each specimen to use as a working electrode. All the specimens were molded in epoxy resin (Struers Ltd., Epofix Resin) to carried out different tests [21]. The exposed surface of the molded specimen was grounded with SiC abrasive paper from #1000 to #4000 grit size. For immersion tests, the specimens were taken out from the resin after polished [21]. Before performing the tests, all the specimens were cleaned in ethanol and in highly purified water using an ultrasonic bath.

3.2.2 Solutions

Three 0.5 M Cl^- solutions with different metal cations were used as test solutions; 0.1 mM $MgCl_2$ (Mg_{sol}), 0.1 mM $ZnCl_2$ (Zn_{sol}), and 0.1 mM $AlCl_3$ (Al_{sol}) and their Cl^- concentration was adjusted to 0.5 M by NaCl. In this experiment, 0.5 M NaCl (Na_{sol}) was used as a reference solution. Water used in this study was highly purified; distilled two times and further purified by water purifier (MILLIPORE, Simplicity UV). All chemicals used in this study were special analytical grade and obtained from Kanto Chemical Co. Ltd.

Corrosion reactions are mostly depended on the pH of the aqueous solution [33, 34]. It is essential to control the pH of an aqueous solution for a better understanding of the individual effect of metal cations on the corrosion of stainless steel. The pH of used solutions was adjusted between 5.7 and 5.8 by 0.1 M NaOH (Table 3.1) before the tests. The pH of the solutions before

and after immersion tests was measured by the pH meter (Eutech Instruments Pte. Ltd., Cyber-Scan 6000).

3.2.3 Immersion tests

Specimens were immersed in the solutions at 25° C for 56 d (8 weeks). During the immersion tests, the solutions were open to the air. The mass of the specimens was measured using a microbalance (METTLER TOLEDO MX5, Pro FACT) before and after the immersion tests, and the corrosion rates were calculated from the mass change [21].

Before and after the immersion tests, the surfaces of the specimens were observed by a digital camera (Nikon, D80-DSLR) and scanning electron microscope using secondary electrons imaging (SEM, JEOL Ltd., JSL6510-LA). The surface of the immersed specimens was analyzed by X-ray photoelectron spectroscope (XPS, JEOL Ltd., JPS-9200) using a monochrome Al Kα X-ray source (1486.6 eV). The area of the specimen surface analyzed by the XPS was 3 × 3 mm. The surface roughness was measured by atomic force microscope (AFM, SPA 400) using dynamic force mode with the cantilever type, SI-DF40. Before the analysis, the immersed specimens were cleaned ultrasonically first in ethanol and then in highly purified water.

3.2.4 Electrochemical tests

Electrochemical tests were performed in a conventional three-electrode cell using a potentiostat (IVIUM TECHNOLOGIES, Pocketstat). Before the tests, the specimens were immersed in the solutions at 25° C for 7 d. A Pt plate and an Ag/AgCl electrode immersed in a saturated KCl solution (SSE) were used as counter and reference electrodes, respectively. The exposed surface area of the working electrode in the solution was 49 mm^2. The potentiodynamic polarization measurements were carried out from immersion potential to the cathodic and anodic direction with a scan rate of 1 mV/s. The cathodic and anodic scan was started separately to obtain the individual electrochemical properties of stainless steel immersed in the solutions with metal cations. The impedance spectra were measured in a frequency range from 100 kHz to 1 mHz and modulation amplitude of 10 mV. For the EIS curve-fitting, the IVIUM software was used. Reproducible data were obtained in all electrochemical measurements.

3.3 Results

3.3.1 Immersion tests

The appearances of solutions and specimens after immersion at 25°C for 56 d in the test solutions are shown in Fig. 3.1. No significant change is observed in the color of the test solutions (Fig. 3.1 (a)) after the immersion. It is very difficult to identify the surface morphological difference from Fig. 3.1 (b) due to the extent of corrosion is very less and few amounts of corrosion products may have formed.

The corrosion rates were calculated from the mass loss after immersion for 56 d in the different solutions. Fig. 3.2 shows the corrosion rate as a function of *X*, and the corrosion rate is gradually decreasing with increasing the value of *X*. The correlation coefficient is -0.92 indicating that corrosion rate is clearly related with *X*. This result indicates that corrosion inhibition ability of metal cations is increased with increasing *X* in 0.5 M Cl^- aqueous solution.

The corrosion inhibition efficiency (η_i) of metal cations was calculated using Eq. (3.1) which were based on the mass loss due to immersion in the solutions.

$$\eta_i\ (\%) = \frac{Na_{ms} - CAT_{ms}}{Na_{ms}} \times 100 \qquad (3.1)$$

Here Na_{ms} is mass loss of specimen in Na_{sol} and CAT_{ms} is mass loss of specimen in solutions. Fig. 3.3 shows the corrosion inhibition efficiency of metal cations as a function of *X* in which the mean value of mass loss data was used. In this experiment, Na_{sol} was used as a reference solution. Therefore, the corrosion inhibition efficiency of Na^+ was considered as zero. The corrosion inhibition efficiency of Al^{3+} and Zn^{2+} are around 20% and 17% respectively.

The pH of the test solutions before and after the immersion tests at 25°C for 56 d are shown in Table 3.1, pH_{int} is the pH of solutions before immersion tests, pH_{corr} is the pH obtained after the immersion tests. The pH was slightly decreased after immersion (pH_{corr}) in all solutions for 56 d (8 weeks) (Table 3.1). Several researchers also reported that the solution pH decreases with the hydrolysis of Fe^{2+} and Fe^{3+} [35, 36]. Additionally, a proton is released into the solution during deprotonation of the passive films on the stainless steel surface in the presence of metal cations [24] and thus pH of solutions is decreased.

The changes in the surface morphology of the specimen were observed after the immersion tests. Fig. 3.4 shows the surface SEM images of specimens. The SEM images exhibit the huge numbers of pits in Na_{sol} and Mg_{sol}. Many pits depict the severe corrosion occurred on the SUS304 surface. A few small pits are observed in the case of Zn_{sol} and Al_{sol}. However, a comparatively smooth surface is observed in both Zn_{sol} and Al_{sol}. It suggests that specimen

surface may be affected by the metal cations in the case of Zn_{sol} and Al_{sol}. These results correspond well to the mass change of specimen after immersed in the solutions.

3.3.2 Surface analysis

The specimen surfaces were analyzed by XPS after the immersion tests to clarify the effect of metal cations on the surface. Fig. 3.5 shows the XPS wide spectra of the specimen immersed in the solutions. In the case of a specimen immersed in Zn_{sol}, clear peaks of Zn2p3/2 and Zn2p1/2 are observed, and it is indicating the presence of Zn on the specimen surface [23, 37]. In the case of a specimen immersed in Al_{sol}, clear peak of Al2p3/2 is observed indicating the presence of Al on the specimen surface [23, 38]. From Fig. 3.5, there are no peaks of Cl2p3/2 (at 200 eV) observed on the specimens immersed in the solutions meaning that chlorine does not exist on the surface. This result suggests that chlorine was unable to form a chemical bond with the corrosion inhibiting species.

The XPS depth analyses were carried out to clarify the distribution or incorporation of metal cations in passive films. There are no peaks observed of Na1s and Mg1s on the specimen in the wide spectra (Fig. 3.5). However, XPS narrow spectra with depths of Na1s and Mg1s along with Zn2p3/2 and Al2p3/2 were carried out (due to the low resolution of wide spectra) to determine the specific depth locations of each element and chemical state. Fig. 3.6 shows the XPS narrow spectra of Na1s, Mg1s, Zn2p3/2, and Al2p3/2 with depths of specimen surface after the immersion tests. Fig. 3.6 (a) and (b) show the Na1s and Mg1s spectra with depths of the specimen immersed in Na_{sol} and Mg_{sol} respectively. From 0 nm to 16 nm depth, no peaks of both Na1s and Mg1s are observed. These results signify that both Na and Mg did not exist on the surface. Fig. 3.6 (c) shows the Zn2p3/2 spectra with depths of the specimen immersed in Zn_{sol}. Peaks are observed at 1022.6 eV from 0 nm to 6 nm depth which is related to the peak of Zn^{2+} [21, 23]. Fig. 3.6 (d) shows the Al2p3/2 spectra with depths of a specimen immersed in Al_{sol}. Peaks are observed at 74.4 eV from 0 nm to 16 nm depth which is related to the peak of Al^{3+} [23].

Fig. 3.7 shows the narrow spectra with depths of Fe2p3/2, O1s, and Cr2p3/2 of specimen immersed in the Zn_{sol} and Al_{sol}. Fig. 3.7 (a) and (b) show the Fe2p3/2 spectra with depths of the specimen immersed in the Zn_{sol} and Al_{sol} respectively. In both case, peaks are observed at 707.05 eV which are related to the peak of Fe [39]. The peak intensity of Fe is increased with increasing the depth. Very small peaks are appeared at 710.2 eV and at 711.2 eV which are related to the peaks of Fe^{2+} and Fe^{3+} respectively [39]. In both cases, the peak of metallic iron, and the peaks of Fe^{2+} and Fe^{3+} on the surface are negligible. Fig. 3.7 (c) and (d) show the

Cr2p3/2 spectra with depths of specimen immersed in Zn_{sol} and Al_{sol} respectively. Both of the cases, peaks are observed at 574.4 eV from 0 nm to 16 nm depth which is related to the peak of Cr [40]. Peaks are also observed at 576.9 eV from 0 nm to 6 nm depth which is related to the peak of Cr^{3+} [40], and high intensity is noticed from 0 nm to 1 nm depth. Fig. 3.7 (e) and (f) show the O1s spectra with depths of specimen immersed in Zn_{sol} and Al_{sol} respectively. Both of the cases, peaks are observed and it can be separated into two peaks, one peak at 530.6 eV which is related to the peak of O^{2-} [39, 40], and another peak at 531.8 eV which is related to the peak of OH^- [39, 40].

From the XPS results of Fig. 6 and Fig. 3.7, it is demonstrated that both Zn^{2+} and Al^{3+} existed on the surface and the peaks of these cations were related to the peaks of $Zn(OH)_2$ and $Al(OH)_3$ respectively [21, 23, 37, 38]. From the previous report, mild steel in Cl^- aqueous solution [21-23], metal cation made a chemical bond with the passive films and formed a metal cation layer which inhibited the corrosion reactions and protected the dissolution of metal. Therefore, it is expected that Zn^{2+} and Al^{3+} existed on the surface as hydroxides and it further formed a chemical bond with the passive films by a de-hydroxylation process which was led to metal cation layer on the surface of SUS304 in the solution [24]. The metal cation layer would have good protective ability against the Cl^- attack in the solution and inhibits the corrosion reactions of SUS304. XPS quantification data of surface (0 nm) are shown in Table 3.2. The higher atomic percentage of Al2p3/2 (24.17) is observed than the atomic percentage of Zn2p3/2 (14.96). These results suggest that Al^{3+} was distributed more than Zn^{2+} on the surface layer, and consequently the specimen immersed in the Al_{sol} showed lower corrosion rate than the specimen immersed in the Zn_{sol} (as shown in Fig. 3.2).

The surface roughness was measured by an atomic force microscope and the recorded 3D images of surface topography are shown in Fig. 3.8. These images show the distinctive rough surface of the specimen immersed in the solutions with a metal cation. Comparatively, smooth surface is observed of a specimen immersed in the Al_{sol}. To quantify the surface roughness, mean roughness factor (R_a) [41, 42] was determined from the respective images. The calculated R_a values are shown in Table 3.3. The roughness of the specimen surface was increased due to immersion in the solutions. However, the roughness of specimen immersed in the Al_{sol} shows the lowest value than other solutions indicating the metal cation layer formation on the specimen surface. These results correspond well to the surface morphological change observed by SEM.

3.3.3 Electrochemical tests

The open circuit potentials of SUS304 were measured in solutions and are shown in Fig. 3.9. All the measured values are confined between -0.15 V and -0.25 V. Only slight difference is observed in the case of Mg_{sol}, Zn_{sol}, and Al_{sol} as compared to the Na_{sol}. However, after 3000 s, Na_{sol} induces the most negative open circuit potential.

Fig. 3.10 shows the cathodic and anodic polarization curves. From the cathodic polarization curves, it is found that Zn_{sol} and Al_{sol} show lower current density (indicated by an arrow in Fig. 3.10) and slightly acts as a cathodic inhibitor as compared to the Na_{sol} and Mg_{sol}. In the anodic polarization curves, the current density is increasing with increasing the potential in all the solutions. At a certain higher potential, the current density is increased suddenly and that potential is mentioned as pitting potential. Na_{sol} shows the lowest pitting potential as compared to the other solutions, and Zn_{sol} and Al_{sol} show lower current density (indicated by an arrow in Fig. 3.10) as compared to the Na_{sol} and Mg_{sol}. These results suggest that both Zn_{sol} and Al_{sol} act as a cathodic and anodic inhibitor.

EIS measurements were carried out to clarify the initial corrosion behavior of the SUS304 and the effect of metal cations on the properties of the passive film. Fig. 3.11 (a) shows the impedance plots and Fig. 3.11 (b) shows the phase shift plots (Bode diagram) of the specimen in different solutions with metal cations. The impedance and phase shift shows different magnitude in each solution with metal cations. The fitted lines are calculated by Randle's equivalent circuit model (Fig. 3.11 (c)) [43-45]. All the experimental spectra can be well described by this equivalent circuit. The equivalent circuit model consists of solution resistance (R_{sol}), charge-transfer resistance (R_{ct}), and constant phase element (CPE), Q. The calculated [46-49] mean values of electrochemical impedance parameters are listed in Table 3.4. Q represents the structure of the solution/metal interface and the area of defects in the protective film on the surface [22, 50]. Otani et. al [22] reported that the decrease in Q value indicates that Zn^{2+} can decrease the defect in the protective film on mild steel. From Table 3.4, the lower value of Q is observed in Zn_{sol} and Al_{sol} as compared to the Na_{sol} and Mg_{sol}. Therefore, it is expected that the specimen immersed in Zn_{sol} and Al_{sol} have relatively perfect film as compared to the film formed on the specimen immersed in the Na_{sol} and Mg_{sol}.

The magnitude of impedance at low frequencies in the Bode diagram implies the corrosion resistance of the SUS304 in the solution. Zn_{sol} and Al_{sol} show the larger magnitude of impedance at a lower frequency (Fig. 3.11 (a)) as compared to the Mg_{sol} and Na_{sol}. Larger phase shift also observed at a lower frequency for both Zn_{sol} and Al_{sol} as compared to the Mg_{sol} and Na_{sol} (Fig. 3.11 (b)). These results suggest that both Zn^{2+} and Al^{3+} have the corrosion inhibitory

effect on SUS304 in 0.5 M Cl^- aqueous solution. The results obtained from the electrochemical tests are in good agreement with the results from the immersion tests and surface analysis.
The values of R_{ct} as a function of *X* are shown in Fig. 3.12 (a). The R_{ct} increases with increasing the value of *X*, and the correlation coefficient is 0.92, signifying that R_{ct} is closely related to *X*. High R_{ct} indicates that the charge transfer rate is low and the steel has high corrosion resistance in the solution. It signifies that Zn_{sol} and Al_{sol} expose higher corrosion resistance than Na_{sol} and Mg_{sol}. Fig. 3.12 (b) shows the changing of R_{ct} with mass loss of specimen immersed in the solutions in which mean values of both parameters have been used. Al_{sol} shows the highest R_{ct} than other solutions, and Al_{sol} has the lowest mass loss than other solutions with metal cation. This result indicates that the solutions with a metal cations which have large *X*, exhibit higher R_{ct} and consequently implies the lower mass loss in the solution. The correlation coefficient is -0.98 indicating that R_{ct} and mass loss are closely related to each other.

3.4 Discussions

The present results shown in the above sections indicate that the harder metal cations played an important role in suppressing the corrosion initiation process by forming a layer on the passive films. It is expected that both zinc and aluminum may form a chemical bond with the passive films by de-hydroxylation process [24]. The formation of hydroxides and de-hydroxylation process are depended on the metal cation hardness, *X* [23]. Metal cations with large *X* are able to form a layer on the steel surface. The mechanism of which the metal cations with large *X* form a layer on the surface and suppress the corrosion reactions will be discussed below based on the model of the passive film proposed by Okamoto and Shibata [51-53] and the HSAB concept [27, 54, 55] (Fig. 3.13).
Okamoto and Shibata proposed the following passive film model for stainless steels [51-53]. The passive films of stainless steel contain a huge amount of bound water which are connected with the metal atoms and oxygen atoms. The atoms are arranged in passive films like a bridge on the steel surface (Fig. 3.13 (a)). When the passive films on the stainless steel surface are ruptured by Cl^-, the re-passivation process takes place immediately [56-58].
According to the HSAB concept, metal cations with large *X* incorporate in the passive films and attract the electron pair of the oxygen atom in H_2O or OH^- in the passive films, and finally stimulates the deprotonation process (Fig. 3.13 (b)). It is considered that the protons are replaced with the hard metal cations and form a metal cation layer on the passive films (Fig. 3.13 (c)). The layer of metal cation protects the passive films from Cl^- attack and inhibits the corrosion reactions of stainless steel. On the other hand, metal cations with small *X*, do not

have the ability to make a layer with the passive films, and thus Cl^- can arrive on the metal surface by destroying the passive films and initiate the metal dissolution reactions.

3.5 Conclusion

- The corrosion behavior of the stainless steel in the 0.5 M Cl^- aqueous solution was changed with *X*, and corrosion rates were closely correlated with *X*.
- SEM surface images showed some pits on the specimen immersed in the Na_{sol}, Mg_{sol}, and Zn_{sol}, whereas, the number of pit was different. Comparatively, smooth surface was observed on the specimen immersed in the Al_{sol}.
- Zn_{sol} and Al_{sol} showed higher impedance and higher charge transfer resistance as compared to Na_{sol} and Mg_{sol}.
- From the XPS results, Zn^{2+} and Al^{3+} were existed on the steel surface as hydroxides and formed a layer by incorporating in the passive films through the de-hydroxylation process.
- The layer of metal cation would have good protecting ability against Cl^- attack as well as corrosion reactions on the steel surface.

Table 3.1 pH of the solutions used for immersion tests, initial value (pH_{int}), after immersion of specimens (pH_{corr}).

Test solutions	pH_{int}	pH_{corr}
Na_{sol}	5.8	4.3
Mg_{sol}	5.7	4.2
Zn_{sol}	5.7	4.3
Al_{sol}	5.7	4.5

Table 3.2 XPS quantification data of specimen immersed in the solutions (atomic %)

Specimen immersed in solution	Fe2p3/2	O1s	Cr2p3/2	Zn2p3/2	Al2p3/2
Zn_{sol}	16.35	24.67	12.11	14.96	-
Al_{sol}	15.05	22.10	10.31	-	24.17

Table 3.3 AFM surface roughness data of SUS304 immersed in the solutions with metal cation at 25°C for 56 d.

Solutions	Average surface roughness, R_a (nm)	
	Before immersion	After immersion
Na_{sol}	4.67	27.71
Mg_{sol}	4.62	13.69
Zn_{sol}	4.65	8.25
Al_{sol}	4.60	7.14

Table 3.4 The simulated mean values of electrochemical impedance parameters of SUS304 after immersion in the solutions for 7 d.

Solutions	R_{sol} (Ωcm^2)	R_{ct} ($M\Omega cm^2$)	Q ($\mu s^n \Omega^{-1} cm^{-2}$)	n
Na_{sol}	15.57	0.97	12.55	0.89
Mg_{sol}	15.28	1.18	9.05	0.91
Zn_{sol}	15.77	2.51	3.95	0.86
Al_{sol}	15.84	3.21	8.51	0.87

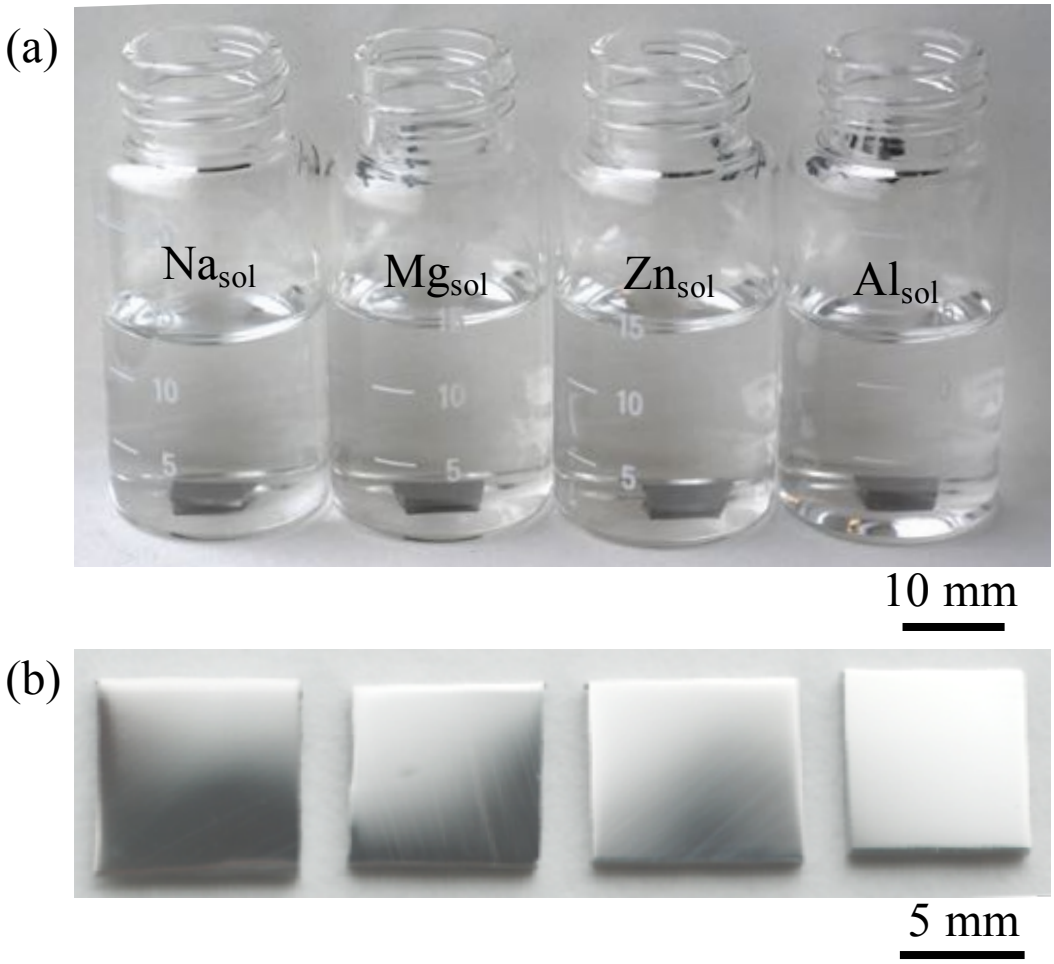

Fig. 3.1 Appearance of (a) solutions and (b) specimens after immersed in the solutions at 25°C for 56 d.

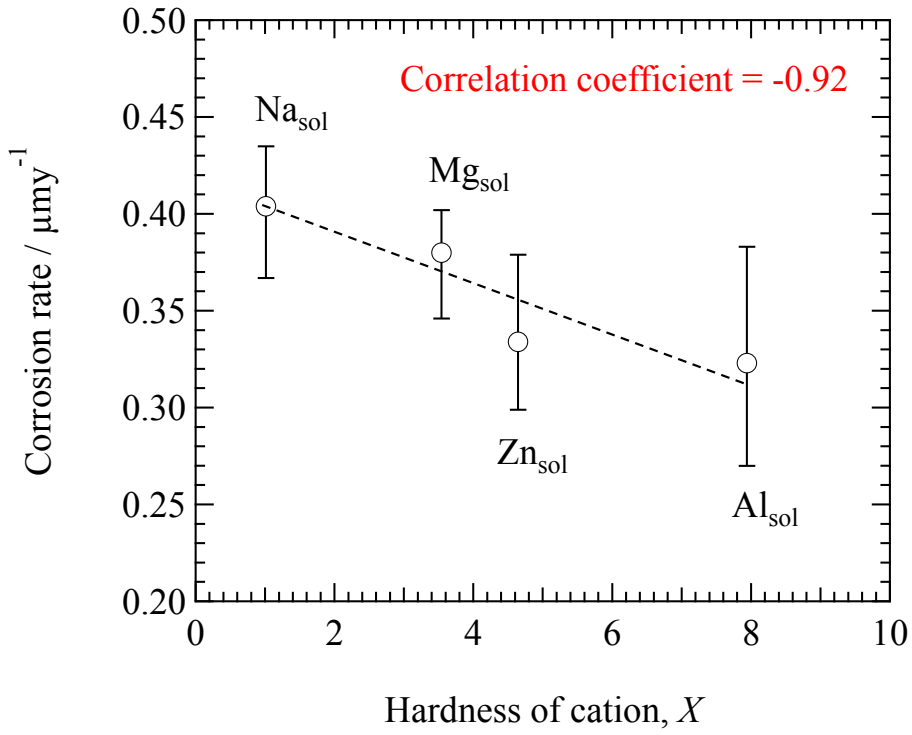

Fig. 3.2 Corrosion rate as a function of *X*.

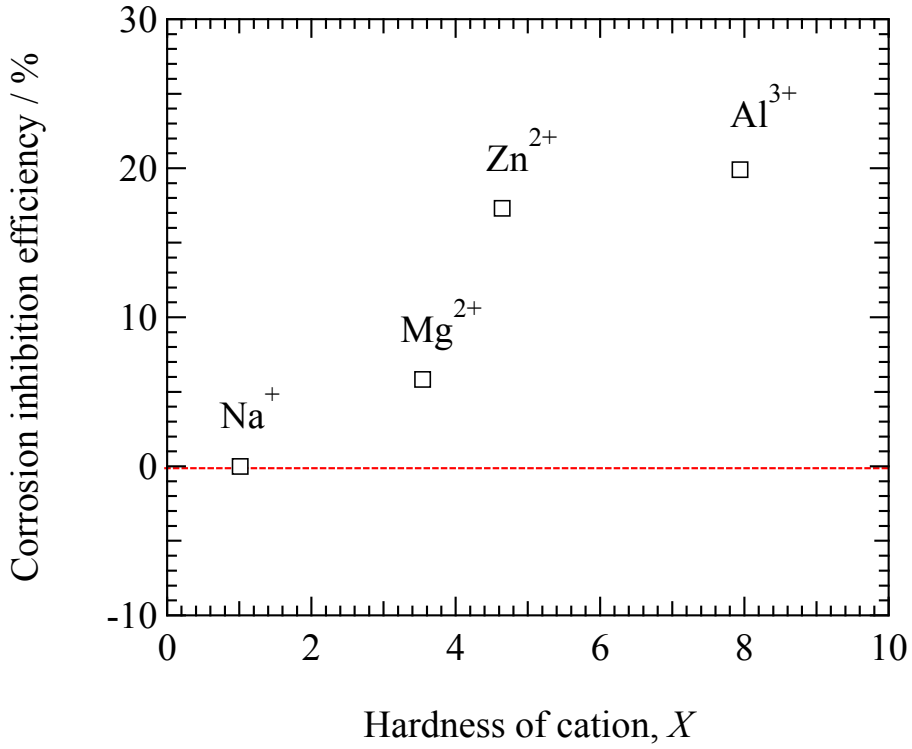

Fig. 3.3 Corrosion inhibition efficiency of metal cations as a function of *X*.

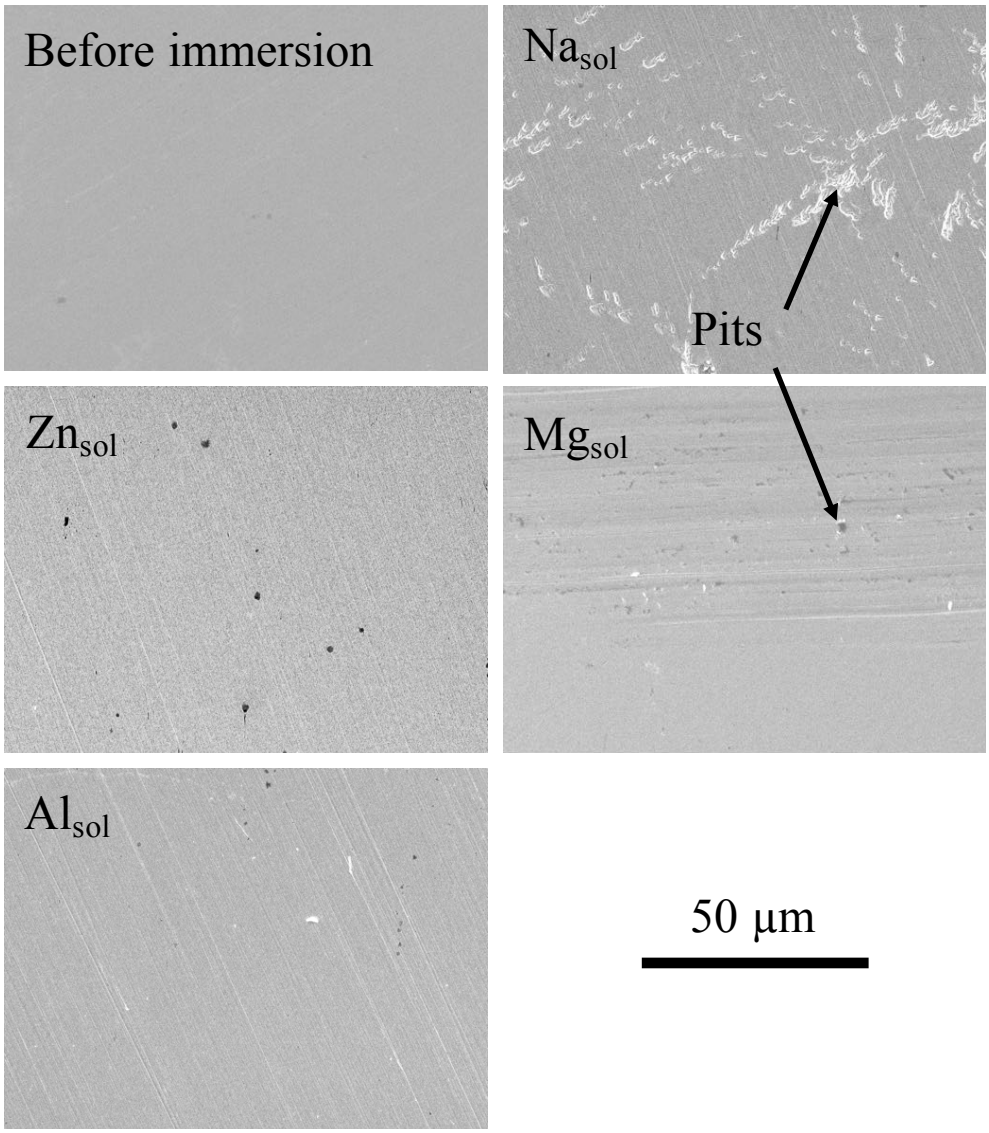

Fig. 3.4 Surface SEM images of specimen after immersion in the solutions at 25°C for 56 d.

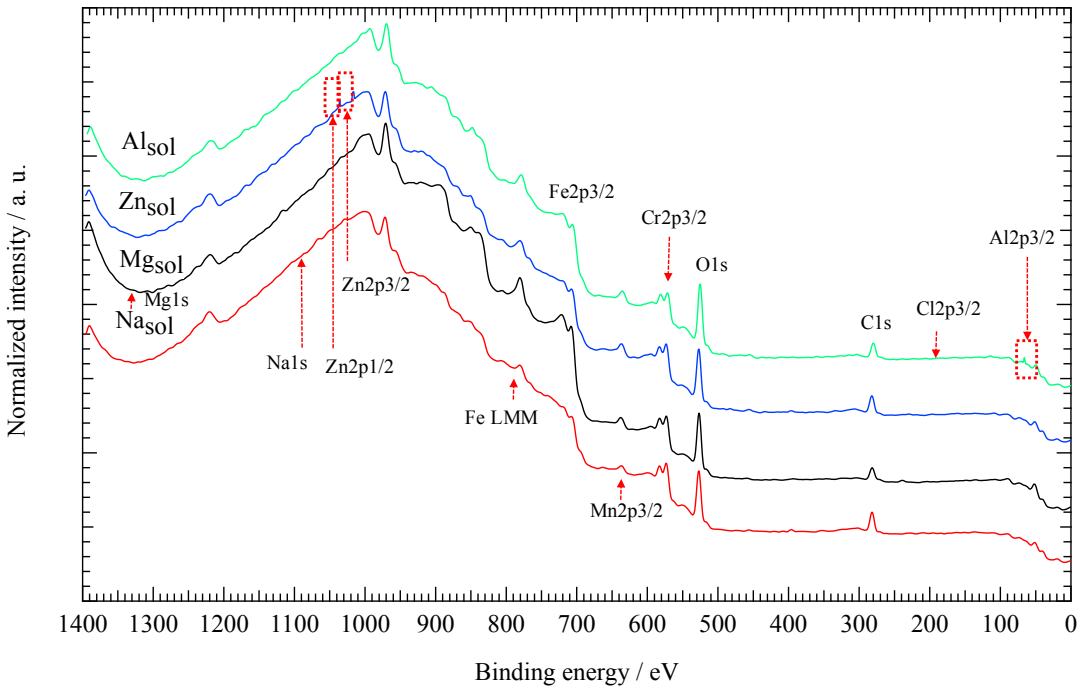

Fig. 3.5 XPS wide spectra of specimen surface after immersion in the solutions.

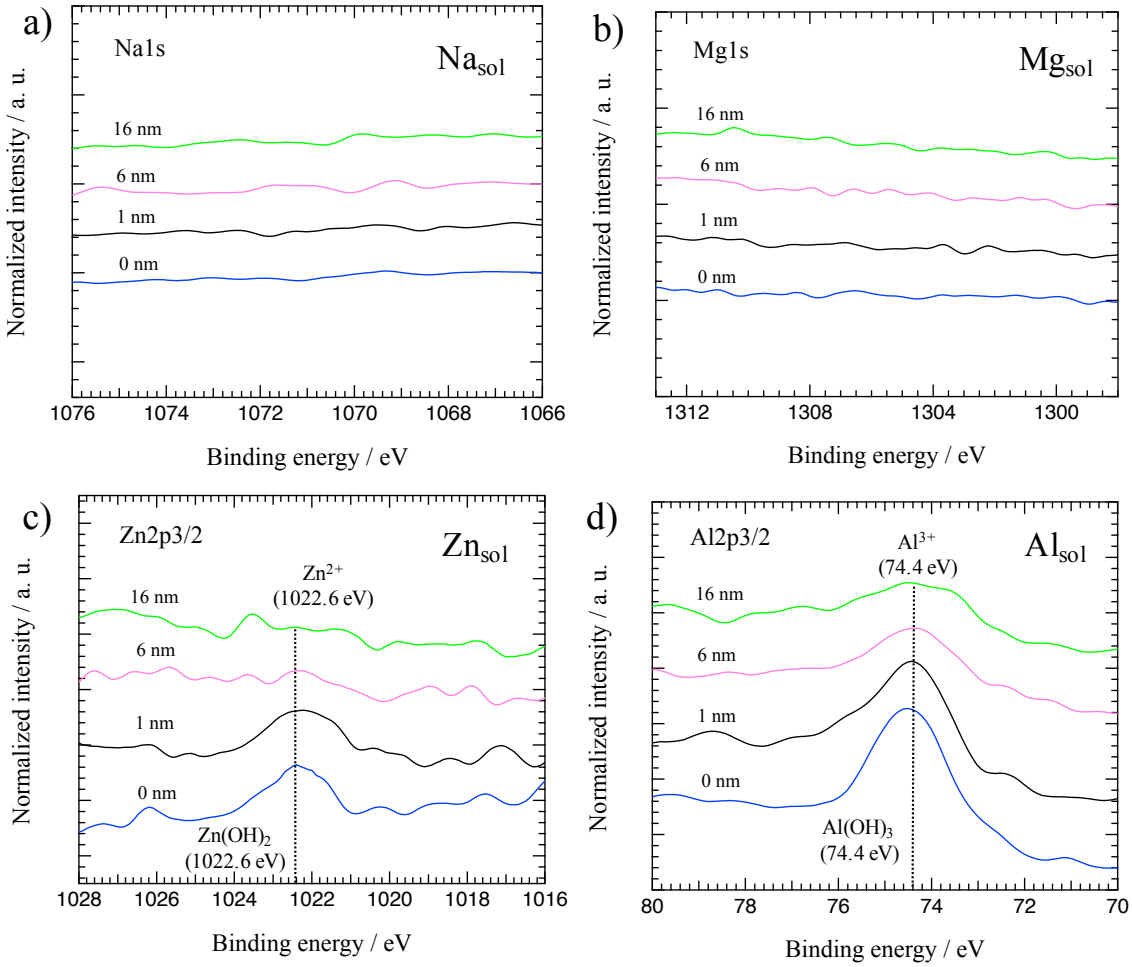

Fig. 3.6 XPS narrow spectra of metal cations with depth a) Na1s peaks of specimen immersed in Na_{sol}, b) Mg1s peaks of specimen immersed in Mg_{sol}, c) Zn2p3/2 peaks of specimen immersed in Zn_{sol}, d) Al2p3/2 peaks of specimen immersed in Al_{sol}.

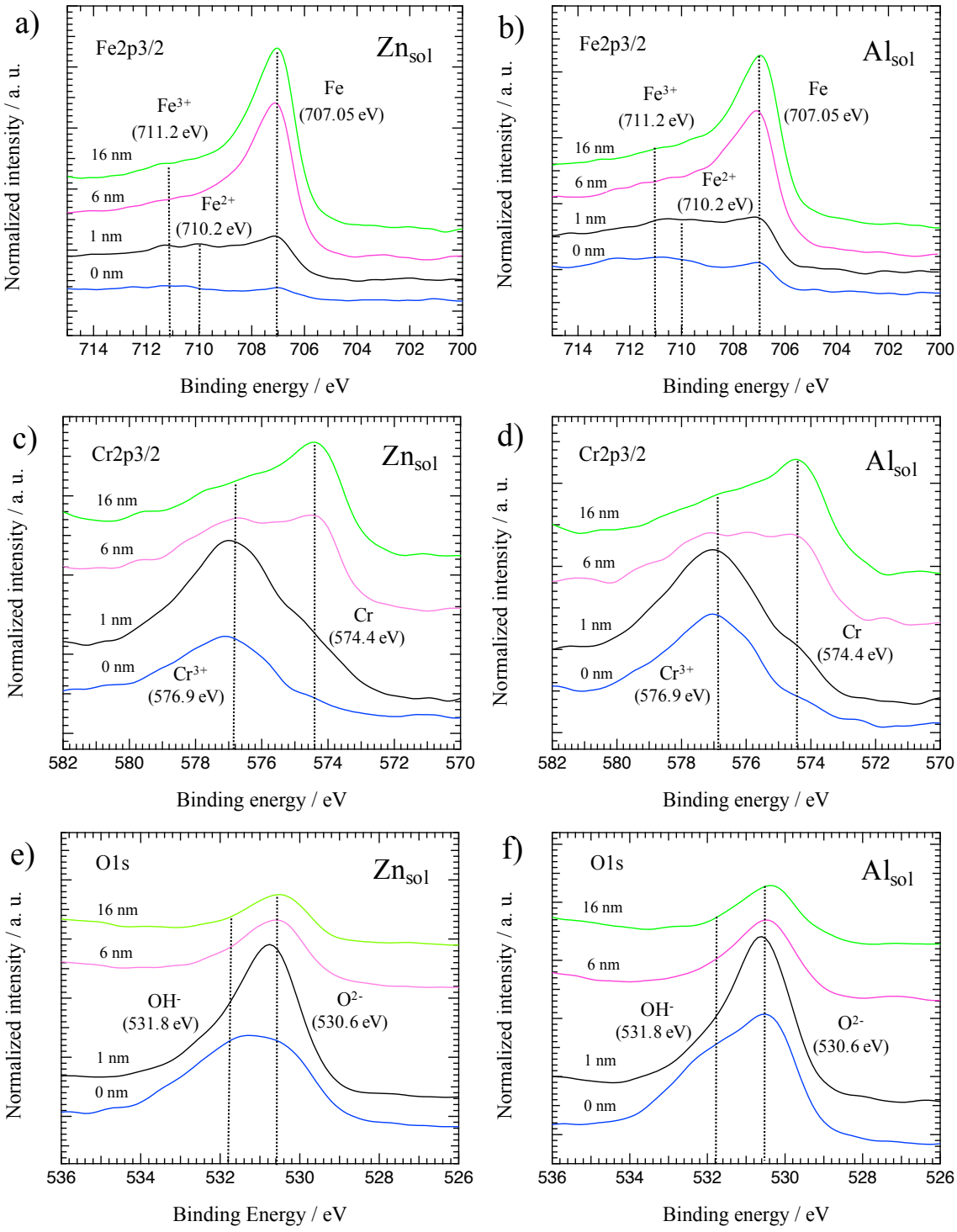

Fig. 3.7 XPS narrow spectra with depth a) Fe2p3/2 c) Cr2p3/2 and e) O1s peaks of specimen immersed in Zn_{sol}, b) Fe2p3/2 d) Cr2p3/2 and f) O1s peaks of specimen immersed in Al_{sol}.

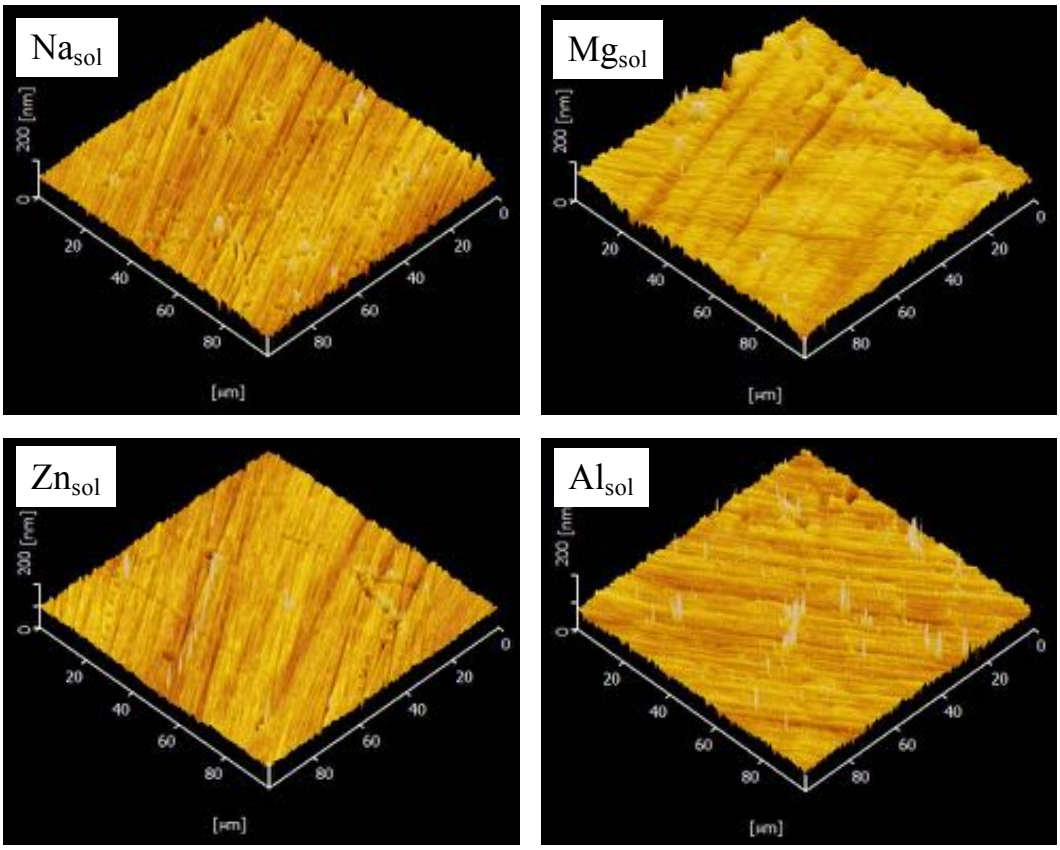

Fig. 3.8 AFM 3D images of specimen immersed in the solutions at 25°C for 56 d.

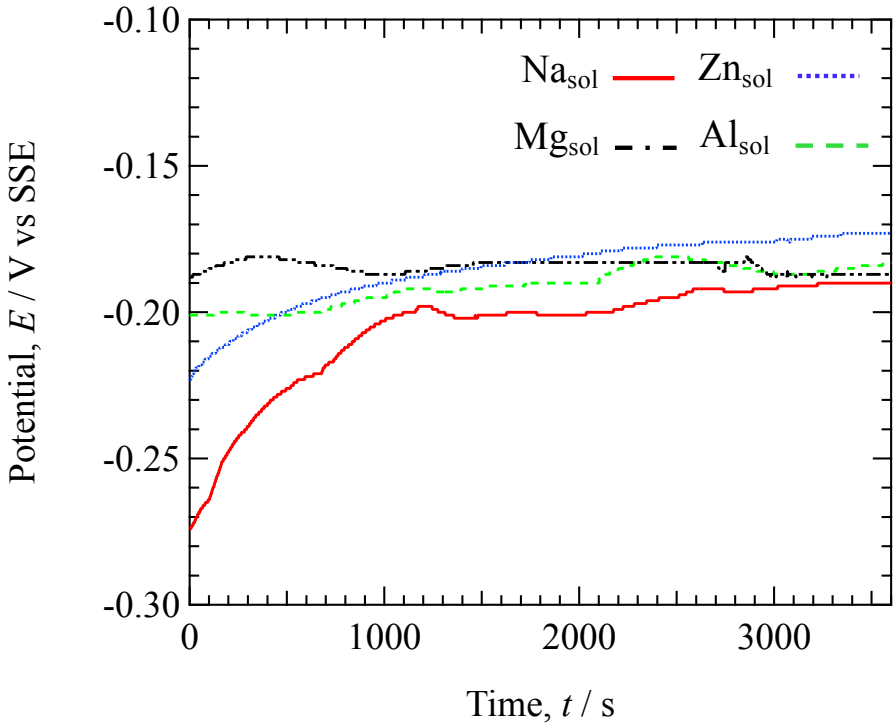

Fig. 3.9 Open circuit potential after immersion for 7 d in the different solutions with metal cations.

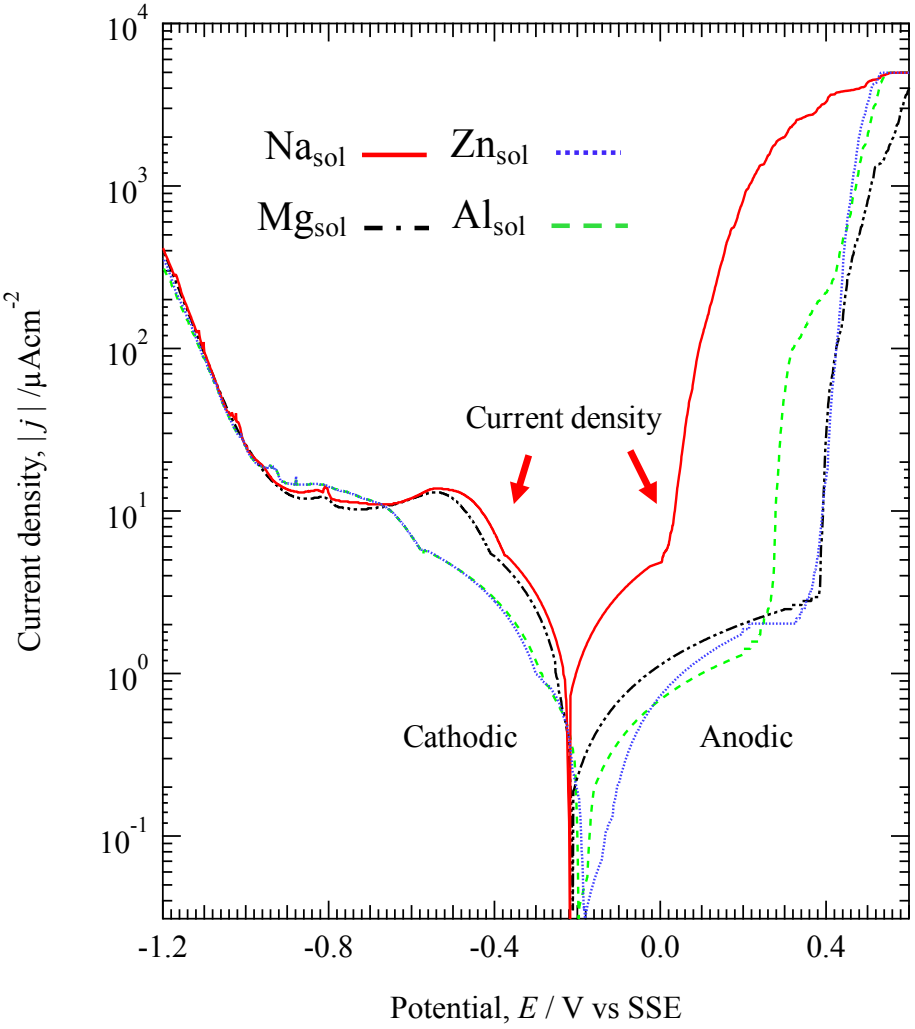

Fig. 3.10 Polarization curves of specimen immersed in the different solutions with metal cations.

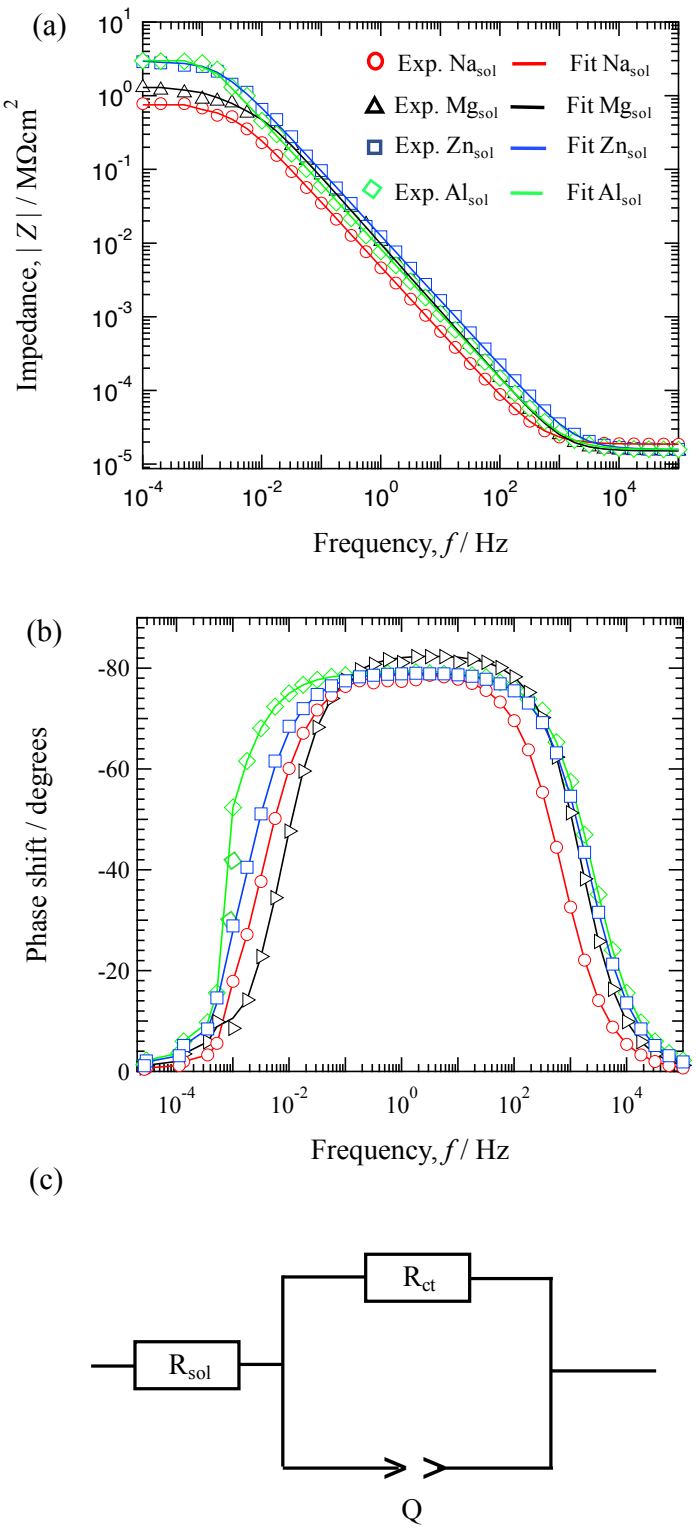

Fig. 3.11 Results of EIS in the solution with different metal cations after immersion for 7 d, Bode diagram of (a) impedance and (b) phase shift plot, (c) equivalent circuit model used to fit the EIS data.

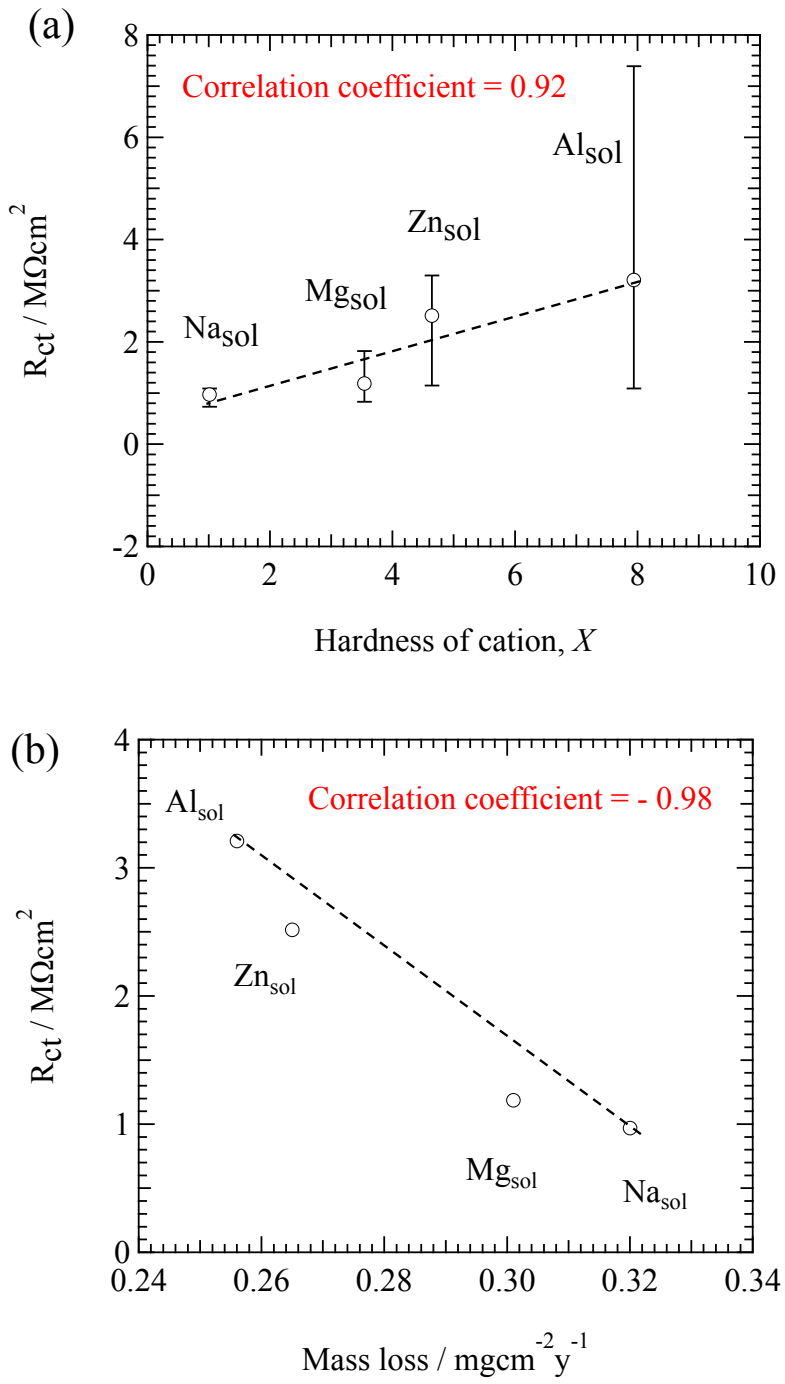

Fig. 3.12 (a) Changing of R_{ct} as a function of *X*, (b) Changing of R_{ct} with mass loss of specimen immersed in the solutions.

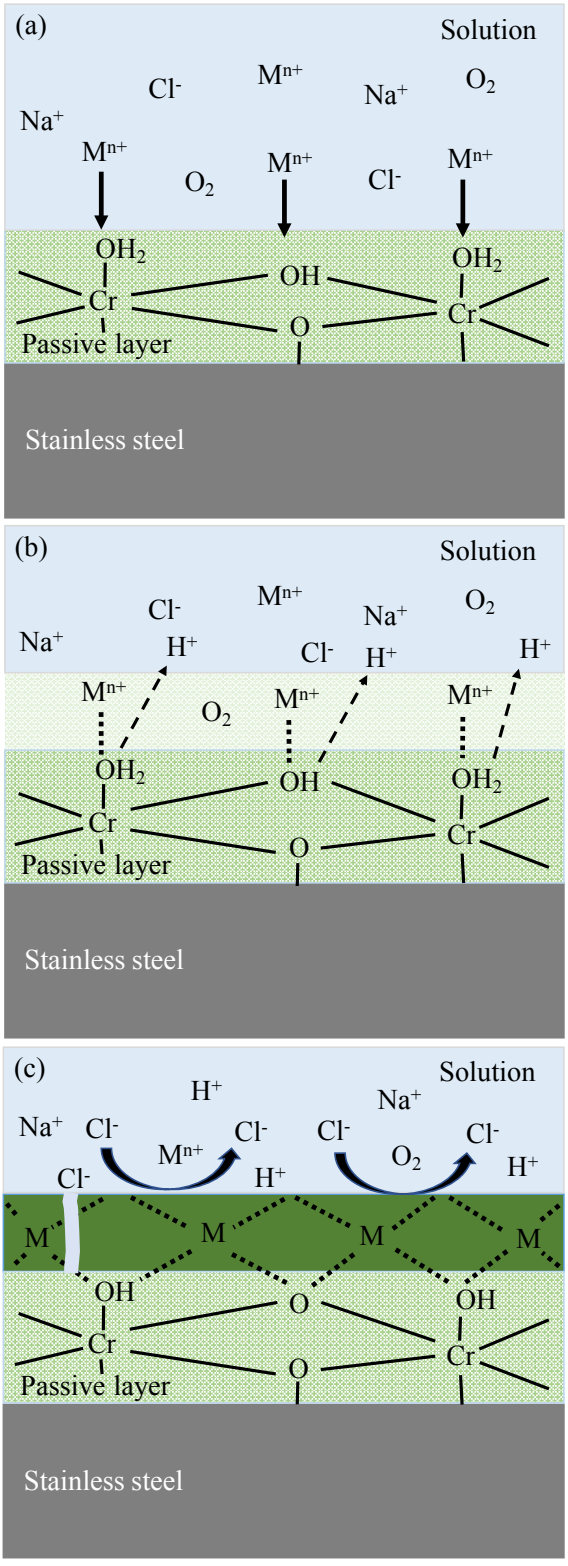

Fig. 3.13 (a) Schematic representation of the passive films structure with hard metal cations in 0.5 M Cl^- aqueous solution (M^{n+} = Zn^{2+}, Al^{3+}). (b) deprotonation process accelerated by hard metal cations, M^{n+}. (c) formation of metal cation layer on the passive films by hard metal cations.

References

1. P. D. Krell, S. Li and H. Cong, Corros. Sci., 122 (2017) 41-52.
2. T. Takei, M. Yabe and F. G. Wei, Corros. Sci., 122 (2017) 80-89.
3. K. S. Raja muthu kumar, P. Vijian, J. Samu Solomon, L. John Berchmans, Int. J. of Emerging Technology and Advanced Eng., 2 (2012) 178-182.
4. S. Hastuty, A. Nishikata and T. Tsuru, Corros. Sci., 52 (2010) 2035-2043.
5. S. T. Kim, S. H. Jeon, I. S. Lee and Y. S. Park, Corros. Sci., 52 (2010) 1897-1904.
6. X. Yu, S. Chen, Y. Liu and F. Ren, Corros. Sci., 52 (2010) 1939-1947.
7. J. Kovac, C. Alaux, T. J. Marrow, E. Govekar and A. Legat, Corros. Sci., 52 (2010) 2015-2025.
8. M. Behpour, S. M. Ghoreishi, M. Khayat Kashani and N. Soltani, Mat. and Corros., 60 (2009) 895-898.
9. J. Starosvetsky, D. Starosvetsky, B. Pokroy, T. Hilel, R. Armon, Corros. Sci., 50 (2008) 540-547.
10. S. J. Yuan, S. O. Pehkonen, Y. P. Ting, E. T. Kang, and K. G. Neoh, Ind. Eng. Chem. Res. 47 (2008) 3008-3020.
11. Z. S. Smialowska and J. Mankowski, Corros. Sci., 18 (1978) 953-960.
12. C. O. A. Olsson and D. Landolt, Electrochim. Acta 48 (2003) 1093-1104.
13. G. Okamoto, Corros. Sci., 13 (1973) 471-489.
14. E. McCafferty, Introduction to corrosion science, Springer, 2010, pp. 283-286.
15. T. Shibata, Corros. Sci., 49 (2007) 20-30.
16. L. A. Krebs and J. Kruger, International symposium; 8th, passivity of metals and semiconductors, Electrochem. Soc., Pennington, NJ, 2001, pp. 561-569.
17. T. Shibata, Corros. Sci., 31 (1990) 413-423.
18. N. Sato, Corros. Sci., 31 (1990) 1-19.
19. D. D. Macdonald and M. U. Macdonald, Corros. Sci., 31 (1990) 424-430.
20. R. Nishimura and K. Kudo, Corros. Sci., 31 (1990) 479-484.
21. Md. S. Islam, K. Otani and M. Sakairi, Corros. Sci., 131 (2018) 17-27.
22. K. Otani, Md. S. Islam and M. Sakairi, J. Electrochem. Soci., 164 (2017) C498-C504.
23. K. Otani, M. Sakairi, Corros. Sci., 111 (2016) 302-312.
24. S. Zhang, T. Shibata, T. Haruna, Corros. Sci., 47 (2005) 1049-1061.
25. M. G. A. Khedr and A. M. S. Lashien, Corros. Sci., 33 (1992) 137-151.
26. S. Tsujikawa and S. Okayama, Corros. Sci., 31 (1990) 441-446.
27. K. E. Heusler, Corros. Sci., 31 (1990) 597-606.

28. C. S. O'dell, B. F. Brown, R. T. Foley, Corrosion, 36 (1980) 183-200.
29. D. M. Drazic and L. Z. Vorkapic, Corros. Sci., 18 (1978) 907-910.
30. H. C. Gatos, Corrosion, 12 (1956) 32-40.
31. J. N. Esposito, G. Economy, W. A. Byers, J. B. Esposito, F. W. Pement, R. J. Jacko, C. A. Bergmann, in: Proc. 5th Int. Sympo. Environmental degradation of materials in nuclear power systems-water reactors, American Nuclear Society, (1992) 495-503.
32. C. J. Wood, W. J. Marbel, M. Prystupa, M. J. Hudson, D. L. Wilkens, in: Proc. of 5th Inter. Conf. on Water chemistry of nuclear reactor systems, vol. 1, BNES, (19890 111-120.
33. K. F. Ankinpelumi, Investigation the effect of pH level on corrosion rate, University of Lagos, Lagos, (2012).
34. I. A. Ammar and S. Riad, J. Phys. Chem., 62 (1958) 150-154.
35. F. H. Sweeton and C. F. Baes Jr., J. Chem. Thermodynamics, 2 (1970) 479-500.
36. L. N. Mulay and P. W. Selwood, J. Am. Chem. Soc., 77 (1955) 2693-2701.
37. G. Deroubaix, P. Marcus, Surf. Interface Anal. 18 (1992) 39-46.
38. J. A. Taylor, J. Vac. Sci. Technol. 20 (1982) 751-755.
39. K. Song, Y. Lee, M. R. Jo, K. M. Nam and Y. M. Kang, Nanotechnology 23 (2012) 505401-505406.
40. S. Ningshen, M. Sakairi, K. Suzuki and S. Ukai, Corros. Sci., 78 (2014) 322-334.
41. R. R. L. De Oliveira, D. A. C. Albuquerque, T. G. S. Cruz, F. M. Yamaji and F. L. Leite, Federal University of São Carlos, Campus Sorocaba, Brazil, (2011) 147-174.
42. A. K. Satapathy, G. Gunasekaran, S. C. Sahoo, Kumar Amit, P. V. Rodrigues, Corros. Sci., 51 (2009) 2848-2856.
43. I. Martinez, C. Andrade, Corros. Sci., 50 (2008) 2948-2958.
44. A. Popova, M. Christov, A. Vasilev, Corros. Sci., 49 (2007) 3290-3302.
45. D. A. Lopez, S. N. Simison and S. R. de Sanchez, Corros. Sci., 47 (2005) 735-755.
46. P. C. Torres, T. J. Mesquita and R. P. Nogueira, J. Phys. Chem. 119 (2015) 4136-4147.
47. M. E. Orazem, I. Frateur, B. Tribollet, V. Vivier, S. Marcelin, J. Electrochem. Soci., 160 (2013) C215-C225.
48. B. Hirschorn, M. E. Orazem, B. Tribollet, V. Vivier, I. Frateur and M. Musiani, Electrochim. Acta, 55 (2010) 6218-6227.
49. G. J. Brug, A. L. G. Van Den Eeden, M. S. Rehbach and J. H. Sluyters, J. Electroanal Chem., 176 (1984) 275-295.
50. M. Mahdavian and R. Naderi, Corros. Sci., 53 (2011) 1194-1200.

51. G. Okamoto, T. Shibata, in: R. P. Frankenthal, J. Kruger (Eds.), The Electrochemical Society Inc., Princeton, NJ, (1978) 646-677.
52. G. Okamoto, T. Shibata, Corros. Sci., 10 (1970) 371-378.
53. S. Ahrland, J. Chatt, N. R. Davies, Quart. Rev. London, 12 (1958) 265-276.
54. G. Okamoto, T. Shibata, Nature, 206 (1965) 1350.
55. R. G. Pearson, J. Am. Chem. Soc., 85 (1963) 3533-3539.
56. M. Haginuma, S. Ono, M. Sambongi, K. Takeda, K. Tachibana, K. Ishigure, in: Proc. of 1998 JAIF Inter. Conf. on Water Chem. in Nuclear Power Plants, Japan Atomic Industrial Forum, Inc., (1998) 122-129.
57. T. M. Angeliu, P. L. Andresen, Corrosion, 52 (1996) 28-35.
58. L. W. Niedrach, W. H. Stoddard, Corrosion, 42 (1986) 546-549.

Chapter 3 has been oriented from the following article

[Md. S. Islam, K. Otani and M. Sakairi, Corrosion inhibition effects of metal cations on SUS304 in 0.5 M Cl^- aqueous solution, *Corros. Sci*., 140 (2018) 8-17.]

Chapter 4

Corrosion inhibition of steel substrate by metal cations in concentrated Cl^- aqueous solutions

4.1 Introduction

Coated steels are extensively used as various constructional material due to low cost and good mechanical and anti-corrosion properties than other steels. Zinc coated steel is one of the most common materials and has wide applications in automobiles, buildings, bridges, marine platforms [1-4]. In the environment that contains Cl^-, main factors of steel corrosion are the concentration and corrosive nature of the Cl^-, and the passive film is generally destroyed by this ion in an aqueous environment [5-8]. It is well known that the Cl^- concentration reaches a high level on the steel surface during the drying situation of the atmospheric environment. There are many studies have been carried out about the corrosion of zinc coated steel in the Cl^- aqueous environment at high concentration [9-13].

Sun et al. [14] reported that ZnO and $Zn(OH)_2$ are produced as corrosion products when zinc coated steel is exposed in an aqueous environment and corrosion protection ability is attributed by these corrosion products. Tsuru [15] proposed that Zn^{2+} is dissolved from the corrosion products and adsorb onto the steel and prevent further corrosion of the steel substrate. Same phenomena occur while carbon steel is exposed in the aqueous solution with Zn^{2+} [16]. The cation adsorbs as hydroxides onto the steel substrate and suppresses the corrosion reactions of steel. There are many researchers reported that metal cations (Zn^{2+} and Al^{3+}) can reduce the corrosion of carbon steel by adsorbing onto the steel substrate in aqueous solution [16-20]. Islam et al. [16] reported that Zn^{2+} effectively inhibits the corrosion of mild steel in 10 mM Cl^- aqueous solution. They also proposed a mechanism of mild steel corrosion inhibition by metal cations. Otani et al. [17, 18] investigated the effects of metal cations (Zn^{2+} and Al^{3+}) on mild steel corrosion in model freshwater and explained that metal cations make a layer on the passive film that inhibits the corrosion reactions in the solution. They also reported that Zn^{2+} effectively improve the corrosion inhibition ability of gluconates in model freshwater [19]. In some nuclear power reactors, Zn^{2+} are also added into the working fluid for suppressing corrosion of the reactor component materials [20].

Zinc coated steel is protected by the galvanic reactions or sacrificial anodic reaction of Zn [21]. However, the zinc coating on steel is not fully corrosion protected or sufficient for long time protection of steel in the environment that contains Cl^- at high concentration. Because, once

the coating is consumed by the sacrificial anodic reaction in the presence of aggressive Cl^-, severe corrosion happens on the steel surface. Therefore, it is needed to clarify the role of Zn^{2+} on carbon steel corrosion in such environment that contains Cl^- at high concentration. In this experiment, the effects of Mg^{2+} and Al^{3+} have also been carried out, because some of the coated layers of the steel contain Mg and Al.

4.2 Experimental

4.2.1 Specimens

A carbon steel sheet was cut into 7 × 7 × 0.7 mm in size and was used as specimens. The chemical composition (wt.%) of specimen used for all the experiments as follows: C = 0.02; Mn = 0.18; P = 0.015; Si = 0.01; S < 0.01, and balance Fe. Prior to the experiments, the specimens were abraded with #240 to #4000 grit size of SiC abrasive paper and then it was ultrasonically cleaned with ethanol and in highly purified water.

4.2.2 Test Solutions

Three different salt solutions of 0.1 mM $MgCl_2$ (Mg_{sol}), 0.1 mM $ZnCl_2$ (Zn_{sol}) and 0.1 mM $AlCl_3$ (Al_{sol}) were prepared and their Cl^- concentration was adjusted to 0.5 M by NaCl and were used as the tests solutions. In this experiment, 0.5 M NaCl (Na_{sol}) was used as a reference solution. Highly purified water was used to prepare experimental solutions. The pH of the solutions was adjusted to 5.8 by 0.1 M NaOH. The measurements of the pH were carried out using the pH meter (Eutech Instruments Pte. Ltd., Cyber-Scan 6000). All chemicals used in this study were special analytical grade and obtained from Kanto Chemical Co. Ltd.

4.2.3 Immersion Tests

Immersion tests were carried out at 25°C for 3 d in stationary condition. During the immersion, the solutions were open to the air. The appearances of specimens and solutions were observed by a digital camera (Nikon, D80). Before and after the tests, the specimens were cleaned in ethanol and then in highly purified water using an ultrasonic bath. The mass of the specimens was measured using a micro-balance (METTLER TOLEDO MX5, Pro FACT), and the corrosion rates were calculated from the mass change [16]

4.2.4 Surface characterizations

The surface morphological changes due to immersion in the solutions were observed by scanning electron microscope (SEM, JEOL Ltd., JSL6510-LA). The surface roughness was measured from 3 D image by atomic force microscope (AFM, SPA400; cantilever: SI-DF40) [22, 23]. The surface of the immersed specimens was analyzed by X-ray photoelectron spectroscope (XPS, JEOL Ltd., JPS-9200) using a monochrome Al Kα X-ray source (1486.6 eV). Before the surface characterizations, the immersed specimens were cleaned ultrasonically by ethanol and then in highly purified water.

4.2.5 Electrochemical tests

Electrochemical measurements were carried out in a three-electrode cell using a potentiostat (Pocketstat, IVIUM TECHNOLOGIES). Open-circuit potential (OCP) was measured for 1 h at room temperature and the potentiodynamic measurements were carried out in the cathodic and anodic direction with a scan rate of 1 mV/s. A platinum plate and an Ag/AgCl electrode (SSE) immersed in a saturated KCl solution were used as counter and reference electrodes, respectively. EIS measurements were carried out at OCP in the frequency range from 10 kHz to 1 mHz, and modulation amplitude of 10 mV. Reproducible data were obtained in all electrochemical measurements.

4.2.6 Corrosion inhibition efficiency of metal cations

The corrosion inhibition efficiency (η_i) of metal cations was calculated from the mass loss by Eq. (4.1).

$$\eta_i\ (\%) = \frac{Na_{ms} - CAT_{ms}}{Na_{ms}} \times 100 \quad (4.1)$$

Here Na_{ms} is the mass loss of specimen immersed in Na_{sol} and CAT_{ms} is the mass loss of specimen immersed in Mg_{sol}, Zn_{sol}, and Al_{sol}.

The corrosion inhibition efficiency (η_e) of metal cations was also calculated from the EIS by Eq. (4.2).

$$\eta_e\ (\%) = \frac{CAT_{ct} - Na_{ct}}{Na_{ct}} \times 100 \quad (4.2)$$

Here Na_{ct} is the charge transfer resistance (R_{ct}) of specimen immersed in Na_{sol} and CAT_{ct} is the R_{ct} of specimen immersed in Mg_{sol}, Zn_{sol}, and Al_{sol}. From equation (4.1) and (4.2), the corrosion inhibition efficiency of Na^+ is zero.

4.3 Results

4.3.1 Immersion tests

Fig. 4.1 (a) shows the appearance of solutions and specimens at the start of immersion, and (b) shows the appearance of solutions and specimens after the immersion tests for 3 d at 25°C. Fig. 4.1 (c) shows the appearance of the specimen surface before immersion and Fig. 4.1 (d) shows the appearance of the specimen surface after the immersion tests. After the immersion, brown-red corrosion products are observed in all the solutions (Fig. 4.1 (b)). Less amount of brown-red corrosion products is observed in the case of Zn_{sol} as compared to the other solutions. The solution color also different in Zn_{sol} as compared to the other solutions. The pH of solutions before (pH_{int}) and after (pH_{corr}) the immersion tests is shown in Table 4.1. The pH has been increased a bit after the immersion tests in all the case. The corrosion rates were calculated from the mass change during the immersion. Several researchers [16-19] introduced the hardness of metal cation, *X* to explain the effect of metal cations on corrosion loss of steel in freshwater and in Cl^- aqueous solution. The *X* is not a suitable corrosion indicator regarding corrosion of mild steel in freshwater and in Cl^- aqueous solution [16, 17]. However, mass losses or corrosion rates were plotted as a function of *X* to find out the relation between them in the environment that contains Cl^- at high concentration in this study. Fig. 4.2 shows the corrosion rate as a function of *X* (hardness of metal cation). Each of the solutions shows different corrosion rate and Zn_{sol} shows the lowest corrosion rate among other solutions. The correlation coefficient is -0.32 indicating that the corrosion rate is not closely related with *X*. The results of immersion tests indicate that Zn_{sol} has the better corrosion inhibition effect on carbon steel as compared to the other solutions used in this study.

4.3.2 Surface characterizations

The corrosion rates of specimens immersed in the solutions are different in each solution of metal cation. The surface of the specimens may be affected by the metal cations. To clarify this matter, the surface morphological changes were observed by SEM. Fig. 4.3 shows the surface SEM images of specimens and different surface morphologies are observed for the different solutions. SEM images represent the clear grain boundaries and pits in the case of Na_{sol}, Mg_{sol}, and Al_{sol} that reflect the severe corrosion. A few numbers of pits are observed on the specimen immersed in Zn_{sol}. The results suggest that the corrosion of carbon steel may be affected with the metal cations in the solutions and Zn^{2+} may form hydroxides with the OH^- of the oxide film

that inhibited the corrosion reactions [16, 17]. These results correspond well with the corrosion rate.

The surface roughness was measured by atomic force microscopy and the 3D images are shown in Fig. 4.4. Different surface roughness is observed for different solutions with metal cations. The average surface roughness (R_a) was calculated from the respective 3D images to enumerate the surface roughness. The calculated R_a values are listed in Table 4.2. The specimen immersed in the Zn_{sol} shows the lowest R_a among other solutions. These results correspond well to the surface observation by SEM.

For better consideration of the effects of different metal cations on the oxide film, the specimen surfaces were analyzed by XPS after the immersion tests. Fig. 4.5 shows the XPS wide spectra of a specimen immersed in the solutions with metal cations. This figure clearly shows the peaks of Zn2p1/2 and Zn2p3/2 after immersion in the Zn_{sol}. Fig. 4.5 also includes the narrow spectra of Zn 2p3/2. XPS analysis results show that there is no peak of Na 1s, Mg 1s and Al2p3/2 on the specimen after immersed in the respective solution signifying that Na^+, Mg^{2+}, and Al^{3+} cannot form a chemical bond with the oxide film on the carbon steel surface in the solution. The clear peak of Zn^{2+} among all experimental metal cations meaning that only Zn^{2+} remains on the carbon steel after immersion in the solution and Zn^{2+} may form a chemical bond with the oxide film. The previous paper demonstrated that Zn^{2+} formed a chemical bond with the oxide film that leads to the formation of a layer which inhibited the corrosion reactions and protected the dissolution of metal [16-18]. The results obtained from XPS analysis were a good agreement with corrosion rate and surface images.

4.3.3 Electrochemical tests

The open circuit potentials (OCP) of the specimen measured in the solutions with metal cations are shown in Fig. 4.6. All the measured values of OCP are decreased with time. However, the OCP reached almost a stable value at around 3000 s of immersion in the solution. Slight difference can be noticed in which the Na_{sol} shows the most negative open-circuit potential and Zn_{sol} shows the most positive one.

Potentiodynamic polarization curves are shown in Fig. 4.7. From the cathodic polarization curves (Fig. 4.7 (a)), it is found that Zn_{sol} shows lower current density as compared to the other solutions. From the anodic polarization curves (Fig. 4.7 (b)), the passivation region is not observed and the current density in Zn_{sol} is less than that in the other solutions. Therefore, it is assumed that the iron oxide film partially remained and was affected by metal cations in the

solutions. Na_{sol} shows the highest current density among used solutions both in cathodic and anodic polarization curves. In other words, Zn_{sol} acts as both cathodic and anodic inhibitor as compared to the other solutions.

Fig. 4.8 shows the Bode diagram of (a) impedance and (b) phase shift in the solutions with metal cations after immersion for 1 h. The fitted lines calculated by Randle's equivalent circuit model [24-26] are also shown in Fig. 4.8 (a), (b), and the used equivalent circuit model is shown in Fig. 4.8 (c). The fitted lines correspond well to the experimental data. The equivalent circuit model consists of solution resistance (R_{sol}), charge-transfer resistance (R_{ct}), and constant phase element (Q). Among experimental solutions, Zn_{sol} shows the highest impedance at low frequency (Fig. 4.8 (a)). The higher phase shift is also observed in Zn_{sol} (Fig. 4.8 (b)) than other solutions. The magnitude of impedance at low frequencies in the Bode diagram indicates the corrosion resistance of specimen in the solutions.

The electrochemical impedance parameters are calculated using the Eq. (4.3) [27-30]. The calculated values of electrochemical impedance parameters are listed in Table 4.3.

$$Z = \mathrm{R_{sol}} + \frac{\mathrm{R_{ct}}}{1+ (j\omega)^n \mathrm{QR_{ct}}} \tag{4.3}$$

High R_{ct} means that the specimen has high corrosion resistance in the corresponding solution. From Table 4.3, Zn_{sol} shows the highest R_{ct} than other solutions. Zn_{sol} also shows the lowest value of Q than other solutions of the metal cation (Table 4.3). The Q represents the structure of the solution/metal interface and the area of defects in the passive film on the surface [19, 31]. Islam et al. [16] and Otani et al. [17] reported that the decrease in Q indicates that Zn^{2+} can decrease the defects in the passive film on carbon steel. This result indicates that relatively perfect oxide film is formed on the specimen immersed in Zn_{sol}. Therefore, the results obtained from EIS tests suggest that the specimen immersed in the Zn_{sol} has high corrosion resistance due to the formation of perfect film compare to the other solutions used in this study.

It is considered that the mass loss of specimen is directly related to the charge transfer resistance (R_{ct}). If the R_{ct} of a solution is high, the mass loss of specimen should be low. To clarify this matter, the relationship between the mean values of both parameters have been examined. Fig. 4.9 shows the relationship between charge transfer resistance (R_{ct}) and mass loss of specimen immersed in the solutions. The correlation coefficient is -0.99 indicates that R_{ct} and mass loss are closely related to each other, and Zn_{sol} shows the highest R_{ct} and lowest mass loss among other solutions. The results of electrochemical tests well correspond with the immersion tests and surface characterizations.

4.3.4 Corrosion inhibition efficiency of metal cations

From the above experimental results, it has been confirmed that metal cations have an effective inhibitory influence on carbon steel corrosion in the solutions and Zn^{2+} shows the highest corrosion inhibition effect among other metal cations used in this study. To elucidate the corrosion inhibition effect, the efficiency of corrosion inhibition of metal cations was calculated depending on the immersion tests and electrochemical tests. Fig. 4.10 (a) shows the corrosion inhibition efficiency (η_i) of metal cations based on the immersion tests in which mean values of mass losses have been used. Fig. 4.10 (b) also shows the corrosion inhibition efficiency (η_e) of metal cations based on the electrochemical tests in which mean values of charge transfer resistance (R_{ct}) have been used. In both cases, Zn^{2+} shows the highest corrosion inhibition efficiency than other metal cations used in this study.

4.4 Discussions

From the experimental results, it has been confirmed that Zn^{2+} remains on the steel surface after the immersion tests. It is assumed that Zn^{2+} forms a chemical bond with the oxide film and make a layer that decreases the defect points in the film. Whereas, the other metal cations used in this study cannot remain on the surface or unable to make such kinds of bond with the oxide film. Fig. 4.11 (a) shows the schematic images of the corrosion process on carbon steel in the solution with metal cations (M^{n+}= Na^+, Mg^{2+}, and Al^{3+}). The metal cations (M^{n+}= Na^+, Mg^{2+}, and Al^{3+}) cannot make a layer on the defect site of the oxide film. Therefore, Cl^- destroy the film easily at the defect point, and then corrosion occurred resulting in the formation of grain boundaries and huge numbers of pits on the immersed specimen as shown in Fig. 4.3. Fig. 4.11 (b) shows the schematic images of the corrosion inhibition process of carbon steel by Zn^{2+} in the solution. Zn^{2+} forms a chemical bond with the OH^- of the oxide film and make a metal cation layer. The metal cation layer decreases the defect points on the oxide film. From this reason, the specimen immersed in the Zn_{sol} would have fewer defect points in the oxide film as compared to the other solutions. Therefore, Zn^{2+} layer has good protective ability against the Cl^- attack in the solutions.

From the above discussions, it can be proposed that the high and longtime corrosion resistance of Zn coated steel substrate is attributed to the formation of the Zn^{2+} layer on the oxide film of steel.

4.5 Conclusion

- The corrosion behavior of carbon steel is changed in the solutions with metal cations, however, it is not closely related with the hardness of metal cation, *X*.
- The surface morphologies dependent on the metal cations (Na^+, Mg^{2+}, Zn^{2+}, and Al^{3+} contained by 0.5 M Cl^- aqueous solution) is observed by SEM and AFM. The surface of the specimen immersed in the solution containing Zn^{2+} (Zn_{sol}) shows the lowest roughness as compared to the others.
- Zn^{2+} is detected by XPS on the specimen surface after immersion in the Zn_{sol} and, however, Na^+, Mg^{2+} and Al^{3+} do not exist in the surface after the immersion in respective solutions.
- It is assumed that Zn^{2+} forms a chemical bond with the OH^- of the oxide film, and then forms a protective layer that decreased the defects in the film. Therefore, the Zn layer acts as a barrier to the corrosion reactions.

Table 4.1 pH of the solutions before (pH_{int}) and after (pH_{corr}) the immersion tests.

Test solutions	pH_{int}	pH_{corr}
Na_{sol}	5.8	6.2
Mg_{sol}	5.8	6.2
Zn_{sol}	5.8	6.3
Al_{sol}	5.8	6.3

Table 4.2 Surface roughness of specimen obtained by AFM after immersion in the solutions with different metal cations at 25°C for 3 d.

Solutions	Average surface roughness, R_a (nm)	
	Before immersion	After immersion
Na_{sol}	4.53	164.30
Mg_{sol}	4.56	155.70
Zn_{sol}	4.65	78.08
Al_{sol}	4.62	136.00

Table 4.3 The calculated mean values of EIS parameters of carbon steel immersed in the solutions for 1 h.

Solutions	R_{sol} (Ωcm^2)	R_{ct} ($k\Omega cm^2$)	Q ($\mu s^n \Omega^{-1} cm^{-2}$)	n
Na_{sol}	17.16	3.03	206.67	0.83
Mg_{sol}	18.50	3.22	193.33	0.83
Zn_{sol}	18.16	4.74	154.00	0.82
Al_{sol}	17.66	3.64	180.00	0.85

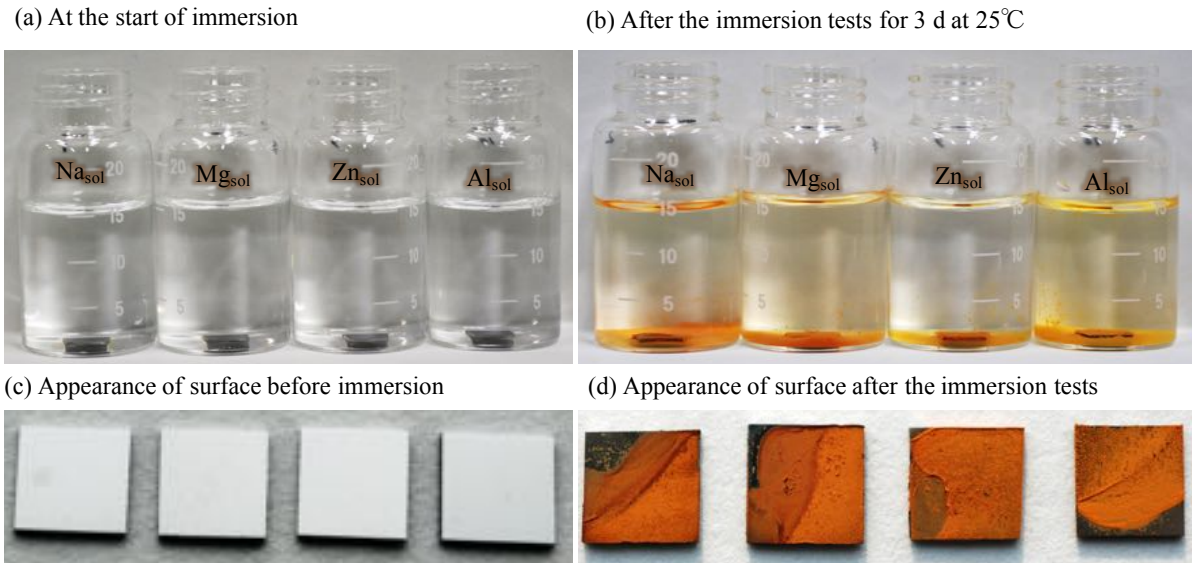

Fig. 4.1 Appearance of solutions and specimens (a) at the start of immersion and (b) after the immersion tests for 3 d at 25°C, and appearance of specimen surface (c) before immersion, (d) after the immersion tests.

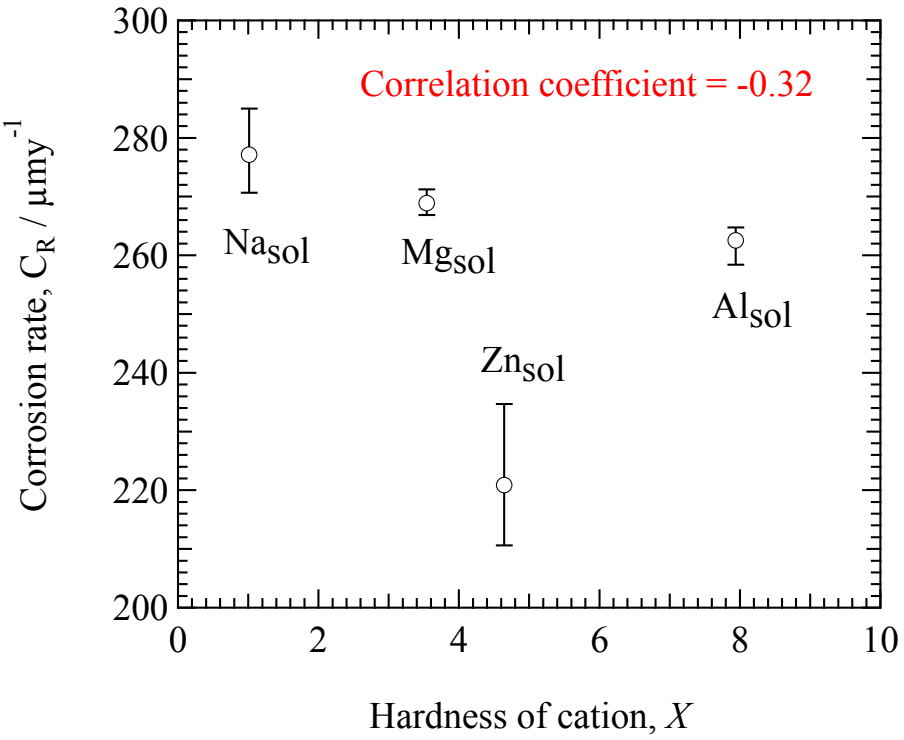

Fig. 4.2 Corrosion rate as a function of X.

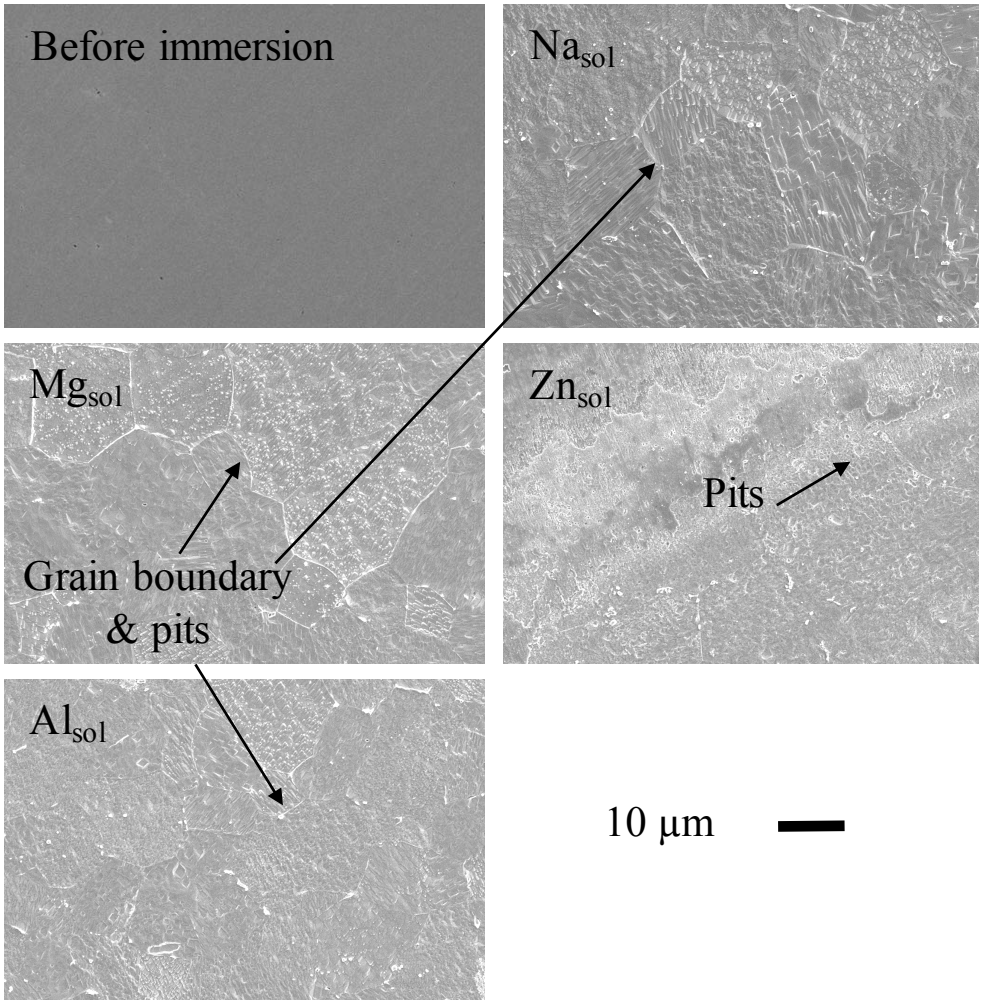

Fig. 4.3 SEM images of specimen immersed in the solutions at 25°C for 3 d.

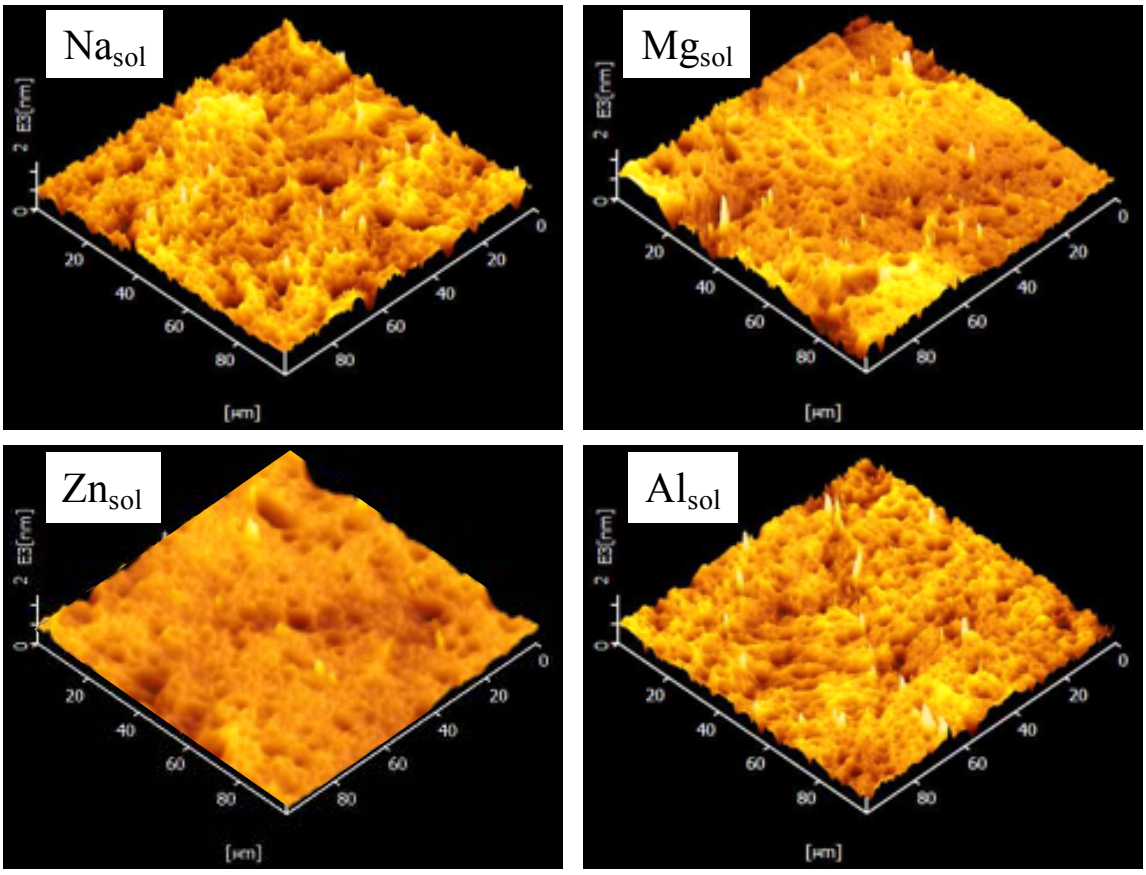

Fig. 4.4 AFM 3 D images of specimen immersed in the solutions at 25°C for 3 d.

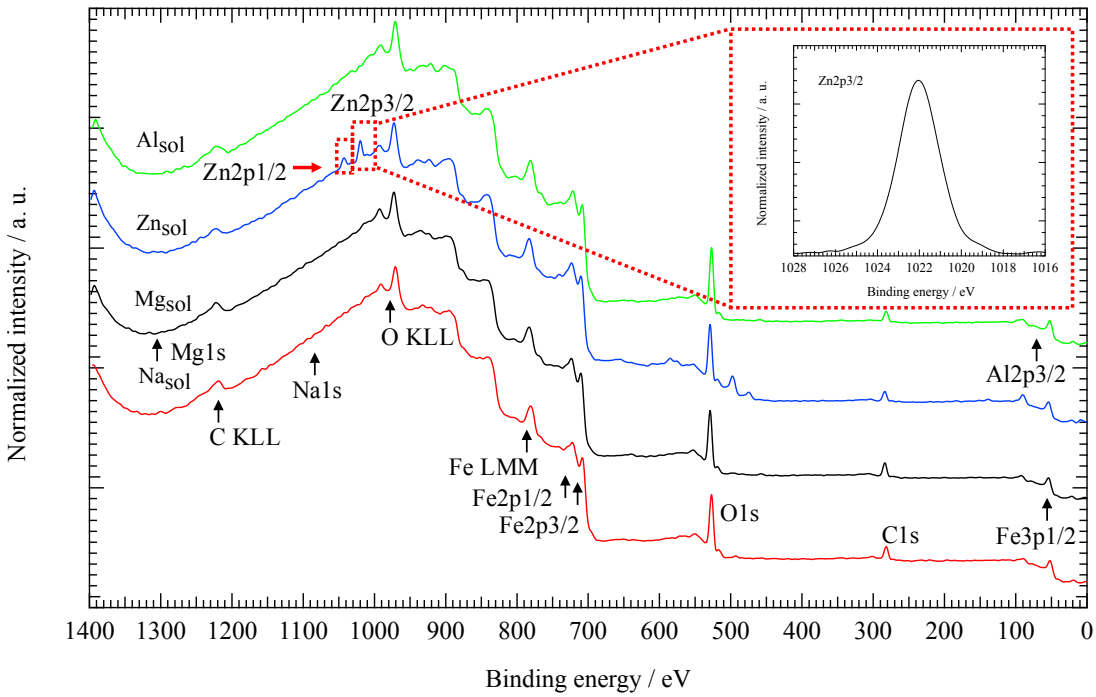

Fig. 4.5 XPS wide spectra (inset XPS narrow spectra of Zn 2p3/2) of specimens after the immersion tests.

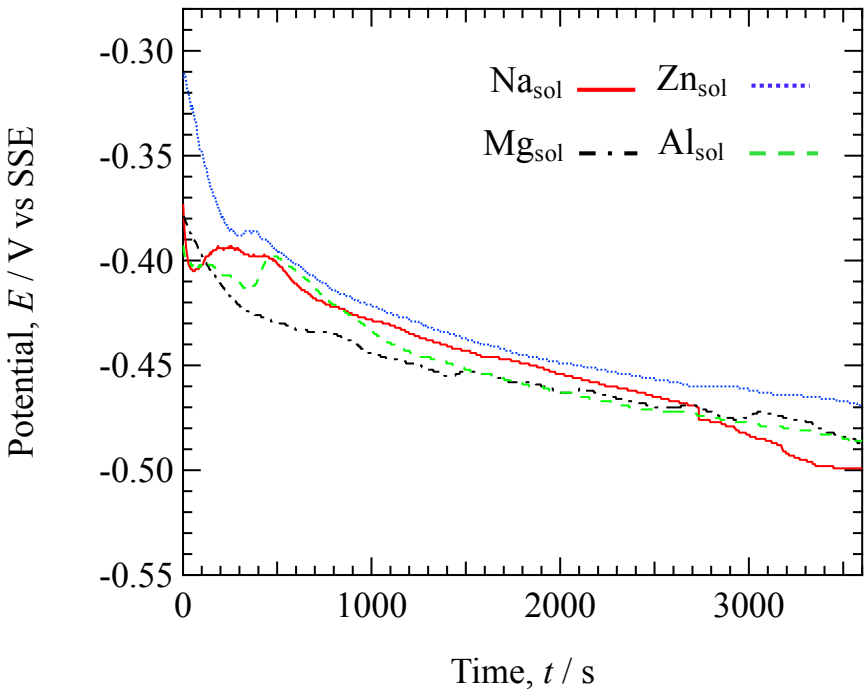

Fig. 4.6 Open circuit potential of specimen immersed in the solutions.

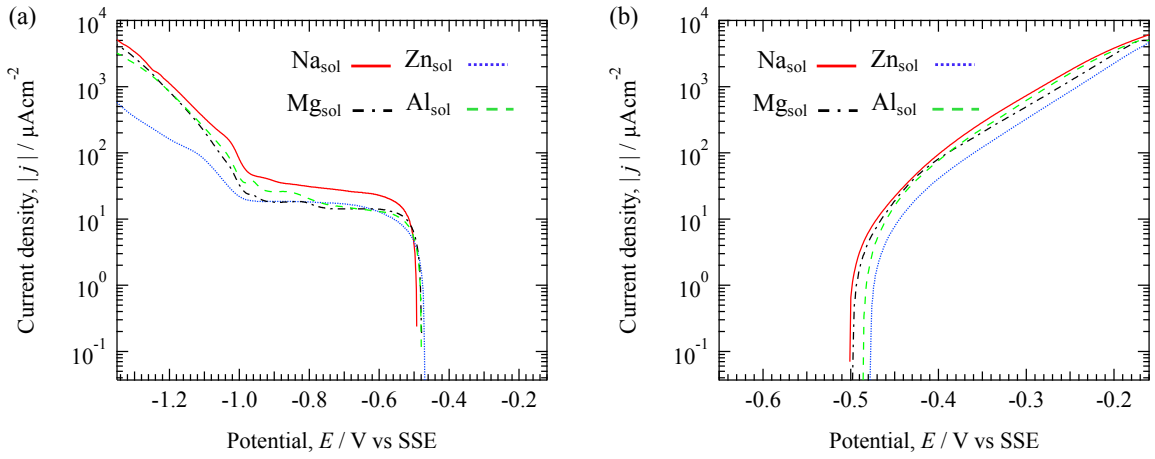

Fig. 4.7 Potentiodynamic (a) cathodic and (b) anodic polarization curves of specimen after immersion in the solutions for 1 h.

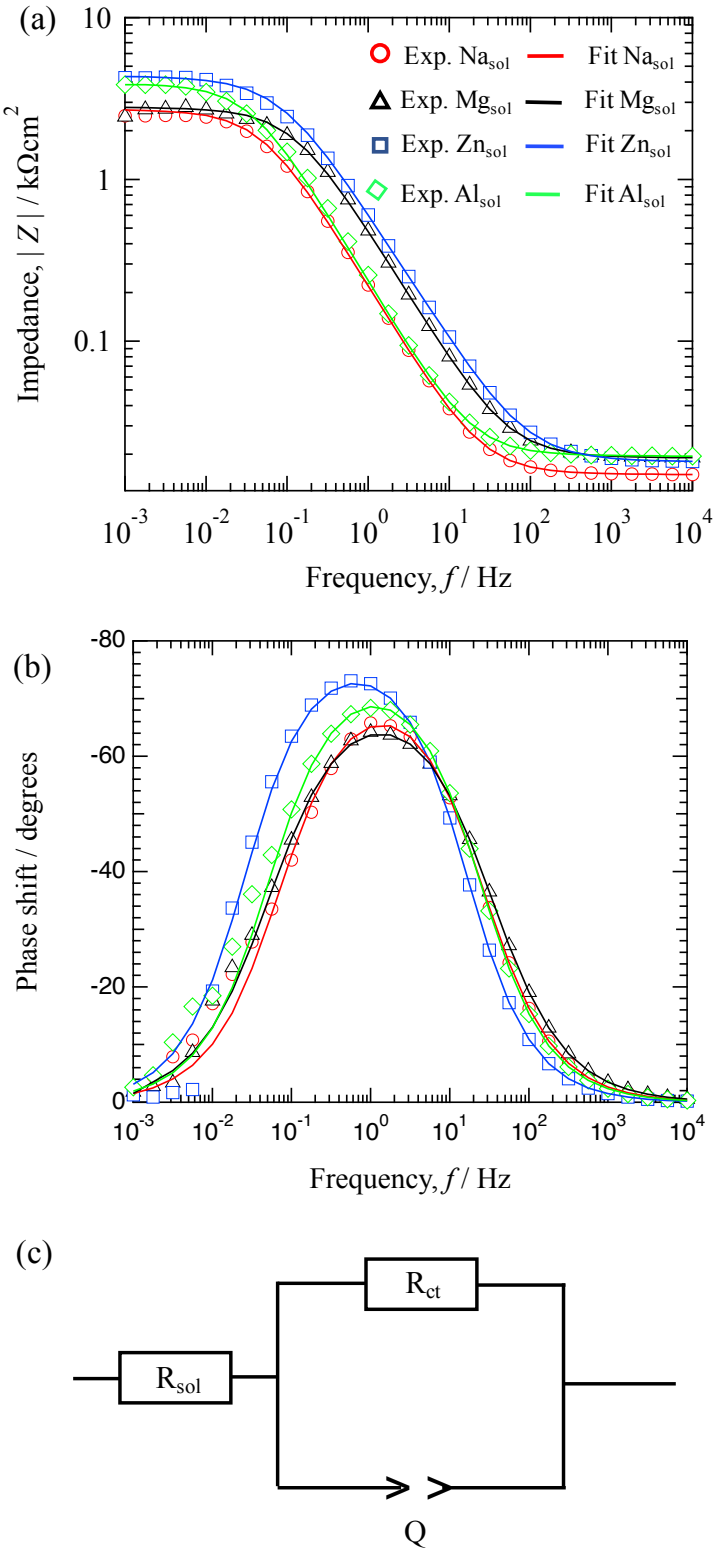

Fig. 4.8 EIS results of specimen after immersion in the solutions for 1 h, Bode diagram of (a) impedance and (b) phase shift, and (c) equivalent circuit used to fit the EIS data.

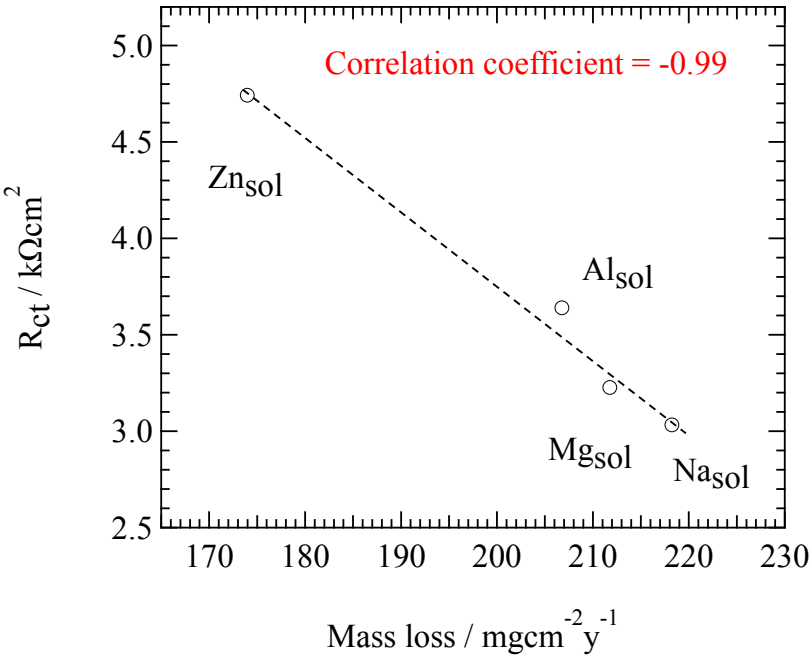

Fig. 4.9 Relationship between charge transfer resistance (R_{ct}) and mass loss of specimen immersed in the solutions.

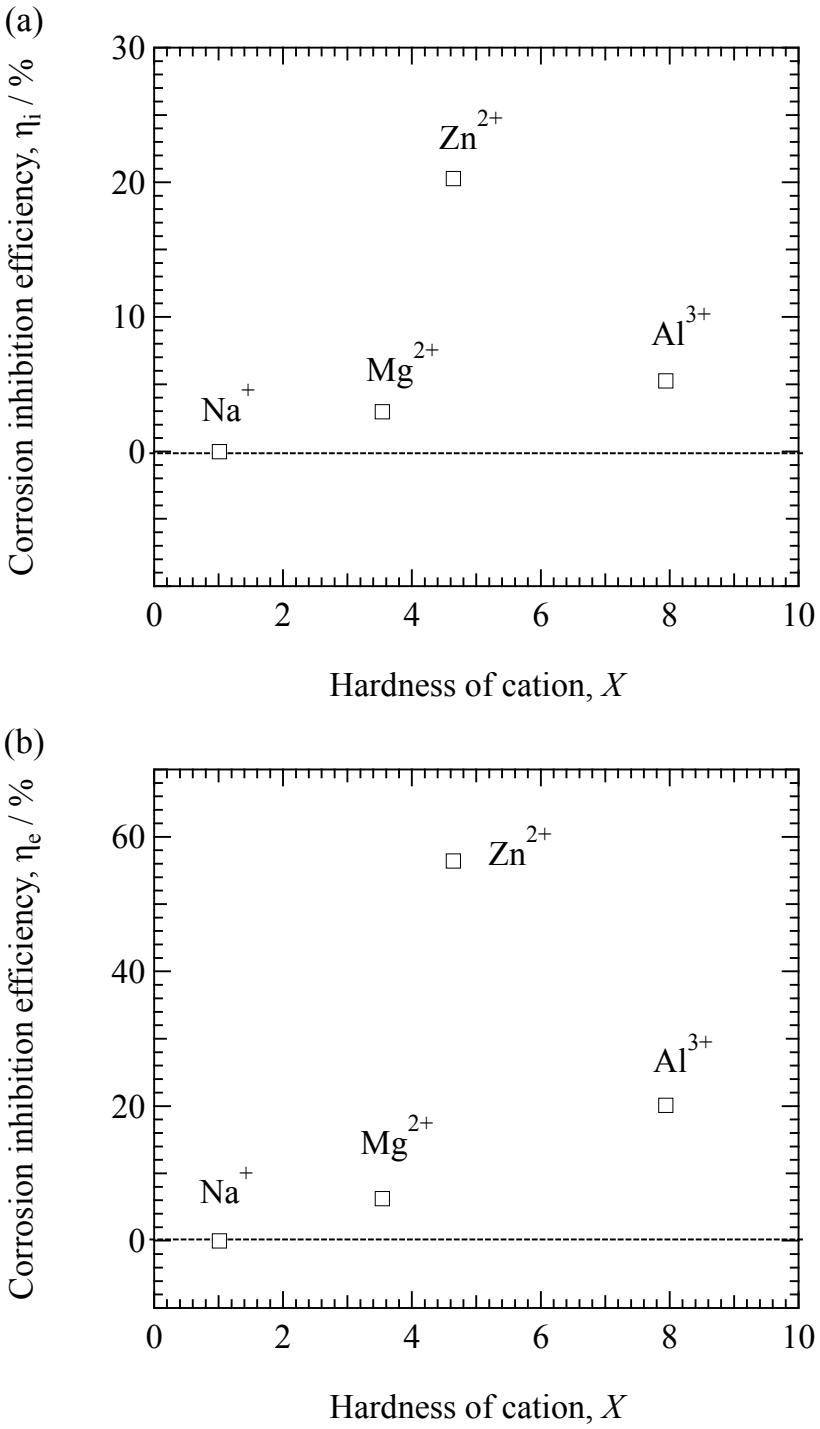

Fig. 4.10 Corrosion inhibition efficiency of metal cations as a function of *X*, (a) based on the immersion tests (b) based on the electrochemical tests.

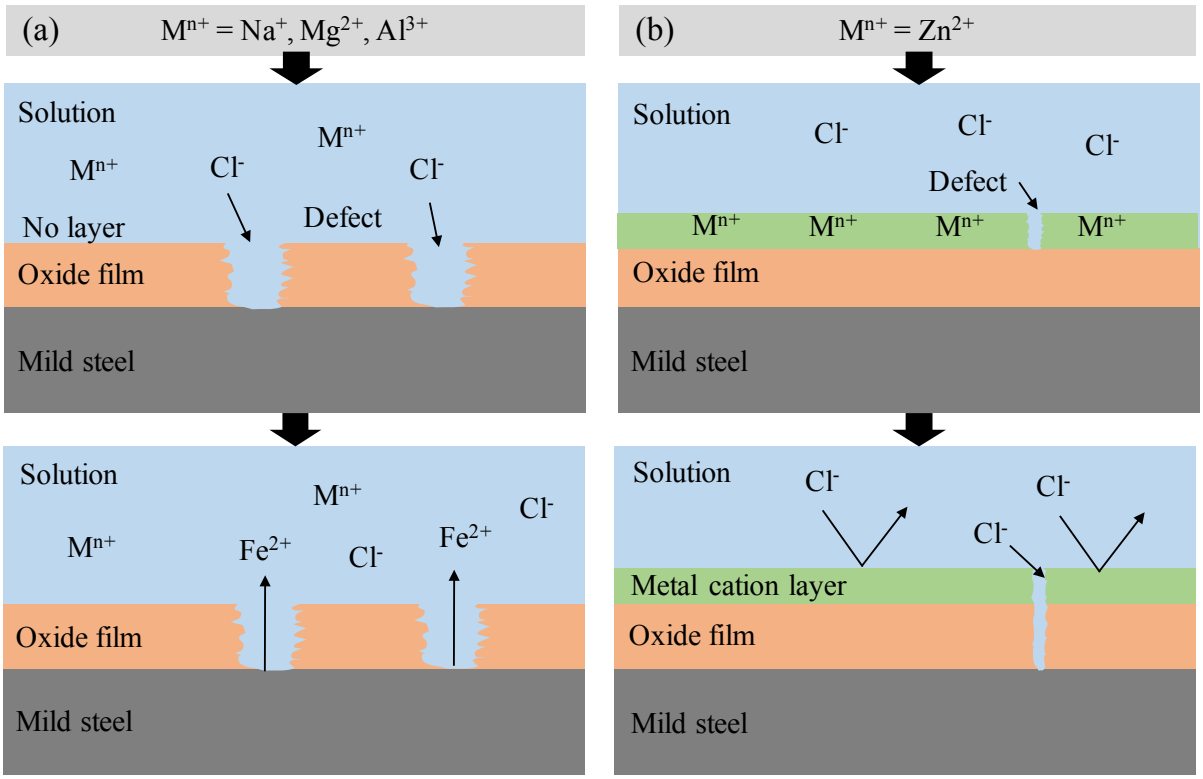

Fig. 4.11 (a) Schematic images of the corrosion process on carbon steel in the solutions with metal cations (M^{n+}= Na^{+}, Mg^{2+} and Al^{3+}). (b) schematic images of the corrosion inhibition process on carbon steel by Zn^{2+} in the solution.

References

1. Y. Y. Chen, S. C. Chung and H. C. Shih, Corros. Sci., 48 (2006) 3547-3564.
2. El-Sayed M. Sherif, A. A. Almajid, A. K. Bairamov and E. Al-Zahrani, Int. J. Electrochem. Sci., 7 (2012) 2796-2810.
3. B. L. Lin, J. T. Lu and G. Kong, Corros. Sci., 4 (2008) 962-967.
4. M. A. Amin, H. H. Hassan and S. A. Rehim, Electrochem. Acta, 53 (2008) 2600-2609.
5. H. J. Engell and N. D. Stolica, Arch. eisenhuttenw, 30 (1959) 239-248.
6. H. J. Engell, Electrochim. Acta, 22 (1977) 987-993.
7. K. G. Weil and D. Menzel, Z. elektrochem., 63 (1959) 669-673.
8. R. T. Foley, Corrosion, 26 (1970) 58-70.
9. B. M. Durodola, J. A. O. Olugbuyiro, S. A. Moshood, O. S. Fayomi and A. P. I. Popoola, Int. J. Electrochem. Sci., 6 (2011) 5605-5616.
10. L. Shuan, Z. Xia, Z. Haichao, S. Huyuan and C. Jianmin, Chinese J. Oceanology and Limnology, 35 (2017) 423-430.
11. E. Kornienko, R. Ossenbrink and V. Michailov, Corros. Sci., 69 (2013) 270-280.
12. A. Diaconu, C. Solomon, L. Benea, V. Dumitrascu and L. Mardare, The aannals of 'dunarea de jos' University of Galati, 3 (2015) 34-39.
13. M. Sakairi, K. Itabashi, Y. Uchida and H. Takahashi, Tetsu-to-Hagané, 92 (2006) 68-74.
14. H. Sun, S. Liu and L. Sun, Int. J. Electrochem. Sci., 8 (2013) 3494-3509.
15. T. Tsuru, Zairyo-to-Kankyo, 59 (2010) 404-409.
16. Md. S. Islam, K. Otani and M. Sakairi, Corros. Sci., 131 (2018) 17-27.
17. K. Otani, M. Sakairi, Corros. Sci., 111 (2016) 302-312.
18. K. Otani, M. Sakairi, R. Sasaki, A. Kaneko and Y. Seki, J. Solid State Electrochemical, 18 (2014) 325-332.
19. K. Otani, Md. S. Islam and M. Sakairi J. Electrochem. Soci., 164 (2017) C498-C504.
20. C. J. Wood, W. J. Marbel, M. Prystupa, M. J. Hudson and D. L. Wilkens, Proc. of 5th Inter. Conf. on water chemistry of nuclear reactor systems, BNES, (1989) 111-120.
21. E. Tada and H. Kaneko, ISIJ International, 51 (2011) 1882-1889.
22. R. R. L. De Oliveira, D. A. C. Albuquerque, T. G. S. Cruz, F. M. Yamaji and F. L. Leite, Federal University of São Carlos, Campus Sorocaba, Brazil, (2011).
23. A. K. Satapathy, G. Gunasekaran, S. C. Sahoo, Kumar Amit and P. V. Rodrigues, Corros. Sci., 51 (2009) 2848-2856.
24. I. Martinez and C. Andrade, Corros. Sci., 50 (2008) 2948-2958.
25. A. Popova, M. Christov and A. Vasilev, Corros. Sci., 49 (2007) 3290-3302.

26. D. A. Lopez, S.N. Simison and S.R. de Sanchez, Corros. Sci., 47 (2005) 735-755.
27. B. Hirschorn, M. E. Orazem, B. Tribollet, V. Vivier, I. Frateur and M. Musiani, Electrochim. Acta, 55 (2010) 6218-6227.
28. M. E. Orazem, I. Frateur, B. Tribollet, V. Vivier and S. Marcelin, J. Electrochem. Soci., 160 (2013) C215-C225.
29. P. C. Torres, T. J. Mesquita and R. P. Nogueira, J. Phys. Chem. 119 (2015) 4136-4147.
30. G. J. Brug, A. L. G. Van Den Eeden, M. S. Rehbach and J. H. Sluyters, J. Electroanal Chem., 176 (1984) 275-295.
31. M. Mahdavian and R. Naderi, Corros. Sci., 53 (2011) 1194-1200.

Chapter 4 has been oriented from the following article

[Md. S. Islam, K. Otani and M. Sakairi, Role of metal cations on corrosion of coated steel substrate in model aqueous layer, *ISIJ International*, 58 (2018) 1616-1622.]

Chapter 5

Temperatures consequence on the mild steel corrosion inhibition by metal cations in high pH Cl^- aqueous solutions

5.1 Introduction

Mild steels are very common and widely used metallic material due to low cost and good mechanical properties. These steels are used in the room temperature and in high temperatures environments such as boilers, liquid transportation pipelines, and machinery parts. Corrosion of steel is a serious problem that depends on some important factors such as dissolved oxygen, the concentration of Cl^-, pH, and temperature of the environment. There are many studies have been carried out on corrosion of mild steel in aqueous environments [1-8]. Passive films on the surface have a great influence on corrosion inhibition of steel, and the stability and structure of the passive films depend on the environmental conditions. The passive films are usually destroyed in presence of anions especially Cl^- [9-12], and after the destruction of the passive films, metal dissolution starts with a coupled of electrochemical reactions (cathodic and anodic reactions).

There are several studies have been carried out that metal cations inhibit the corrosion of steel in aqueous solutions [13-26]. Drazic *et al*. [13] explained that Cd^{2+}, Mn^{2+}, and Zn^{2+} inhibited the corrosion of iron by lowering the hydrogen evaluation reaction rate in H_2SO_4 solutions at room temperature. Leidheiser Jr. *et al*. [14, 15] explained that some metal cations act as effective corrosion inhibitors under certain experimental condition. They reported that Sn^{2+} and Pb^{2+} effectively inhibited the corrosion of iron and steel in acid solutions by changing the protective nature of oxide on the surface, and Co^{2+} and Ni^{2+} effectively inhibited the corrosion of galvanized steel in 3% NaCl solutions by forming an insoluble barrier layer at the metal surface. Application of rare earth (RE) metal cation as a corrosion inhibitor was first proposed by Goldie and McCarrol in 1984. Khedr *et al*. [16, 17] reported the effect of some metal cations (K^+, Mg^{2+}, Cu^{2+}, Zn^{2+}, Hg^{2+}, Cd^{2+}, Co^{2+}, and Ni^{2+}) on the corrosion of aluminum in neutral and acid Cl^- solutions. In some nuclear power reactors, zinc ions are added into high temperature water for suppressing corrosion of the reactor component materials [18]. Zhang *et al*. [19] reported that the inhibition effect of metal cations (Na^+, Ca^{2+}, Mn^{2+}, and Zn^{2+}) to intergranular stress corrosion cracking of sensitized type-304 stainless steel in 10^{-5} mol L^{-1} sulfate solutions, and they described that hard metal cation forms a layer on the surface by bonding with the surface film. Amadeh *et al*. [20] introduced the usages of rare earth metal cations (Ce^{4+} and

La^{4+}) as corrosion inhibitors for carbon steel in aerated NaCl solution. Otani *et al*. [21] reported that the inhibition effects of metal cations (Na^+, K^+, Ca^{2+}, Mg^{2+}, Zn^{2+}, and Ni^{2+}) on corrosion of A3003 aluminum alloy in model tap water at room temperature, and they [22] also reported that Zn^{2+} and Al^{3+} significantly inhibited the corrosion of mild steel in model fresh water. Islam *et al*. [23-25] reported that Zn^{2+} inhibited the corrosion of mild steel in Cl^- aqueous solution at room temperature, and they [26] also explained that Al^{3+} significantly inhibited the corrosion of type-304 stainless steel in 0.5 mol L^{-1} Cl^- aqueous solution at room temperature. Several researchers also reported that metal cations significantly enhanced the inhibition performance of some corrosion inhibitors [27-34]. Therefore, it has been established that metal cations significantly inhibit the corrosion of metal in aqueous solutions.

Almost all of the studies regarding the corrosion inhibition of metal by metal cations have been carried out at room temperature, and the inhibition effects were not fully explained as well. Moreover, it is still not fully elucidated the mechanism of corrosion inhibition effect of metal cations on mild steel in freshwater with a high pH at different temperatures. In the case of boiler feed water, the pH is usually controlled at a value of higher than 9.5 [35-38] to avoid the formation of carbonic acid (H_2CO_3) and its species (HCO_3^-) [39]. Therefore, the experimental tests were carried out in freshwater with a high pH (9.5). The present research purpose is to clarify the mechanism of inhibition effects of metal cations on corrosion of mild steel at different temperatures in the high pH simulated freshwater.

5.2 Experimental

5.2.1 Specimens

The composition (mass%) of mild steel samples used for this experiment was as follows: C = 0.02; Mn = 0.18; P = 0.015; S < 0.01; and Fe = balance. The mild steel sheet of 0.7 mm thickness was cut into 7 × 7 mm to carried out different tests. For the potentiodynamic polarization and EIS measurements, each specimen was connected to a conductive wire and embedded in epoxy resin leaving the exposed surface. For the immersion corrosion tests, the specimens were also embedded in resin leaving the exposed surface. For both experiments, the exposed surface of specimens was mechanically abraded with a series of SiC abrasive paper up to #4000 grit size. In the case of immersion tests, the abraded specimens were removed from the resin beforehand the tests. Before the experimental tests, all the specimens were ultrasonically cleaned in ethanol and in highly purified water.

5.2.2 Test solutions

Three different salt solutions of 10^{-4} mol L^{-1} $MgCl_2$ (Mg_{sol}), 10^{-4} mol L^{-1} $ZnCl_2$ (Zn_{sol}) and 10^{-4} mol L^{-1} $AlCl_3$ (Al_{sol}) were prepared. The Cl^- concentration also plays an important role in corrosion of metals, therefore, the Cl^- concentration of all solutions was adjusted to 10^{-3} mol L^{-1} by NaCl, which is similar to that of generally freshwater [22]. These solutions were used as test solutions together with 10^{-3} mol L^{-1} NaCl (Na_{sol}) which was used as a reference solution. The pH of the solutions was adjusted to about 9.5 using 10^{-1} mol L^{-1} NaOH (Table 5.1). Fig. 5.1 shows the condition of solutions before the experiment.

The pH of the solutions before and after immersion tests was measured by the pH meter (Eutech Instruments, Cyber-Scan 6000). Water used in this experiment was highly purified (MILLIPORE, Simplicity UV). Before the experiment, all the test solutions were colorless and transparent (Fig. 5.1). All the chemicals used in this study were commercially available special grade and were obtained from Kanto Chemical Co. Ltd.

5.2.3 Immersion tests

Specimens were immersed in each solution at 25, 50 and 80°C for 1, 2 and 3 d. Immersion tests were carried out with three replicates of each solution in each temperature at a time. The exposed surface area of the specimens was 0.49 cm^2, and the test was carried out by keeping the solutions open to the air. The mass of the specimen before and after the tests were measured using a microbalance (METTLER TOLEDO MX5, Pro FACT) to obtain the mass change. Corrosion rates (C_R) and the corrosion inhibition efficiencies (η_i) of metal cations were calculated based on the mass loss during the immersion tests by the Eqs. (5.1) and (5.2) [23-26].

$$C_R\ (\mu m/y) = \frac{M_1 - M_2}{D \times S \times t} \times 365 \times 10000 \qquad (5.1)$$

Here M_1 (g) is the mass of the specimen before immersion, M_2 (g) is the mass of the specimen after immersion, D (g/cm^3) is the density of the specimen, S (cm^2) is the surface area of the specimen and t (d) is the immersion time.

$$\eta_i\ (\%) = \frac{Na_{CR} - CAT_{CR}}{Na_{CR}} \times 100 \qquad (5.2)$$

Here Na_{CR} is the corrosion rate of specimens immersed in the Na_{sol}, and CAT_{CR} is the corrosion rate of specimens immersed in Mg_{sol}, Zn_{sol}, and Al_{sol}, and the corrosion inhibition efficiency of Na^+ is considered zero.

A digital camera (Nikon, D80) was used for taking the photograph of the sample surface and the glass bottle overview before and after immersion, a scanning electron microscope (SEM,

JEOL, JSL6510-LA) was used for high magnification observation of the sample surface. The red color corrosion products (rust) formed on the specimen surface after immersion in the solutions was analyzed by X-ray diffraction (XRD, Rigaku, SmartLab). For the processing of XRD data, integrated X-ray powder diffraction software (PDXL2) was used. The surface roughness [40, 41] was measured by atomic force microscope (AFM, SPA400) using dynamic force mode with the cantilever type, SI-DF40. X-ray photoelectron spectroscope (XPS, JEOL, JPS-9200) was used for surface analysis. During the XPS analysis, Al Kα was used as an X-ray source (1486.6 eV), and the measurement region of photoelectrons was 3 × 3 mm. The XPS depth analysis was carried out by sputtering of Ar ion. The sputtering time was converted to depth by the sputtering rate of SiO_2. Before the surface observation and analysis, the immersed specimens were cleaned ultrasonically first in ethanol and then in highly purified water.

5.2.4 Electrochemical measurements

Electrochemical tests were performed in a conventional three-electrode cell using a potentiostat (IVIUM TECHNOLOGIES, Pocketstat) connected to a personal computer. The tests were carried out with three replicates of each solution at 25, 50 and 80°C. Before the tests, the specimens were immersed in the solutions for 1 h at these temperatures. A Pt plate was used as the counter electrode and the reference electrode was Ag(s)|AgCl(s)|Cl^- (aqueous, saturated KCl) (SSE). The exposed surface area of the specimen (working electrode) in the solution was 0.49 cm^2. The polarization measurements were carried out from immersion potential to the cathodic and anodic direction with a scan rate of 60 mV/min. The cathodic and anodic scan was started individually to obtain the specific electrochemical properties of mild steel immersed in the solutions with metal cations. The EIS measurements were carried out at open circuit potential in the frequency range from 10 kHz to 1 mHz and modulation amplitude of 10 mV. The IVIUM software was used to fit the EIS data.

5.3 Results and discussions

5.3.1Immersion tests

The appearances of solutions and specimens after immersion in the solutions for 1, 2 and 3 d at 25, 50 and 80°C are shown in Fig. 5.2. The brightness of the solutions is different and the Zn_{sol} is brighter as compared to the other solutions after 3 d immersion at 80°C. Red corrosion products are observed on the specimens and in the solutions. The appearances (red) and the

brightness of the solutions may indicate the degree of corrosion of steel in the solutions. Fig. 5.3 a) and b) show the appearances of the specimen surfaces after immersion in the solutions for 3 d at 25, 50 and 80°C before the ultrasonic cleaning and after the ultrasonic cleaning respectively. All the cases red corrosion products (rust) are found on the specimen surface (Fig. 5.3 a)).

The pH of the test solutions before and after immersion for 3 d at 25, 50 and 80°C are shown in Table 5.1, where pH_{int} is the initial pH of solutions and pH_{corr} is the pH obtained after immersion tests. The pH is decreased after immersion (pH_{corr}) in all solutions. Several researchers also reported that the pH of solutions in such cases decreases with the hydrolysis of Fe^{2+} and Fe^{3+} [42, 43].

The mass of specimens was measured after immersion in the solutions at 25, 50 and 80°C for 1, 2 and 3 d. Fig. 5.4 a) shows the average mass changes of specimens with time. After 1 d immersion in the solutions, it is found that the average mass changes of specimens immersed in Mg_{sol}, Zn_{sol}, and Al_{sol} are nearly the same, whereas the average mass change of the specimen immersed in Na_{sol} is different. The average mass changes of the specimen are gradually increasing with time. After 2 and 3 d immersion, each solution shows the different mass change, and Na_{sol} shows the highest mass change and Zn_{sol} shows the lowest mass change as compared to the other solutions at these temperatures.

Fig. 5.4 b shows the corrosion rates at different temperatures. The corrosion rate is gradually increasing with increasing the temperature. Na_{sol} shows the highest and Zn_{sol} shows the lowest corrosion rate as compared to the other solutions at all these temperatures. This result indicates that Zn_{sol} has better corrosion inhibition ability than other solutions.

5.3.2 Surface observations and analysis

Corrosion behavior of specimens can be clarified by surface morphology changes that are occurred due to immersion in the solutions. Fig. 5.5 shows the SEM images of surface morphology of specimens immersed in the solutions at 25, 50, and 80°C for 1, 2 and 3 d. SEM images clearly indicate the numbers of pits and grain boundaries that are observed on the surface of a specimen immersed in Na_{sol}, Mg_{sol}, and Al_{sol} at all the temperatures. The clearer grain boundaries are observed with increasing the temperatures on the surface of a specimen immersed in Na_{sol}, Mg_{sol}, and Al_{sol}. These clear grain boundaries and pits represent the severe corrosion occurred on the mild steel surface. Some small pits are observed on the surface of the specimen immersed in Zn_{sol}, and the numbers of pits are increased with increasing the

temperatures. The results of surface observations are in good agreement with the corrosion rate as shown in Fig. 5.4 b).

The surface roughness of each specimen was measured by AFM after immersed in the solutions at 25, 50, and 80°C for 3 d, and the AFM-3D images are shown in Fig. 5.6. Different surface roughness is observed of a specimen immersed in the different solutions with metal cations. The average surface roughness (R_a) was calculated from the respective 3D images to enumerate the surface roughness. The calculated R_a values are shown in Fig. 5.7 as a function of temperature. Average surface roughness is increased with increasing the temperature. However, the specimen immersed in the Zn_{sol} shows the lowest R_a as compared to the specimen immersed in the other solutions. Zn related products may be covered the steel surface and thus metal dissolution reactions were inhibited. From this reason, relatively smooth surface is observed on the specimen immersed in Zn_{sol} as compared to the others. These results correspond well to the surface observation by SEM as shown in Fig. 5.5.

The red corrosion products (rust) formed on the specimen surface shown in Fig. 5.3 a) were analyzed by XRD to determine the crystal structure. Fig. 5.8 shows XRD patterns of the corrosion products on specimens after immersion in the solution at 80°C for 3 d. The results indicate that the corrosion products formed on the specimen surface in all the solutions consisted of FeOOH, Fe_3O_4, Fe_2O_3, and Fe, and metal cations are not detected in the corrosion products.

The specimen surfaces were examined by XPS to clarify the existence of metal cations on the mild steel surface after immersion in the solutions. Fig. 5.9 shows the results of XPS analysis of the surface of the specimen immersed in each solution at 25, 50, and 80°C for 1 h. In the wide spectra, Zn2p1/2 and Zn2p3/2 peaks are observed on the specimens immersed in the solution at all temperatures whereas the other peaks of Na1s, Mg1s, and Al2p3/2 are not observed on the specimen immersed in the corresponding solution. This result indicates that only Zn existed on the surface after immersion in the Zn_{sol} at all the experimental temperatures. XPS narrow scan with depth was performed to determine how Zn was distributed in the surface films. The right side of Fig. 5.9 shows the XPS narrow spectra of Zn2p3/2 with depth at 25, 50 and 80°C. At 25°C, sharp peaks of Zn2p3/2 appear with a depth of approximately 100 nm. It means that the thickness of the Zn-layer is about 100 nm. At 50 and 80°C, peaks of Zn2p3/2 also appear and the thickness of the layers is approximately 20 nm and 10 nm respectively. The results suggest that Zn-layer exists on the surface at all temperatures. However, the thickness of the Zn-layer is decreased with increasing the temperature.

XPS narrow scan was analyzed to determine the chemical state of Zn that is existed on the steel surface. Fig. 5.10 shows the XPS narrow scan of Zn2p3/2 at 25, 50, and 80°C. In the case of 25°C (Fig. 5.10 a)), the peak of Zn2p3/2 is observed at 1022.5 eV (binding energy) which is related to the peak of Zn^{2+} and it is indicated to the formation of zinc hydroxide ($Zn(OH)_2$) [44, 45]. Leygraf *et al*. [46] and Winiarski *et al*. [47] reported that the formation of corrosion product of Zn^{2+} as zinc hydroxide ($Zn(OH)_2$) and carbonate based corrosion product as hydrozincite ($Zn_5(CO_3)_2(OH)_6$) on the steel surface at normal temperature. In the case of 50°C and 80°C (Fig. 5.10 b) and c)), the peak of Zn2p3/2 is observed at 1021.4 eV (binding energy) which is also related to the peak of Zn^{2+} and it is indicated to the formation of zinc oxide (ZnO) [44, 45]. Zhang [48] reported that $Zn(OH)_2$ is generally the corrosion product formed in Zn^{2+} containing water in the temperature range 0-30°C, and ZnO is the corrosion product in the temperature range 30-90°C. Winiarski *et al*. [47] also reported that ZnO is formed at the temperature around 60°C. From the XPS results, it can be suggested that Zn^{2+} existed on the specimen surface as zinc hydroxide ($Zn(OH)_2$) and carbonate based zinc corrosion product as hydrozincite ($Zn_5(CO_3)_2(OH)_6$) at 25°C, and at the higher temperatures (50°C and 80°C), Zn^{2+} existed on the specimen surface as zinc oxide (ZnO) after immersion in the solution, and it further made a chemical bond with the passive films which led to a layer of Zn^{2+}. The layers of Zn^{2+} may have protected the steel from the Cl^- attack and inhibited the metal dissolution reactions. The Zn-layer may have also some defects, and the area of defect may be increased with increasing the temperature. The defects of the film led to the formation of pits [34] and the numbers of pits were increased with increasing the temperatures which were shown in Fig. 5.5. From this reason, the metal dissolution rate in Zn_{sol} (Fig. 5.4 b)) also increased with increasing the temperature. Na^+ cannot exist on the steel surface as oxides or hydroxides in the experimental conditions [22-26, 49]. From the mass change after 1 d immersion in the solutions (Fig. 5.4 a)), it is signifying that Mg^{2+} and Al^{3+} may be precipitated as oxides or hydroxides on the steel surface which inhibited the metal dissolution like Zn^{2+}. However, the precipitations of both Mg^{2+} and Al^{3+} might not be stable and cannot form a bond with the surface film with time as larger mass changes were observed compared with Zn_{sol} after 2 and 3 d immersion (Fig. 5.4 a)). From these reasons the corrosion rate in Mg_{sol} and Al_{sol} showed lower than that in Na_{sol} and higher than that in Zn_{sol}, and the lowest corrosion rate was observed in Zn_{sol} as compared to the other solutions (Fig. 5.4 b)) at the experimental temperatures.

5.3.3 Electrochemical tests

5.3.3.1 Polarization curves

From the immersion tests results (surface observations and analysis), Zn_{sol} showed better corrosion inhibition ability than other solutions. The polarization behavior was studied only in Na_{sol} and Zn_{sol} at 25, 50 and 80°C. Fig. 5.11 a) shows the cathodic polarization curves in Na_{sol} and Zn_{sol} at 25, 50 and 80°C. At 25°C, the higher current density is observed in Na_{sol} than that in Zn_{sol} at around the potential -0.5 V, and after the potential at around -1.0 V, there is no significant difference in the current density between Na_{sol} and Zn_{sol}. At 50°C, the higher current density is observed in Zn_{sol} than that in Na_{sol} at around the potential -0.5 V. The potential at -1.0 V, Zn_{sol} shows lower current density than that in Na_{sol}. At 80°C, Na_{sol} shows higher current density than that in Zn_{sol} at the potential around -1.0 V. Fig. 5.11 b) shows the anodic polarization curves in Na_{sol} and Zn_{sol} at 25, 50 and 80°C. Lower current density is observed in Zn_{sol} than that in Na_{sol} at all the experimental temperatures. Therefore, it can be suggested that Zn^{2+} containing solution has inhibition ability both in cathodic and anodic reactions as compared to the Na^{+} containing solution at these temperatures.

5.3.3.2 EIS tests

EIS tests were carried out at 25, 50 and 80°C, and Figs. 5.12 a) to f) show the Bode diagram of impedance and phase shift plots. Fig. 5.12 g) shows the equivalent circuit which was used to fit the experimental data that simulates an electrode with a protective film having defect [34, 50]. The fitted lines are also shown in Figs. 5.12 a) to f) which were calculated by the equivalent circuit (Fig. 5.12 g)). The equivalent circuit consists (Fig. 5.12 g)) of bulk solution resistance (R_{sol}), resistance of the defects in the protective film (R_d), charge transfer resistance at the metal/solution interface inside the defect (R_{ct}), constant phase element of the double layer at the defect interface (Q_{dl}) and the constant phase element of the protective film (Q_f). The fitted lines correspond well to the experimental plots (Figs. 5.12 a) to f)). Some pits were also observed on the specimen immersed in the Zn^{2+} containing solutions (as shown in Fig. 5.5) suggesting that the protective Zn-layer formed on the immersed specimens had some defects that led to the formation of pits [34]. The number of pits on the specimen immersed in the Zn^{2+} containing solution was increased with increasing the temperature (as shown in Fig. 5.5). The magnitude of impedance indicates the corrosion resistance of steel in the solutions [22-24]. From Fig. 8 a) to f), it is found that the impedance and phase shift are decreased with increasing the temperature. However, Zn_{sol} shows the highest impedance and highest phase shift as compared to the other solutions at all the experimental temperatures. These results indicate that

Zn_{sol} has better corrosion resistance ability than the other solutions at the experimental temperatures.

Calculated electrochemical impedance parameters of mild steel after immersion in the solutions for 1 h at different temperatures are shown in Table 5.2. The corrosion resistance (R_c) and the inhibition efficiency (η_e) were calculated by the Eqs. (5.3) and (5.4):

$$R_c\ (k\Omega cm^2) = R_d + R_{ct} \tag{5.3}$$

$$\eta_e\ (\%) = (R_{c\_sol} - R_{c\_ref})/R_{c\_sol} \times 100 \tag{5.4}$$

Where R_{c_sol} and R_{c_ref} are the values of corrosion resistance in the solutions (Mg_{sol}, Zn_{sol}, and Al_{sol}), and in the reference solution (Na_{sol}). From Table 5.2, the η and R_c of Zn_{sol} show the highest value as compared to the other solutions at all the experimental temperatures. These results indicate that the charge transfer may be inhibited by the Zn-layer (in the Zn^{2+} containing solution) that was formed on the steel surface and the inhibition ability was decreased with increasing the temperature. The value of Q_{dl} in Zn^{2+} containing solution (Zn_{sol}) is lower than that in other solutions at all the temperatures. The decrease in Q_{dl} value indicates that the defect in the film is decreased on mild steel [34, 51]. The results obtained from the EIS tests are in good agreement with the immersion tests results.

5.3.4 Corrosion inhibition efficiency

From the experimental results, it was found that the solutions containing different metal cations showed different corrosion rate. Therefore, it is considered that Zn^{2+} and Al^{3+} significantly inhibited the metal dissolution in the solutions, and Zn^{2+} containing solution showed the lowest corrosion rate at all the experimental temperatures (as shown in Fig. 5.4 b)) as compared to the other solutions. The corrosion inhibition efficiencies of metal cations were calculated based on the immersion tests and Fig. 5.13 shows the corrosion inhibition efficiencies of metal cations as a function of temperature in which mean values of mass loss data were used. The corrosion inhibition efficiencies are changed with temperatures. The corrosion rate is increased with increasing the temperature (as shown in Fig. 5.4 b)), however, corrosion inhibition efficiencies of metal cations are increased at a higher temperature (80°C). Because at higher temperature corrosion is rapidly increased in Na_{sol} as compared in the other solutions, and efficiencies were calculated by comparing the Na_{sol}. Zn^{2+} and Al^{3+} show higher corrosion inhibition efficiency at 80°C, and Zn^{2+} shows the highest corrosion inhibition efficiency as compared to the other metal cations at all the experimental temperatures.

5.3.5 Corrosion inhibition mechanism

From the above experimental results, Zn^{2+} effectively inhibited the mild steel corrosion in model fresh water as compared to the other metal cations used in this study at the experimental temperatures. Based on the experimental results, a possible corrosion inhibition mechanism of mild steel by Zn^{2+} can be proposed. Fig. 5.14 shows the Zn^{2+} layer formation on the specimen surface at different temperatures and corrosion inhibition mechanism in the solution. At 25°C, the Zn^{2+} layer is formed on the steel surface (Fig. 5.14 a) and b)). Zn^{2+} layer may not cover all the exposed surface of the steel, and the layer contains some defects. The Cl^- attack at the defects and initiate the metal dissolution (Fig. 5.14 b)). When the temperature is increased to 50°C, the thickness of the Zn^{2+} layer is decreased and the area of the defects is increased (Fig. 5.14 c)). The possible reasons by which the thickness of Zn-layer decreased and the area of the defects increased are as follows:

a) The composition of Zn-layer is changed with temperature as discussed in 'surface observations and analysis.' At 25°C, $Zn(OH)_2$ and $Zn_5(CO_3)_2(OH)_6$ are formed, and at 50 and 80°C, ZnO is formed [44-48]. Thus, the layer thickness is decreased at a higher temperature.

b) Dissolution rate in the layer may increase with increasing the temperature.

c) Some part of the layer may be removed while metal dissolution occurs, and the area of defects increased at a higher temperature.

Due to the above-mentioned reasons, the corrosion rate is increased at a higher temperature as compared to that at a lower temperature. When the temperature is further increased to 80°C, the thickness of the Zn^{2+} layer is decreased and the area of the defects is also increased (Fig. 5.14 d)). From these points of view, the corrosion rate is increased at 80°C as compared to 25 and 50°C. However, Zn^{2+} containing solution showed the lowest corrosion rate as compared to the other solutions at all the experimental temperatures due to inhibition of the corrosion reactions by the Zn^{2+} layer that was formed on the steel surface.

5.4. Conclusion

The effects of metal cations on the corrosion inhibition of mild steel in simulated fresh water at 25, 50 and 80°C were investigated by immersion tests, EIS tests and surface investigations were carried out by SEM, AFM, and XPS. It can be concluded as follows:

- The corrosion rate of steel in each solution obtained from the immersion corrosion tests decreased in the order of $Na_{sol} > Mg_{sol} > Al_{sol} > Zn_{sol}$.
- Comparatively smooth surfaces of the specimens immersed in the Zn_{sol} were observed by SEM and AFM.
- The charge transfer resistance (R_{ct}) from the EIS tests decreased in the order of $Zn_{sol} > Al_{sol} > Mg_{sol} > Na_{sol}$. From this, it was suggested that Zn^{2+} present in the aqueous solution had a function of suppressing corrosion.
- From the XPS analysis of the sample surface immersed in different solutions, only Zn^{2+} was detected on the specimen immersed in the Zn_{sol}.
- Zn^{2+} formed a layer on the surface films and protected the steel surface from Cl^- attack and inhibited the corrosion reactions.

Table 5.1 pH of solutions before and after the immersion tests for 3 d at 25, 50 and 80℃.

Solution of metal cations	pH_{int}	pH_{corr}		
		25°C	50°C	80°C
Na_{sol}	9.6	6.4	6.6	6.4
Mg_{sol}	9.6	6.7	6.8	6.5
Zn_{sol}	9.6	6.5	6.9	6.6
Al_{sol}	9.5	6.6	7.0	6.5

Table 5.2 Calculated electrochemical impedance parameters of mild steel after immersion in the solutions for 1 h at different temperatures.

Solutions	R_c ($k\Omega cm^2$)			Q_{dl} ($\mu s^n \Omega^{-1} cm^{-2}$)			n_{dl}			η (%)		
	25°C	50°C	80°C	25°C	50°C	80°C	25°C	50°C	80°C	25°C	50°C	80°C
Na_{sol}	20.48	2.63	2.26	5.55	2.55	2.40	0.76	0.58	0.58	-	-	-
Mg_{sol}	22.89	2.94	2.45	5.25	2.05	2.38	0.76	0.62	0.64	11	10	7
Zn_{sol}	309.59	7.54	3.15	0.17	0.76	0.48	0.84	0.66	0.65	93	65	28
Al_{sol}	56.98	5.38	2.79	2.45	1.56	0.58	0.81	0.68	0.63	64	51	19

Fig. 5.1 Test solutions condition before the experiment

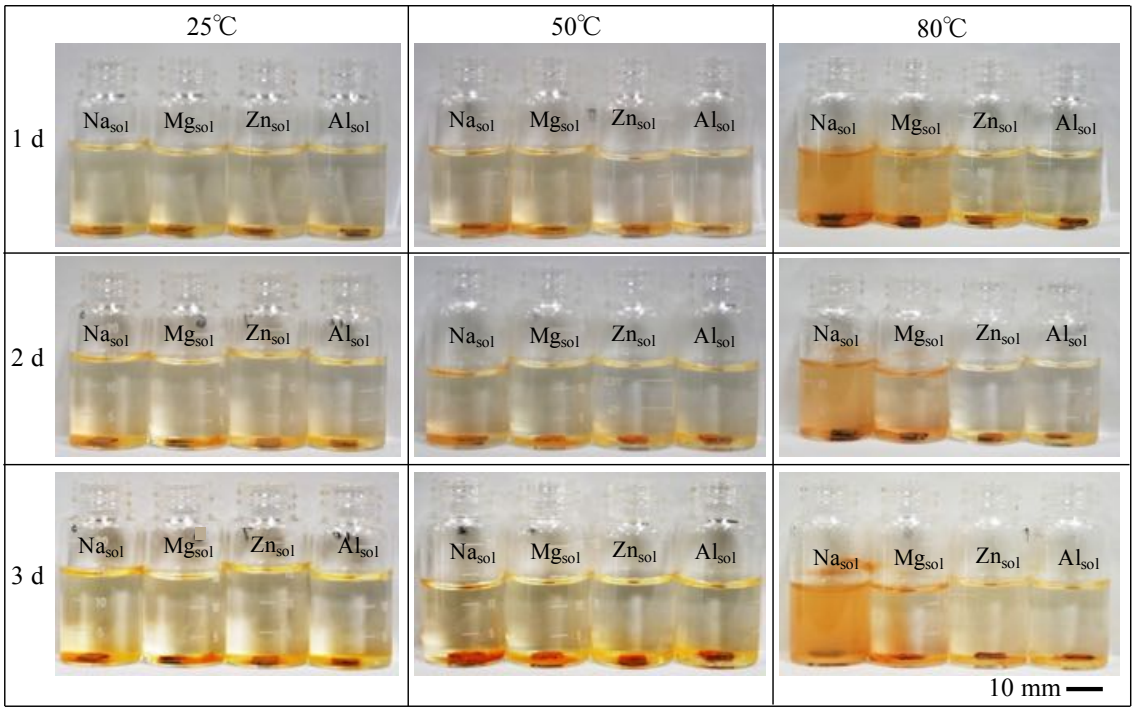

Fig. 5.2 Appearance of solutions and specimens after immersion in the solutions for 1, 2 and 3 d at 25, 50 and 80°C.

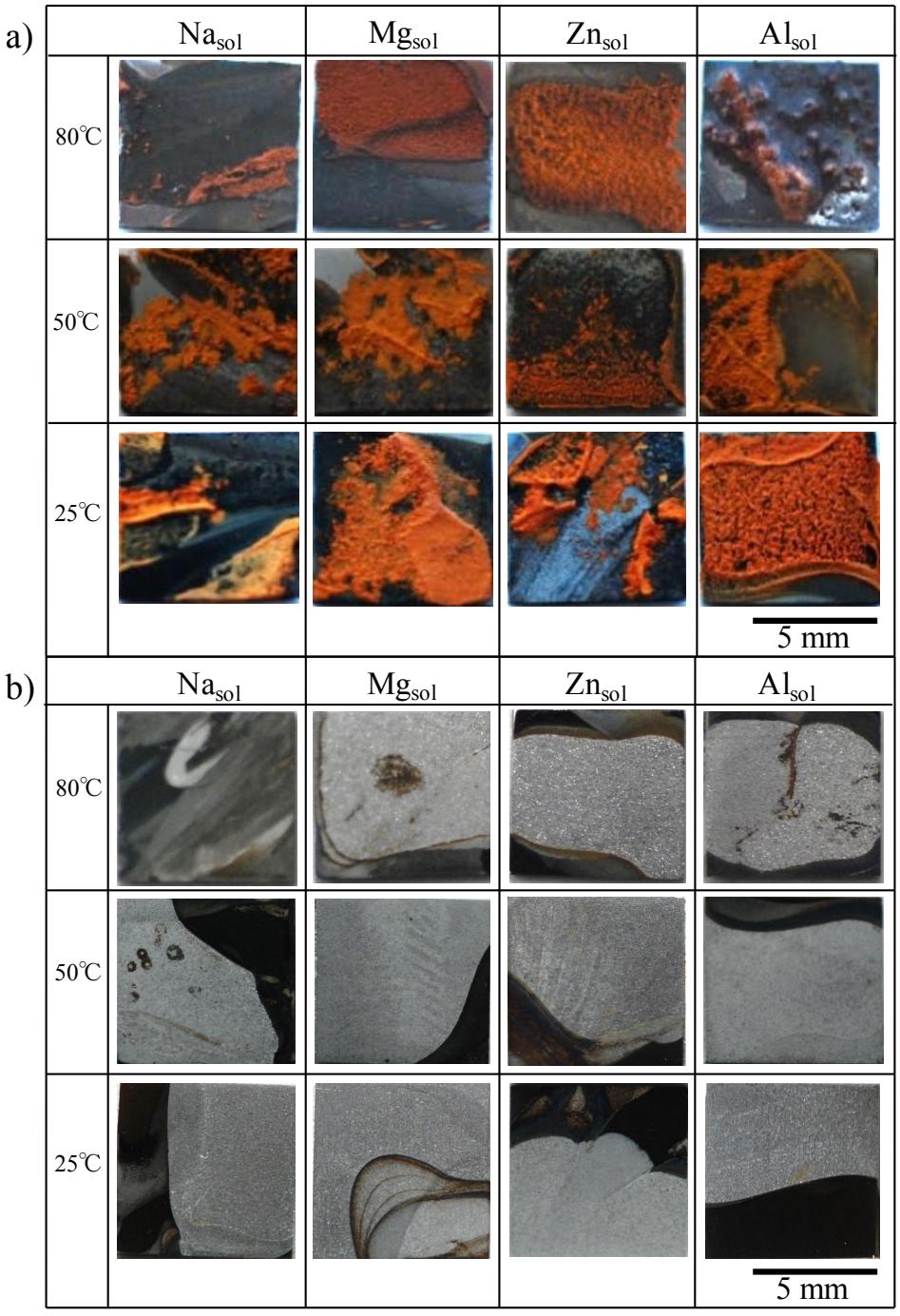

Fig. 5.3 Appearance of specimen surface after immersion in the solutions for 3 d at 25, 50 and 80°C a) before ultrasonic cleaning, b) after ultrasonic cleaning.

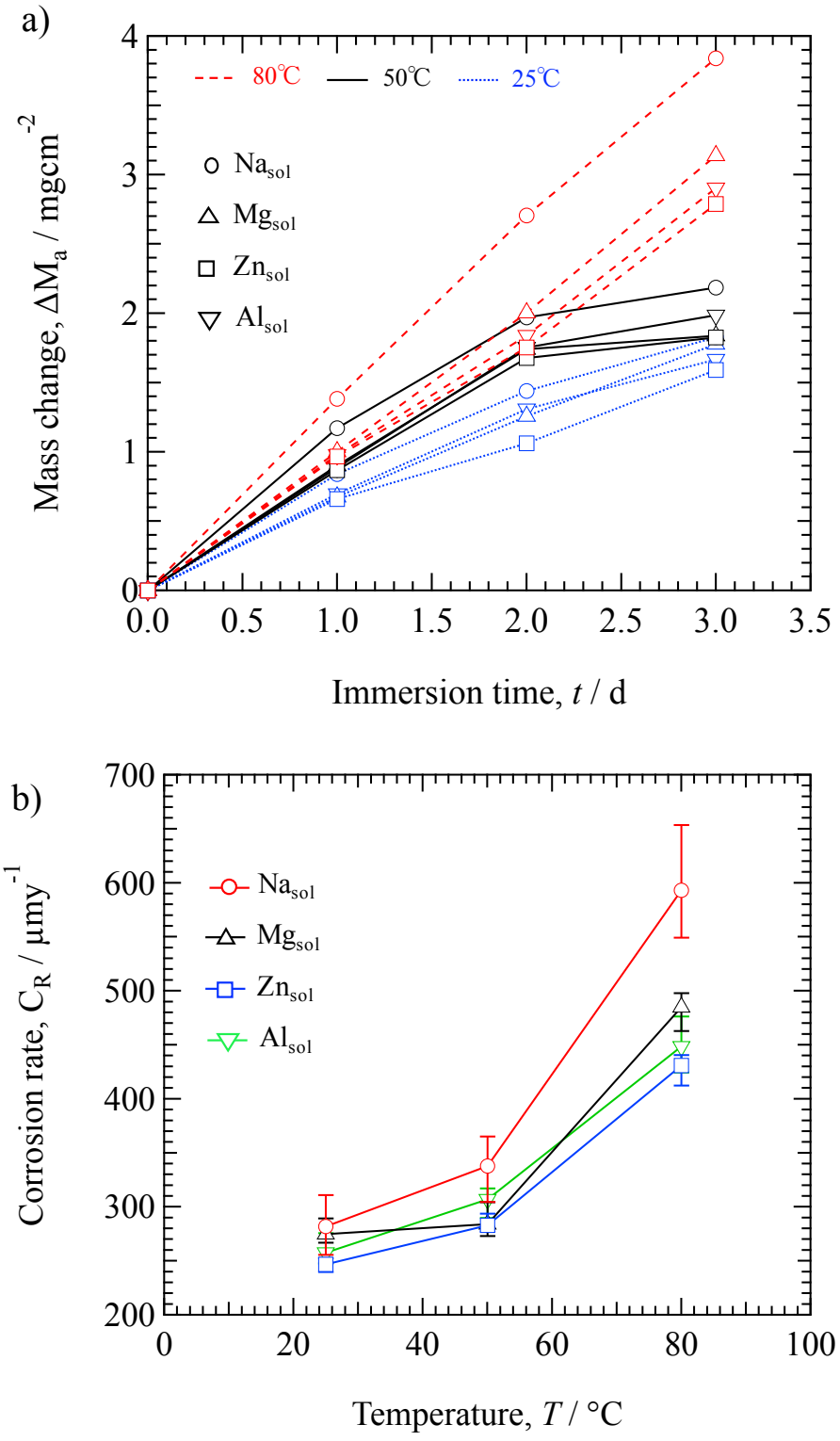

Fig. 5.4 a) Mass changes of specimens with immersion time and b) Corrosion rate at different temperatures.

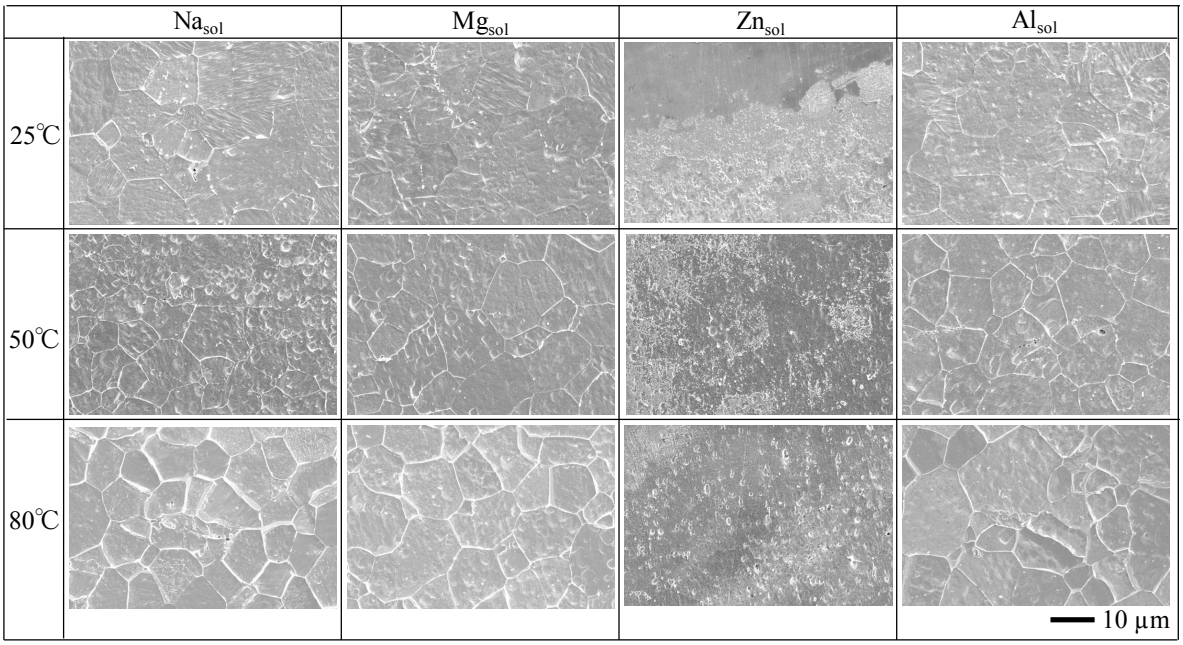

Fig. 5.5 Surface SEM images of specimen after immersion in the solutions for 3 d at 25, 50 and 80°C.

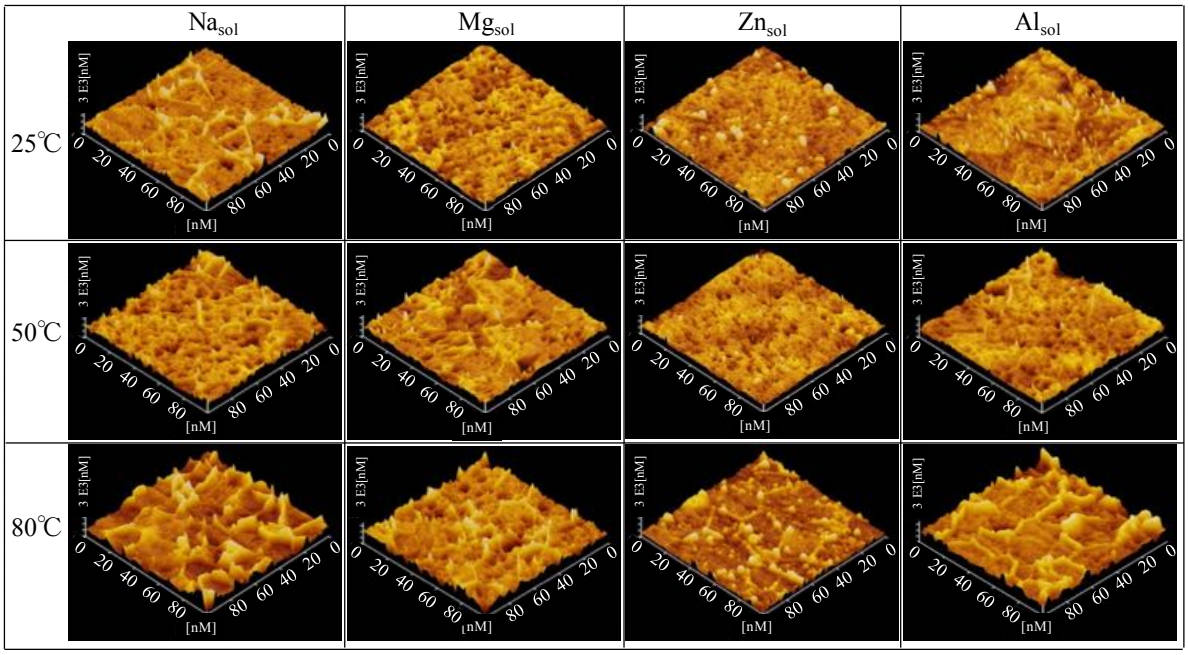

Fig. 5.6 AFM 3D images of specimen surface after immersion in the solutions for 3 d at 25, 50 and 80°C.

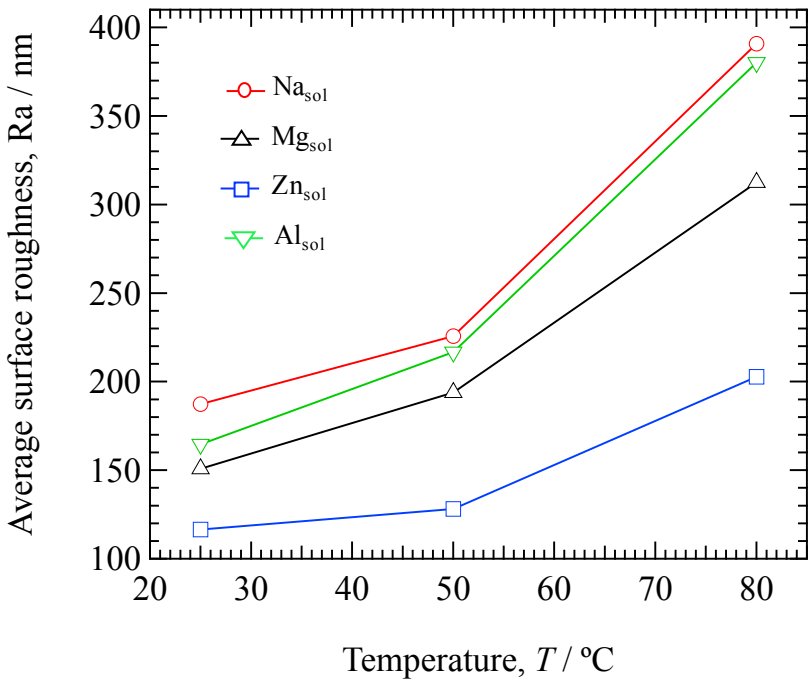

Fig. 5.7 Average surface roughness of specimens as a function of temperature after immersion in the solutions for 3 d.

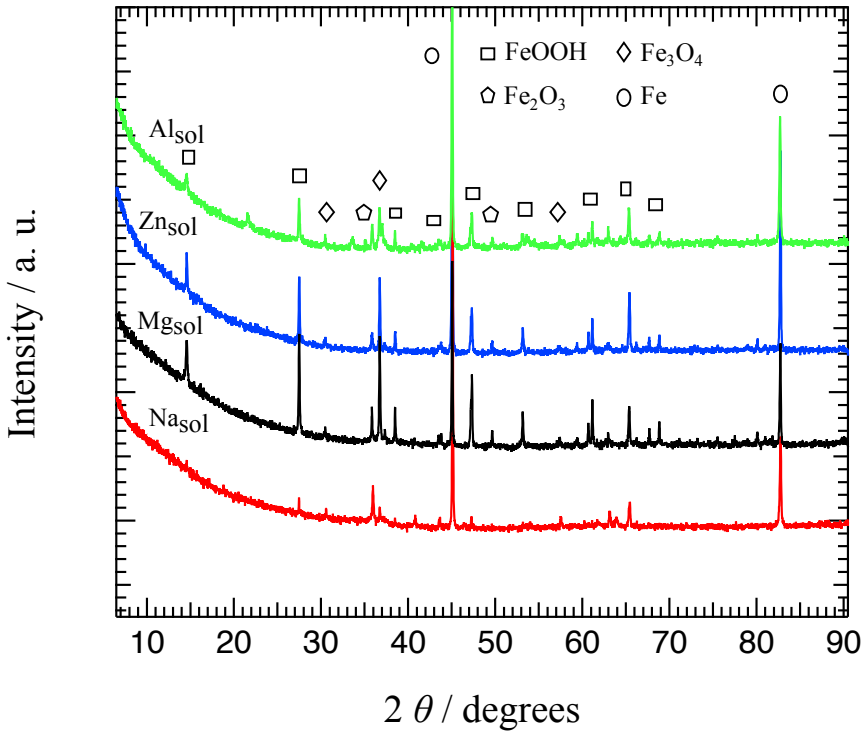

Fig. 5.8 XRD patterns of the corrosion products (rust) formed on specimens after immersion in the solutions for 3 d at 80°C.

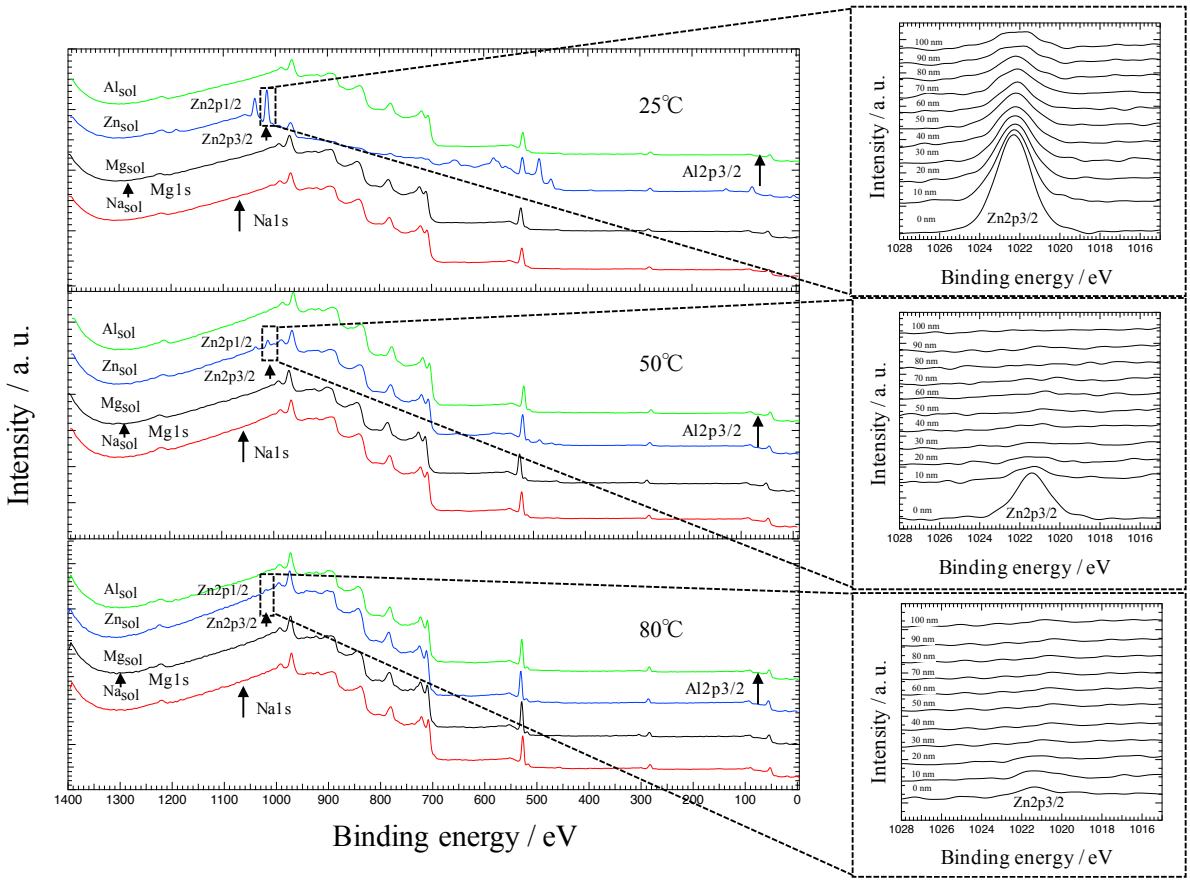

Fig. 5.9 XPS wide spectra of specimen surface after immersion in the solutions for 1 h, and narrow spectra of Zn2p3/2 with depths (inset) at 25, 50 and 80°C.

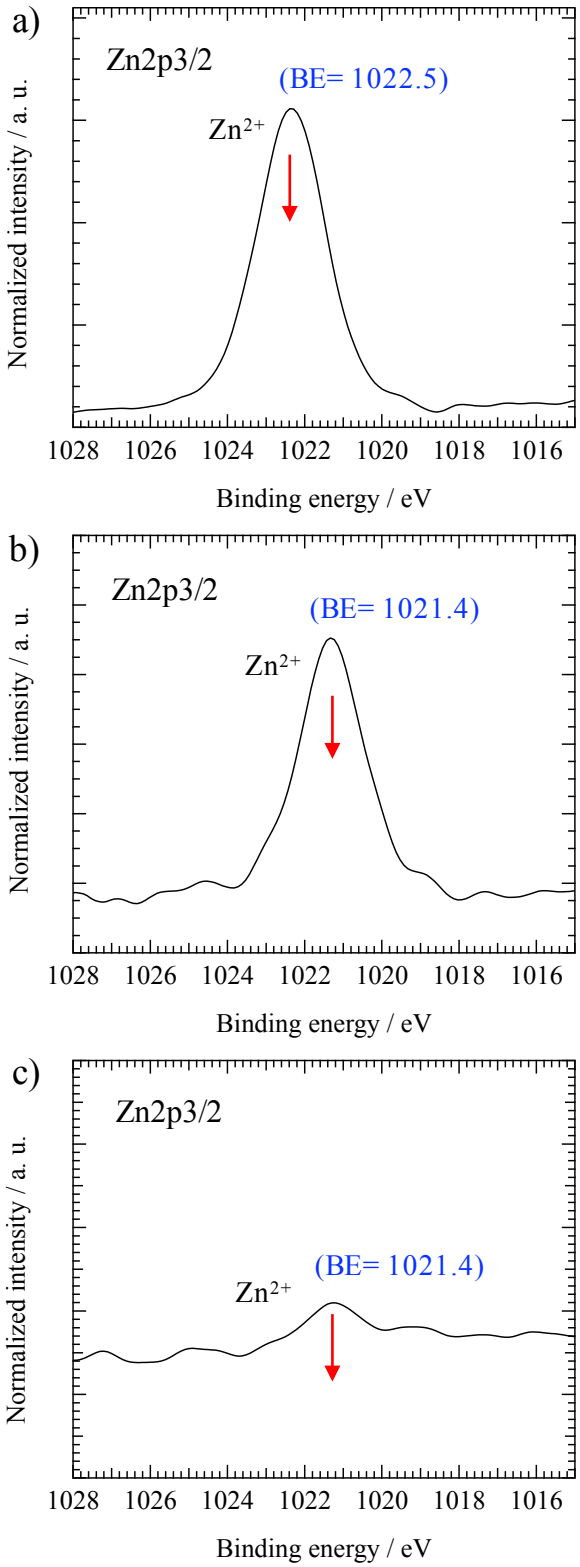

Fig. 5.10 XPS narrow spectra of Zn2p3/2 with chemical state and binding energy of specimen surface after immersion in the solutions for 1 h at a) 25°C, b) 50°C and c) 80°C.

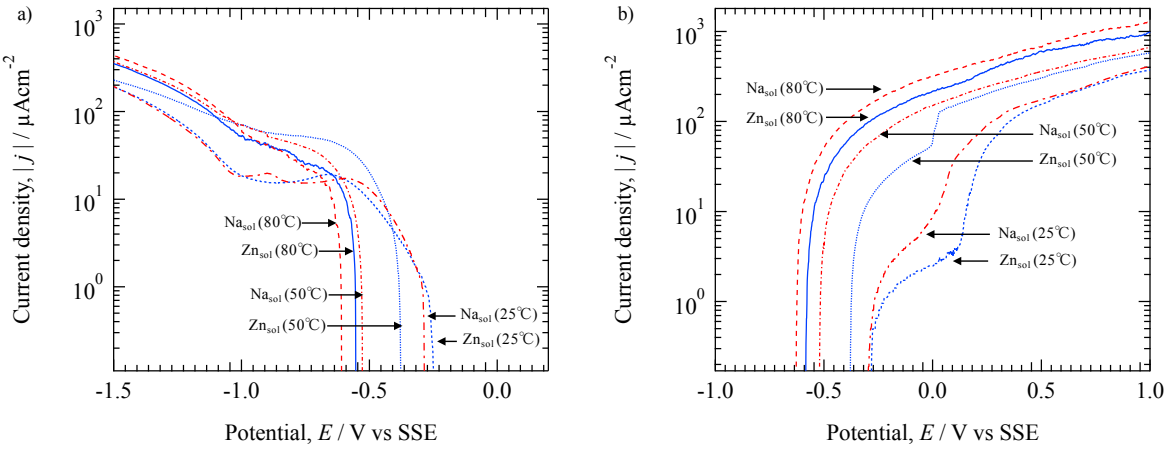

Fig. 5.11 Potentiodynamic a) cathodic and b) anodic polarization curves after immersion in the Na_{sol} and Zn_{sol} for 1 h at 25, 50 and 80°C.

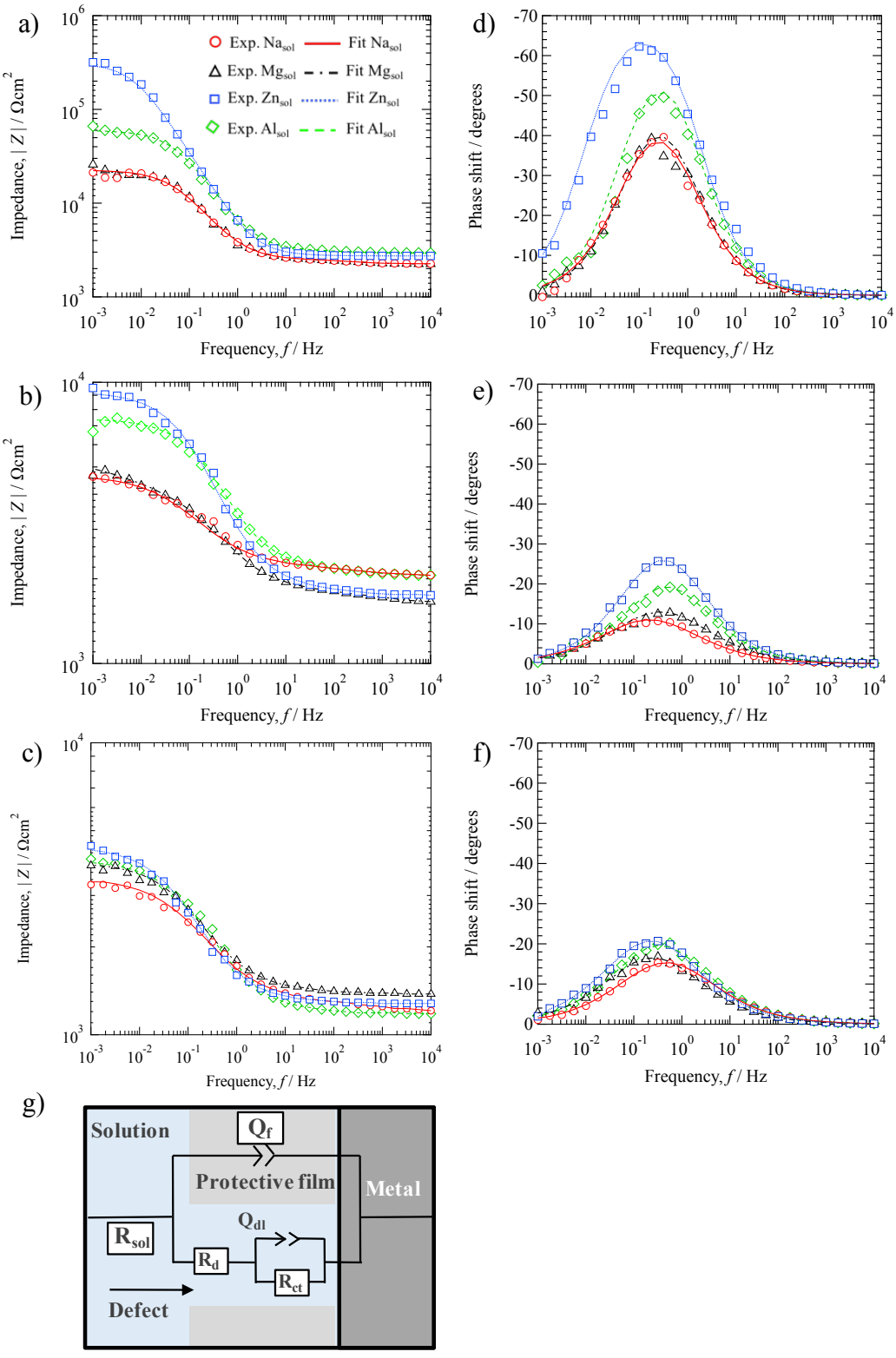

Fig. 5.12 Bode diagram of impedance and phase shift plots a) and d) at 25°C, b) and e) at 50°C, c) and f) at 80°C, and g) Schematic representation of the equivalent circuit of mild steel electrode with a protective film having a defect.

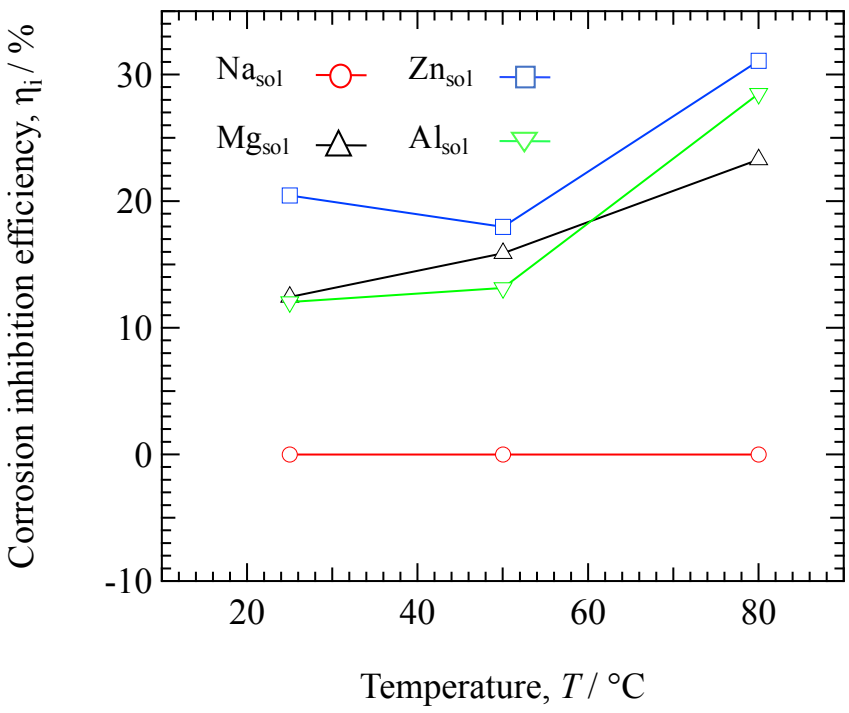

Fig. 5.13 Corrosion inhibition efficiency of metal cations as a function of temperature.

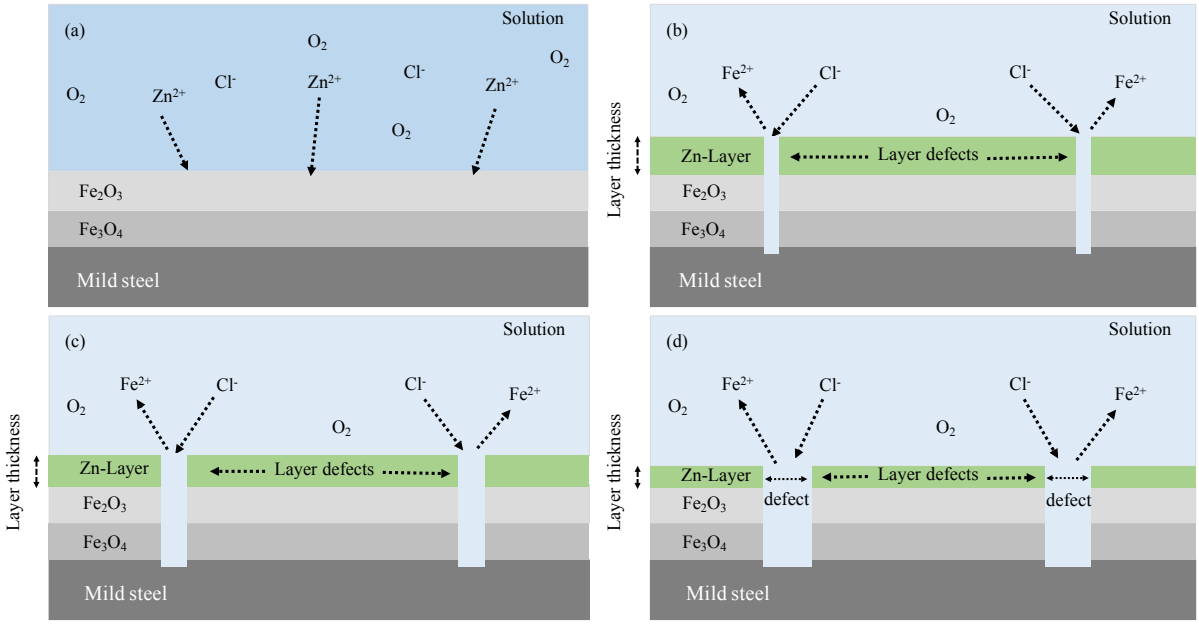

Fig. 5.14 Corrosion inhibition mechanism of mild steel by the Zn-layer at different temperatures, a) Formation of Zn-layer on the steel surface, b) Cl^- attack at the defect sites and initiation of metal dissolution at 25°C, c) decreasing of Zn-layer thickness and increasing of defect area at 50°C, d) decreasing of Zn-layer thickness and increasing of defect area at 80°C.

References

1. C. P. Gardiner and R. E. Melchers, Corros. Sci., 44 (2002) 2665-2673.
2. R. E. Melchers, Corros. Sci., 48 (2006) 4174-4201.
3. G. A. Rassoul and D. R. Rzaige, Iraqi J. Chem. Petroleum Eng., 9 (2007) 37-41.
4. A. C. Uzorh, IJES, 2 (2013) 18-24.
5. H. Xian-jun, Z. Bi-ming, C. Shao-hui, F. Feng and J. Jian-qing, J. Iron Steel Res. Int., 20 (2013) 47-52.
6. G. S. Vasyliev, Corros. Sci., 98 (2015) 33-39.
7. S. Cao, D. Liu, P. Zhang, L. Yang, P. Yang, H. Lu and J. Gui, Scientific Reports, 7 (2017).
8. X. Zheng, M. Gong, Q. Li and L. Guo, Scientific reports, 8 (2018).
9. R. T. Foley, Corros., 26 (1970) 58-70.
10. D. D. Macdonald, J. Electrochem. Soc., 139 (1992) 3434-3449.
11. E. McCafferty, Introduction to Corrosion Science, Springer, (2010) 283-286.
12. Y. Song, G. Jiang, Y. Chen, P. Zhao and Y. Tian, Scientific Reports, 7 (2017).
13. D. M. Drazic and L. Z. Vorkapic, Corros. Sci., 18 (1978) 907-910.
14. H. Leidheiser Jr., Corros., 36 (1980) 339-345.
15. H. Leidheiser Jr. and I. Suzuki, J. Electrochem. Soc., 128 (1981) 242-249.
16. M. G. A. Khedr and A. M. S. Lashien, J. Electrochem. Soc., 136 (1989) 968-972.
17. M. G. A. Khedr and A. M. S. Lashien, Corros. Sci., 33 (1992) 137-151.
18. J. N. Esposito, G. Economy, W. A. Byers, J. B. Esposito, F. W. Pement, R. J. Jacko, C. A. Bergmann, in: Proc. 5th Int. Sympo. Environmental degradation of materials in nuclear power systems-water reactors, American Nuclear Society, (1992) 495-503.
19. S. Zhang, T. Shibata, T. Haruna, Corros. Sci., 47 (2005) 1049-1061.
20. A. Amadeh, S. R. Allahkaram and S. R. Hosseini, Anti-Corrosion Methods and Materials, 55 (2008) 135-143.
21. K. Otani, M. Sakairi, R. Sasaki, A. Kaneko, Y. Seki and D. Nagasawa, J. Solid State Electrochem., 18 (2014) 325-332.
22. K. Otani, M. Sakairi, Corros. Sci., 111 (2016) 302-312.
23. Md. S. Islam, K. Otani and M. Sakairi, Corros. Sci., 131 (2018) 17-27.
24. Md. S. Islam, K. Otani and M. Sakairi, ISIJ International, 58 (2018) 1616-1622.
25. Md. S. Islam and M. Sakairi, J. Electrochem. Soci., 166 (2019) C83-C90.
26. Md. S. Islam, K. Otani and M. Sakairi, Corros. Sci., 140 (2018) 8-17.
27. I. Singh and M. Singh, Corrosion, 43 (1987) 425-429.

28. I. Felhosi, Zs. Keresztes, F. H. Karman, M. Mohai, I. Bertoti and E. Kalman, J. Electrochem. Soc., 146 (1999) 961-969.
29. J. C. Lin, S. L. Chang and S. L. Lee, J. App. Electrochem., 29 (1999) 911-918.
30. J. Telegdi, M. M. Shaglouf, A. Shaban, F. H. Karman, I. Betroti, M. Mohai and E. Kalman, Electrochim. Acta. 46 (2001) 3791-3799.
31. M. Abdallah and M. M. El-Naggar, Mater. Chem. Phys., 71 (2001) 291-298.
32. S. Sathiyanarayanan, C. Jeyaprabha, S. Muralidharan and G. Venkatachari, App. Surf. Sci., 252 (2006) 8107-8112.
33. M. Prabakaran, M. Venkatesh, S. Ramesh and V. Periasamy, App. Surf. Sci., 276 (2013) 592-603.
34. K. Otani, Md. S. Islam and M. Sakairi, *J. Electrochem. Soci.*, 164 (2017) C498-C504.
35. L. I. Pincus, Practical boiler water treatment-introducing air-conditioning system, McGraw-Hill Book Company, New York, (1962) 37-38.
36. S. Basu, Boiler chemistry control and treatment of feed water, Elsevier SciTech Connect, (2015).
37. Handbook of Industrial Water Treatment, General Electric Company, (2012).
38. E. J. Bonner, Water treatment for modern boiler plant in the paper industry, Prime Conference Proc. Instn. Mech. Engrs., (1967) 24-33.
39. I. G. Wenten, Khoiruddin, F. Arfianto and Zudiharto, Desalination 314 (2013) 109-114.
40. A. K. Satapathy, G. Gunasekaran, S. C. Sahoo, K. Amit and P. V. Rodrigues, Corros. Sci., 51 (2009) 2848-2856.
41. R. R. L. De Oliveira, D. A. C. Albuquerque, T. G. S. Cruz, F. M. Yamaji and F. L. Leite, Measurement of the nanoscale roughness by atomic force microscopy: Basic principles and applications, Federal University of São Carlos, Campus Sorocaba, Brazil, (2011).
42. L. N. Mulay and P. W. Selwood, J. Am. Chem. Soc., 77 (1955) 2693-2701.
43. F. H. Sweeton and C. F. Baes Jr., J. Chem. Thermodynamics, 2 (1970) 479-500.
44. R. Al-Gaashani, S. Radiman, A. R. Daud, N. Tabet and Y. Al-Douri, Ceramics Int., 39 (2013) 2283-2292.
45. N. Gogurla, A. K. Sinha, S. Santra, S. Manna and S. K. Ray, Scientific Reports, 4 (2014).
46. C. Leygraf and T. Graedel, Atmospheric Corrosion, *Wiley Interscience*, 131 (2001).
47. J. Winiarski, W. Tylus, K. Winiarska, I. Szczygiel and B. Szczygiel, *J. Spectroscopy*, (2018) 1-14.
48. X. G. Zhang, Corrosion and Electrochemistry of Zinc, Springer, Boston, MA, (1996).

49. M. Pourbaix, Atlas of electrochemical equilibria in aqueous solutions, National Association of Corrosion Engineers, Huston, Texas (1974).
50. F. Vacandio, Y. Massiani, P. Gergaud and O. Thomas, Corros. Sci., 359 (2000) 221-227.
51. M. Mahdavian and R. Naderi, Corros. Sci., 53 (2011) 1194-1200.

Chapter 5 has been oriented from the following article

[Md. S. Islam and M. Sakairi, Corrosion inhibition of mild steel by metal cations in high pH simulated freshwater at different temperatures, *Corros. Sci.*, 153 (2019) 100-108.]

Chapter 6
Inhibition performance of Zn^{2+} concentrations on the corrosion of mild steel in Cl^- aqueous solutions

6.1 Introduction

Modern civilization mostly depends on the utilization of metallic materials. Mild steel is one of the best choice for the consumer and frequently used in the industry and as daily used objects [1-6]. Although the mild steel is characterized by low cost and very good mechanical properties, it has poor corrosion resistance and is readily corroded in many environments [4-6]. Many studies have been carried out on mild steel corrosion in aqueous environments [1-3, 7-14]. Oxide films on the surface strongly influence the corrosion inhibition of these steels. The oxide films are usually destroyed in the presence of anions, especially Cl^- [15-19], and after destroying of the films, metal dissolution proceeds with the anodic and cathodic reactions.

Corrosion control of metal in aqueous solutions is an important issue, and using inhibitors is a common method for corrosion protection. Metal cations are able to inhibit the corrosion of metal in aqueous solutions, and there are some researches have been carried out showing that Zn^{2+} inhibits the corrosion of steel in aqueous solutions [20-29]. Drazic *et al*. [20] stated that Zn^{2+}, Cd^{2+}, and Mn^{2+} inhibited the corrosion of Fe by suppressing the current density in H_2SO_4 solutions. Khedr *et al*. [21, 22] described the effect of some cations (K^+, Mg^{2+}, Cu^{2+}, Zn^{2+}, Hg^{2+}, Cd^{2+}, Co^{2+}, and Ni^{2+}) on the corrosion of aluminum in neutral and acid Cl^- solutions. Zn^{2+} is used in some power plant to suppress the corrosion of the reactor materials [23]. Zhang *et al*. [24] investigated the inhibition effects of metal cations (Na^+, Ca^{2+}, Mn^{2+}, and Zn^{2+}) on intergranular stress corrosion cracking of a sensitized type-304 stainless steel in 10^{-5} M sulfate solutions, and they reported that hard metal cations formed a layer on the steel surface by bonding with the surface films. Otani *et al*. [25] investigated the inhibition effects of metal cations (Na^+, K^+, Ca^{2+}, Mg^{2+}, Zn^{2+}, and Ni^{2+}) on corrosion of the A3003 aluminum alloy in model tap water, and they [26] also described that Zn^{2+} inhibited the corrosion of mild steel in model freshwater significantly. Islam *et al*. [27, 28] reported that Zn^{2+} inhibited the corrosion of mild steel in Cl^- aqueous solutions. They [29] also found that Zn^{2+} inhibited the corrosion of type-304 stainless steel in 0.5 M Cl^- aqueous solution appreciably. Other research has reported that Zn^{2+} enhanced the inhibition of some corrosion inhibitors in aqueous solution significantly [30-35]. Prosek *et al*. [36] stated that the improved corrosion performance is attributed to the inhibition of oxygen reduction by Zn/Mg/Al deposits on the cut edges of coated steels.

Thebault *et al*. [37] reported that Zn^{2+} is more efficient than Mg^{2+} to inhibit cathodic reactions on the steel surface in 0.03 M NaCl solutions. They [38] also reported that the protection mechanism of cut-edge corrosion of galvanized steel sheets in 0.03 M NaCl solution involves galvanic effects and formation of $Zn(OH)_2$ on the steel surface. Tada *et al*. [39] reported that zinc corrosion products deposited on the steel surface by the hydrolysis of Zn^{2+} and inhibited the cathodic reaction of galvanic corrosion of Zn/Steel couples in 0.01 M NaCl solutions. Ogle *et al*. [40] studied the cut-edge corrosion of zinc coated steel in 0.03 M NaCl solution and reported that the steel surface was covered by zinc containing products (ZnO, $3Zn(OH)_2$. $2ZnCO_3$). They [41] also demonstrated that the inhibition of the cathodic reaction can be attributed to the precipitation of zinc-based corrosion products on the active cathode. Sakairi *et al*. [42-44] reported that the corrosion behavior of steel in aqueous solutions was influenced by Zn^{2+}, with a laser irradiation method. Hirasaki *et al*. [45] reported that the anodic current of Fe around the immersion potential decreased with increases of Zn^{2+} concentration in acid solutions.

In summary, it has been established that Zn^{2+} inhibits the corrosion of metals in aqueous solutions significantly. However, details of the effects and mechanism of Zn^{2+} inhibition with different Zn^{2+} concentrations on the corrosion of mild steel in Cl^- aqueous solutions have not been established. The present research proposes to elucidate details of the mechanism of inhibition effects of Zn^{2+} in different concentrations on the corrosion of mild steel in NaCl aqueous solutions.

6.2 Experimental

6.2.1 Specimens

Mild steel sheets of 0.7 mm thickness (compositions in mass%: C = 0.02; Mn = 0.18; P = 0.015; S < 0.01; and Fe - balance) were cut into 7 × 7 mm specimens to carry out the different tests in the present study. For the electrochemical measurements, the specimens were connected to a conductive wire and embedded in epoxy resin leaving an exposed surface. For immersion tests, the specimens were also embedded in resin. The exposed surface of the specimens was mechanically abraded with a series of SiC abrasive papers up to # 4000 grit size. The abraded specimens were removed from the resin before immersion tests and ultrasonically cleaned in ethanol and in highly purified water before the experiments.

6.2.2 Test solutions

Three different solutions of 0.1 mM $ZnCl_2$ ($Zn_{0.1}$), 0.5 mM $ZnCl_2$ ($Zn_{0.5}$) and 1.0 mM $ZnCl_2$ ($Zn_{1.0}$) were prepared and the concentration of Cl^- of the solutions was adjusted to 10 mM by NaCl. These three solutions and 10 mM NaCl (Na_{sol}) were used as test solutions with Na_{sol} regarded as a reference solution. Water used in this study was highly purified (MILLIPORE, Simplicity UV) and the chemicals were commercially available special grade from Kanto Chemical Co. Ltd., Tokyo, Japan.

6.2.3 Immersion tests

The mild steel samples were immersed in the various solutions at 25°C for 3 d. Immersion tests were carried out with three replicates of each solution at a time. The solutions were open to the air during the immersion tests, and the mass of the specimens before and after the tests were measured by a microbalance (MX5, METTLER TOLEDO, Pro FACT). The pH of the solutions before and after the tests was measured by a pH meter (Eutech Instruments, Cyber-Scan 6000). Corrosion rates (C_R) and the corrosion inhibition efficiencies (η_i) of Zn^{2+} with different concentrations were calculated based on the mass loss during the immersion tests by the Eqs. (6.1) and (6.2):

$$C_R\ (\mu m/d) = \frac{M_1 - M_2}{D \times S \times t} \times 10000 \tag{6.1}$$

Where M_1 (g) is the mass of the specimen before immersion, M_2 (g) is the mass of the specimen after immersion, D (g/cm^3) is the density of the specimen, S (cm^2) is the surface area of the specimen and t (d) is the immersion time.

$$\eta_i\ (\%) = \frac{Na_{CR} - Zn_{CR}}{Na_{CR}} \times 100 \tag{6.2}$$

Here Na_{CR} is the corrosion rate of specimens immersed in the Na_{sol}, and Zn_{CR} is the corrosion rate of specimens immersed in the Zn^{2+} containing solutions.

A digital camera (Nikon, D80) was used to take the photograph of specimen surfaces and the appearance of the solutions in glass bottles before and after the immersion tests. A scanning electron microscope (SEM, JEOL, JSL6510-LA) was used for high magnification observations of the specimen surfaces. The surface roughness [46, 47] was measured by an atomic force microscope (AFM, SPA400) using the dynamic force mode with the cantilever type, SI-DF40. An X-ray photoelectron spectroscope (XPS, JEOL, JPS-9200) was used for the surface analysis. During the XPS analysis, Al Kα was used as the X-ray source (1486.6 eV), and the area for the analysis was 3 × 3 mm. The XPS depth analysis was carried out by sputtering with Ar ions. The sputtering time was converted to depth by the sputtering rate of SiO_2. The surfaces of the

specimens were also analyzed by an Auger electron spectroscope (AES, JEOL, JAMP-9500 F). Before the surface observations and analysis, the immersed specimens were cleaned ultrasonically in ethanol and in highly purified water.

6.2.4 Electrochemical tests

Electrochemical tests were carried out at room temperature in each solution in a conventional three-electrode cell using a computer controlled potentiostat (IVIUM TECHNOLOGIES, Pocketstat). The tests were carried out with three replicates in each solution. Before the tests, the specimens were immersed in the solutions for 1 h. An Ag/AgCl electrode (SSE) immersed in a saturated KCl solution was used as the reference electrode and a Pt plate was used as the counter electrode. The exposed surface area of the specimens in the solution was 49 mm^2. The polarization measurements were carried out from immersion potential to the cathodic and anodic directions with a scan rate of 1 mV/s. The electrochemical impedance spectroscopy (EIS) measurements were carried out at open circuit potential in the frequency range from 10 kHz to 1 mHz and modulation amplitude of 10 mV. The IVIUM software was used to analyze the experimental data obtained from the EIS tests.

6.3 Results and discussions

6.3.1 Immersion tests

The appearance of the solutions and specimens before and after the immersion tests are shown in Fig. 6.1, a) and b) respectively. The transparency of the solutions is different from that of the Na_{sol}. Red corrosion products are observed in the solutions and on the specimens (Fig. 6.1 b)). The appearance (red) and the transparency of the solutions would indicate the degree of corrosion of the steel in the solutions. Fig. 6.1 c) shows the appearance of specimen surfaces before immersion and Fig. 6.1 d) shows them after the immersion tests and ultrasonic cleaning in ethanol and in highly purified water. These cleaned specimens were used for further surface analysis. The pH of the solutions was recorded before (pH_{int}) and after the tests (pH_{corr}) is shown in Table 6.1. The pH_{corr} was slightly increased in all solutions due to the formation of OH^- at the metal surface [26, 27, 48]. The differences in pH (ΔpH) between pH_{int} and pH_{corr} are shown in Table 6.1. Large ΔpH is observed in Na_{sol} (Zn free solution) as compared to that in Zn containing solutions. The ΔpH may reflect the extent of corrosion of metal in the solutions. The corrosion rates were calculated from the mass change recorded in the immersion tests. Fig. 6.2 shows the corrosion rate as a function of the Zn^{2+} concentration in the solutions. The solutions show different corrosion rates, and there are deviations from the mean values. Overall,

the mean values of the corrosion rates decrease with increasing Zn^{2+} concentration. The correlation coefficient is -0.98 and the $Zn_{1.0}$ shows the lowest corrosion rate as compared to the other solutions.

6.3.2 Surface observations and analysis

Details of the corrosion behavior as investigated here can be understood by surface morphology changes during the immersion tests. Fig. 6.3 shows the surface SEM images of specimens immersed in the solutions at 25°C for 3 d. The images show a number of pits and grain boundaries on the surface of the specimen immersed in Na_{sol}. Small pits are visible on the surface of the specimens immersed in the Zn containing solutions, with white corrosion products present on the specimen immersed in $Zn_{1.0}$. These solutions contained 10 mM Cl^-, and it is well known that Cl^- destroys the oxide film on the metal surfaces. In these Zn^{2+} containing solutions, Zn related products may cover the steel surface, preventing the Cl^- from destroying the film. However, Zn corrosion products would not cover the steel surface uniformly, and Cl^- corrosion takes place at Zn-free areas on the steel and creates defects by destroying the surface film. These defects on the steel surface may lead to the formation of pits [27, 28, 35]. For these reasons the specimens immersed in the Zn^{2+} containing solutions also show pits, and the number of pits decreases with increasing solution Zn^{2+} concentration.

The surface roughness was measured by AFM before and after the immersion in the solutions at 25°C for 3 d, and the AFM-3D images are shown in Fig. 6.4. The surface roughness (R_a) was measured from 3D images, and Fig. 6.5 shows the surface roughness of the specimens against the Zn^{2+} concentrations of the solutions. In all the case, the surface roughness is increased after the immersion tests. The specimen immersed in the Na_{sol} shows the highest R_a among these immersed specimens, and the surface roughness decreases with increasing solution Zn^{2+} concentration. These results correspond well to the surface observation by SEM as shown in Fig. 6.3.

The specimen surfaces were examined by XPS after immersion in the solutions at 25°C for 3 d, and Fig. 6.6 shows XPS wide scan spectra and narrow scan spectra of Zn2p3/2 at different depths after immersion. In the wide scan spectra (Fig. 6.6 a)), Zn2p1/2 and Zn2p3/2 peaks are observed on the specimens that were immersed in Zn^{2+} containing solutions [26, 27, 49], with no peak of Na1s on these specimens. These results indicate that there was Zn on the steel surface after immersion in the Zn^{2+} containing solutions. The XPS narrow scan measured at different depths was performed to determine the Zn distribution on the surface. In these narrow

scan spectra (Fig. 6.6 b)), there are sharp peaks of Zn2p3/2 are observed in higher Zn^{2+} containing solutions ($Zn_{1.0}$) than that in low concentration ($Zn_{0.1}$). The XPS narrow scan spectra of Zn2p3/2 were studied to clarify the chemical state of the Zn on the steel surface. As shown in Fig. 6.7, Zn2p3/2 peaks are observed on the steel surface (at 0 nm depth) with all specimens at the 1022.2 eV (binding energy), which is related to the peak of Zn^{2+} [27, 28, 35, 50]. Previously, it was suggested that the Zn^{2+} on the steel surface was zinc hydroxide ($Zn(OH)_2$) [27, 28]. Leygraf *et al*. [51] and Winiarski *et al*. [52] reported the formation of corrosion products of Zn^{2+} as zinc hydroxide ($Zn(OH)_2$) and hydrozincite ($Zn_5(CO_3)_2(OH)_6$) on the steel surface at room temperature. In addition, Zhang *et al*. [53] reported that $Zn(OH)_2$ is the corrosion product formed in Zn containing water in the temperature range 0-30°C, and ZnO is the corrosion product in the temperature range 30-90°C. Winiarski *et al*. [52] also reported that ZnO is formed at around 60°C. In summary, the XPS results suggest that the Zn^{2+} layer on the specimen surface is zinc hydroxide ($Zn(OH)_2$) and hydrozincite ($Zn_5(CO_3)_2(OH)_6$). The XPS results also suggest that (Fig. 6.6 b)) the thickness of the Zn layer formed in $Zn_{0.5}$ and $Zn_{1.0}$ is thicker than that in $Zn_{0.1}$.

The specimen surfaces were further analyzed by AES to determine the Zn layer formation and coverage on the steel surface. Fig. 6.8 shows the AES results of the immersed specimens. The left panels of Fig. 6.8 show SEM images of specimen surfaces after immersion in the solution with different Zn^{2+} concentrations, the middle images are enlargements of randomly selected surface areas of the three left panels, and the right plots in Fig. 6.8 show the AES spectra of Zn of different selected areas. The Zn peaks appeared between energies of 975 eV and 995 eV. With $Zn_{0.1}$, only Zn peaks appeared in area-1 and area-3. With $Zn_{0.5}$, Zn peaks appeared in area-1, area-2, and area-5, and with $Zn_{1.0}$, Zn peaks appeared in all of the areas. These results suggest that the surface coverage of the Zn layer may be increased with increasing Zn^{2+} concentration in the solutions.

6.3.3 Electrochemical tests

6.3.3.1 Open-circuit potential

Open circuit potentials of specimens during immersion for 1 h at room temperature are shown in Fig. 6.9. After 3000 s of immersion, all the potentials reach a stable value, and the Na_{sol} shows the lowest potential, the potential increases with increasing Zn^{2+} concentrations in the solutions.

6.3.3.2 Potentiodynamic polarizations

The potentiodynamic cathodic and anodic polarization curves are shown in Fig. 6.10. In the cathodic polarization curves, at around -0.8 V, the lowest current density is observed in the Zn rich solution ($Zn_{1.0}$). The highest current density is observed in the Na_{Sol} as compared to the other used solutions. In the anodic polarization curves, at around -0.15 V, the lowest current density is observed in the Zn rich solution ($Zn_{1.0}$) as compared to the other used solutions. The highest current density is also observed in the Na_{Sol} as compared to the other used solutions. The polarization behavior demonstrates that the presence of Zn^{2+} suppresses the current density in both cathodic and anodic polarizations, and the inhibition effect is increased with increasing the Zn^{2+} concentration in the solutions.

6.3.3.3 EIS

EIS tests were carried out at room temperature after immersion in the solutions for 1 h. Figs. 6.11 a), b) and c) show the Bode diagram of impedance, phase shift plot, and Nyquist plot respectively. The fitted lines are also shown in Figs. 6.11 a), b) and C) which were calculated by an equivalent circuit shown in Fig. 6.12. The equivalent circuit pretends an electrode with a protective film having a defect [35, 54]. The equivalent circuit consists (Fig. 6.12) of bulk solution resistance (R_{sol}), resistance of the defects in the protective film (R_d), charge transfer resistance at the metal/solution interface inside the defect (R_{ct}), constant phase element of the double layer at the interface (Q_{dl}) and the constant phase element of the protective film (Q_f). All the experimental spectra can be well described by the mentioned equivalent circuit, and the fitted lines correspond well to the experimental plots (Figs. 6.11 a), b) and C)). The protective Zn-layer formed on the immersed specimens may have some defects that led to the formation of pits [35]. The magnitude of impedance indicates the corrosion resistance of steel in the solutions [26-29]. From Fig. 6.11 a), it is found that Zn rich solution ($Zn_{1.0}$) shows the highest and the Na_{Sol} shows the lowest impedance among the used solutions. The largest phase shift is observed in the case of Zn rich solution as compared to the other solutions (Fig. 6.11 b)). From the Nyquist plot (Fig. 6.11 c)), semicircle plots are observed in all the solutions. The radius of the semicircle is increased with increasing the Zn^{2+} concentration in the solutions. These results indicate that the corrosion resistance ability of steel is increased with increasing the Zn^{2+} concentration in the solutions.

The used electrochemical impedance parameters are shown in Table 6.2. The corrosion resistance (R_c) and the inhibition efficiency (η_e) were calculated by the Eqs. (6.3) and (6.4):

$$R_c\ (k\Omega cm^2) = R_d + R_{ct} \qquad (6.3)$$

$$\eta_e(\%) = \frac{R_{c\_sol} - R_{c\_ref}}{R_{c\_sol}} \times 100 \quad (6.4)$$

Where R_{c_sol} and R_{c_ref} are the values of corrosion resistance in the Zn^{2+} containing solutions and in the reference solution (Na_{sol}). From Table 6.2, it is found that the η_e and R_c change as follows, $Zn_{1.0} > Zn_{0.5} > Zn_{0.1} > Na_{Sol}$. These results indicate that the charge transfer may be prevented by the Zn-layer that was formed on the steel surface and the prevention ability was increased with increasing the Zn^{2+} concentration in the solutions. The value of Q_{dl} in $Zn_{1.0}$ shows the lowest as compared to the other solutions (Table 6.2). Q_{dl} represents the structure of the metal/solution interface and the area of defects in the protective film on the metal surface [27, 35, 55]. Otani et al. [35] reported that the decrease in Q_{dl} value indicates that Zn^{2+} can decrease the number of defects in the protective film on mild steel in model freshwater. Mahdavian et al. [55] reported that the values of constant phase element of the double layer at the interface (Q_{dl}) of the defects in a protective film depend on the total area of defects in the film. Therefore, the results indicate that zinc may form a protective film with fewer defects on the metal surface immersed in the $Zn_{1.0}$ (as Q_{dl} value is the lowest). At the high concentration ($Zn_{1.0}$), Zn^{2+} may have distributed uniformly on the surface and formed a layer that covered the area of the surface more than the area of the surface covered by the other solutions ($Zn_{0.1}$ and $Zn_{0.5}$). The uniformed and comparatively thicker layer of Zn^{2+} decreased the defect area that protected the surface from the Cl^- attack and the metal dissolution reactions. Consequently, the highest charge transfer resistance was observed in the Zn-rich solution ($Zn_{1.0}$) as compared to the other solutions.

6.3.4 Corrosion inhibition efficiency and mechanism

To establish the relation between the corrosion inhibition and the Zn^{2+} concentration, corrosion inhibition efficiencies were calculated. Fig. 6.13 shows the corrosion inhibition efficiencies of Zn^{2+} as a function of concentration, with the corrosion inhibition of Na^+ alone considered zero. A linear relationship (correlation coefficient = 0.95) is observed between the corrosion inhibition and Zn^{2+} concentration in the solutions (Fig. 6.13), and $Zn_{1.0}$ shows the strongest corrosion inhibition. This result corresponds well with the results from the surface analysis.

From the experimental results, a corrosion inhibition mechanism of mild steel by Zn^{2+} in NaCl aqueous solution can be suggested, and Fig. 6.14 is a schematic of the suggested corrosion inhibition mechanism of Zn^{2+} in the solutions here. When the solution does not contain Zn^{2+}, Cl^- defects in the surface and destroys the surface film. After destroying the surface film, metal dissolution is initiated (Fig. 6.14 a)). In the presence of Zn^{2+} in the solution, a Zn^{2+} layer forms

on the steel surface. The Zn^{2+} layer on the steel surface protects against Cl^- attack and inhibits metal dissolution reactions (Fig. 6.14 b). If the Zn^{2+} concentration is increased in the solution, the coverage of the Zn layer increases and the protection of the steel surface is improved, the corrosion or metal dissolution rate decreases with increasing Zn^{2+} concentration in the solutions.

6.4 Conclusion

The effects of Zn^{2+} concentrations on the corrosion inhibition of mild steel in sodium chloride aqueous solutions were investigated by immersion tests and electrochemical tests. The surface investigations were carried out by SEM, AFM, and XPS.

- The corrosion rate of mild steel decreased with increasing Zn^{2+} concentration in the solutions.
- Surface morphologies and surface roughness depend on the Zn^{2+} concentration in the solutions.
- Both cathodic and anodic currents were suppressed in presence of Zn^{2+} in the solutions.
- Charge transfer resistances were increased with increasing the concentration of Zn^{2+} in the solutions, and Zn rich solution showed the highest corrosion inhibition efficiency.
- The XPS results showed that a Zn^{2+} layer was present on the steel surface. The thickness of the Zn layer depends on the Zn^{2+} concentration of the surrounding solution.
- The Zn layer covered the steel surface and the coverage depends on the Zn^{2+} concentration which inhibited the corrosion reactions in the solutions.

Table 6.1 pH of the solutions before and after the immersion tests

Solutions	Before the immersion tests, pH_{int}	After the immersion tests, pH_{corr}	Difference ΔpH
Na_{sol}	6.9	7.5	0.6
$Zn_{0.1}$	6.9	7.4	0.5
$Zn_{0.5}$	6.8	6.9	0.1
$Zn_{1.0}$	6.6	6.7	0.1

Table 6.2 Calculated electrochemical impedance parameters of mild steel after immersion in the solutions for 1 h at room temperature.

Solutions	R_d ($k\Omega cm^2$)	R_{ct} ($k\Omega cm^2$)	Q_{dl} ($\mu s^n \Omega^{-1} cm^{-2}$)	Q_f ($\mu s^n \Omega^{-1} cm^{-2}$)	n_{dl}	n_f	R_c ($k\Omega cm^2$)	η (%)
Na_{sol}	0.10	4.95	3.34	3.50	0.71	0.69	5.05	-
$Zn_{0.1}$	0.12	21.00	1.19	1.02	0.71	0.72	21.12	76
$Zn_{0.5}$	0.13	37.50	0.98	0.99	0.74	0.72	37.63	87
$Zn_{1.0}$	0.15	62.50	0.85	0.78	0.75	0.73	62.65	92

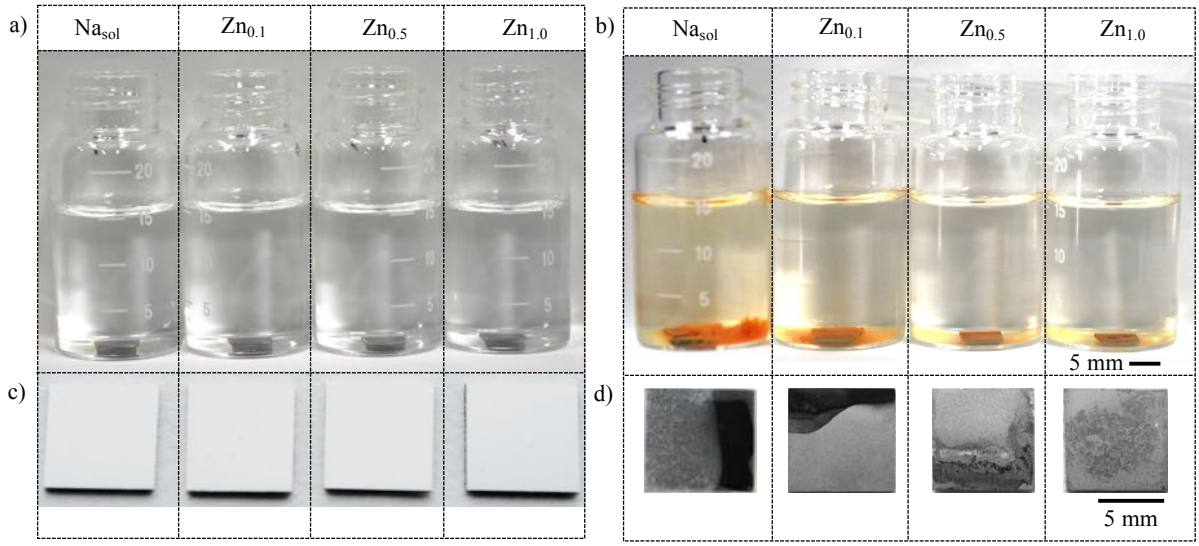

Fig. 6.1 Appearance of solutions a) at the start of immersion and b) after the immersion tests. Appearance of specimen surfaces after ultrasonic cleaning c) before the immersion and d) after the immersion tests.

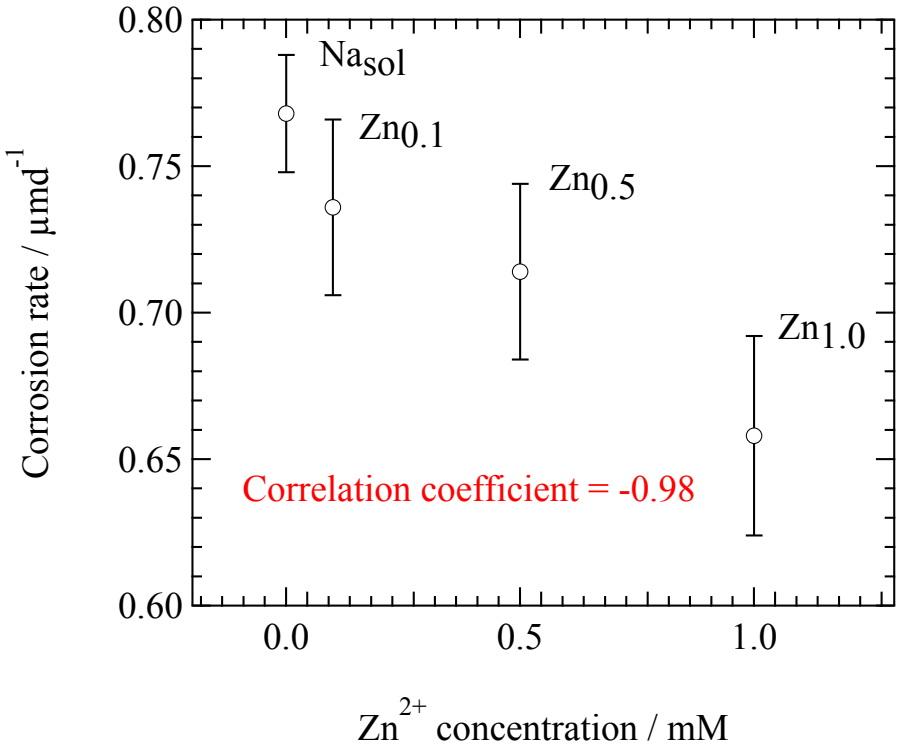

Fig. 6.2 Corrosion rate as a function of Zn^{2+} concentration in the solutions.

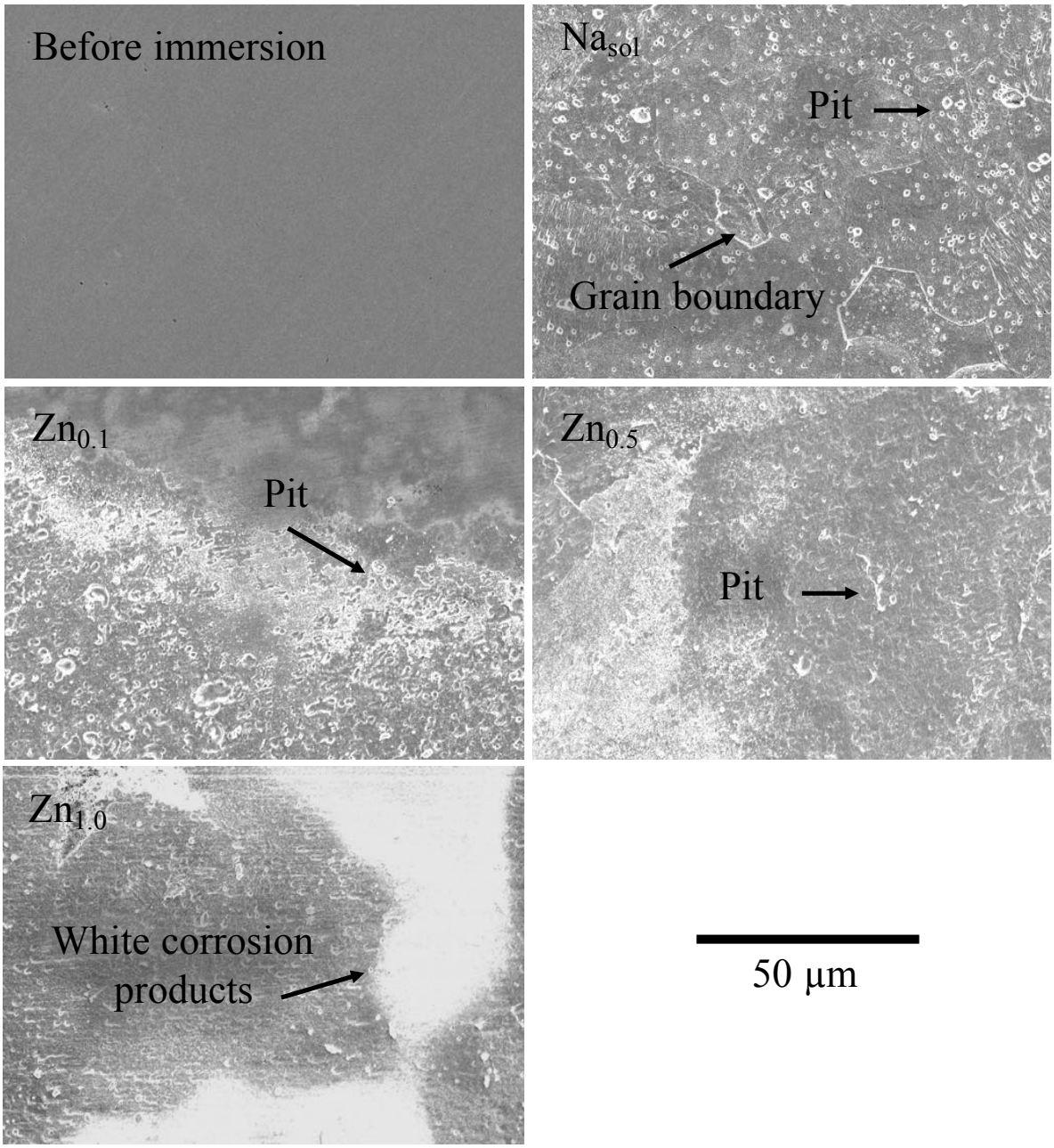

Fig. 6.3 Surface SEM images of specimens after immersion in the solutions for 3 d at 25°C.

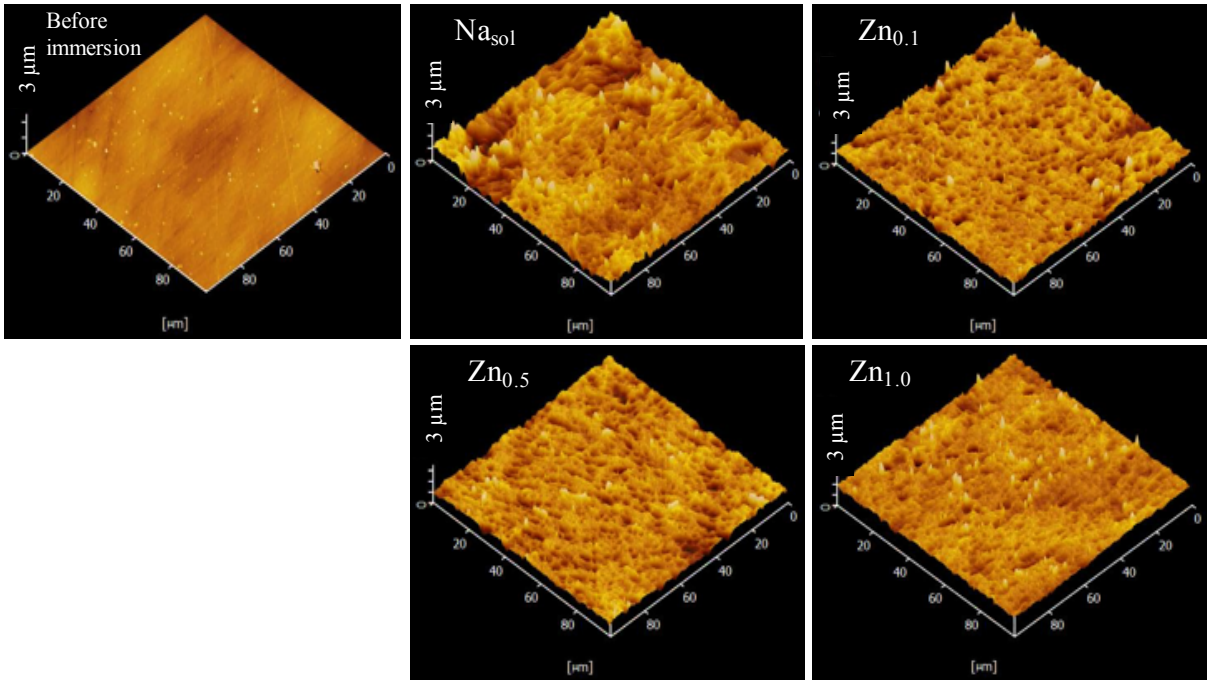

Fig. 6.4 AFM 3D images of the specimen surfaces before and after immersion in the solutions for 3 d at 25°C.

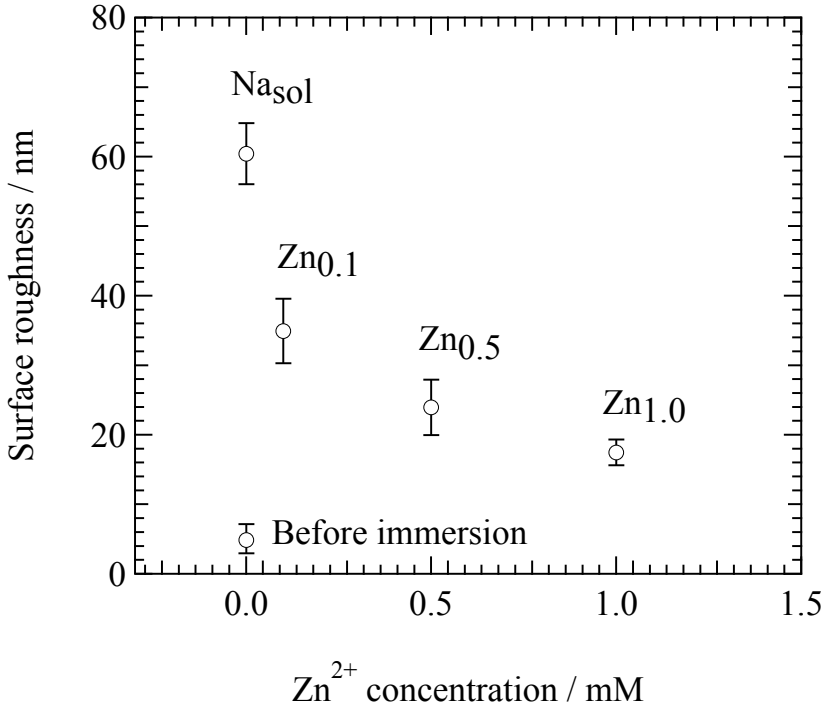

Fig. 6.5 Surface roughness of specimens versus Zn^{2+} concentration before and after immersion in the solutions for 3 d at 25°C.

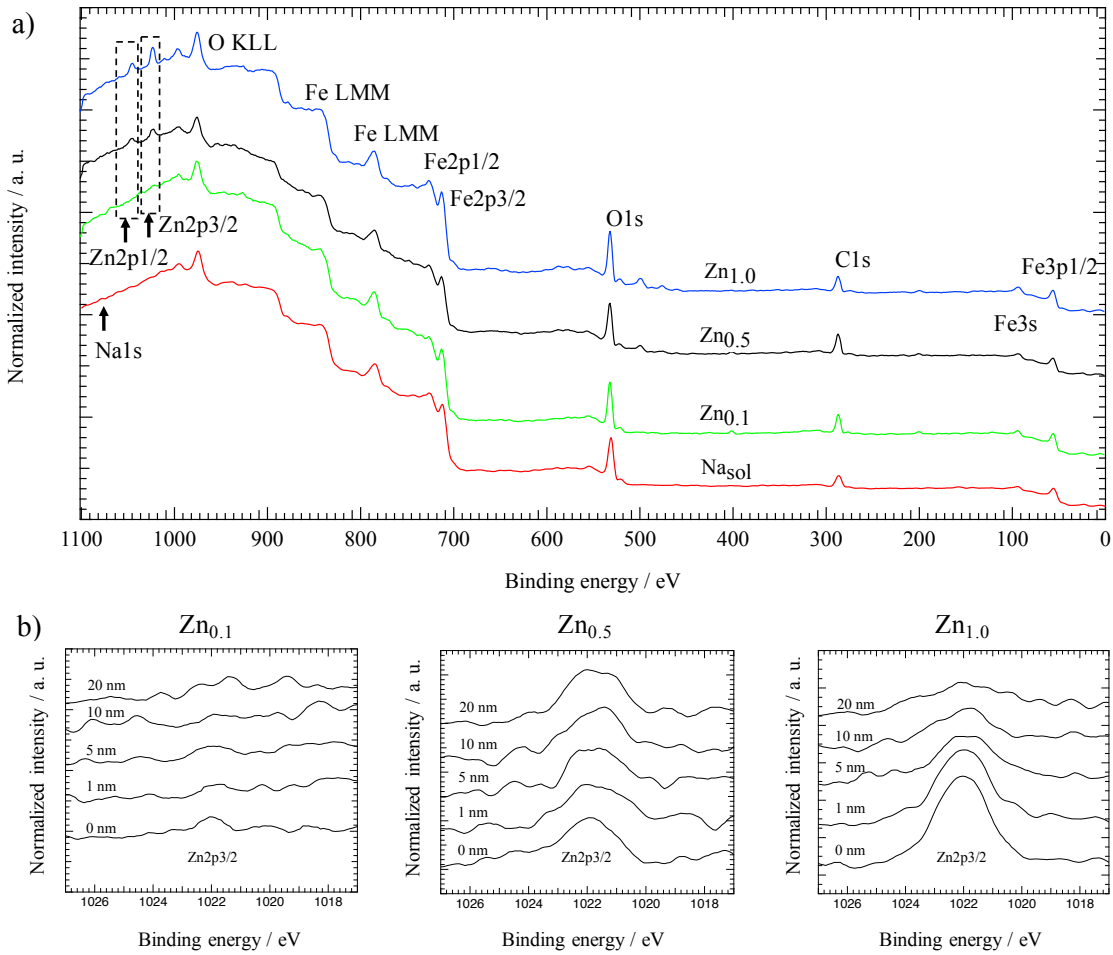

Fig. 6.6 XPS measurements: a) wide scan spectra b) narrow scan spectra of Zn2p3/2 with depth from the specimen surface after immersion in the solutions for 3 d at 25°C.

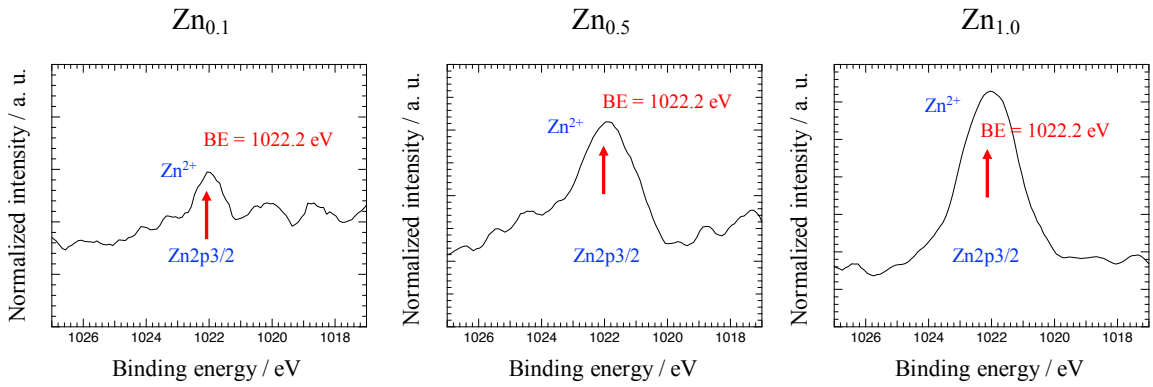

Fig. 6.7 XPS narrow scan spectra of Zn2p3/2 of the specimen surface after immersion in the Zn^{2+} containing solutions for 3 d at 25°C.

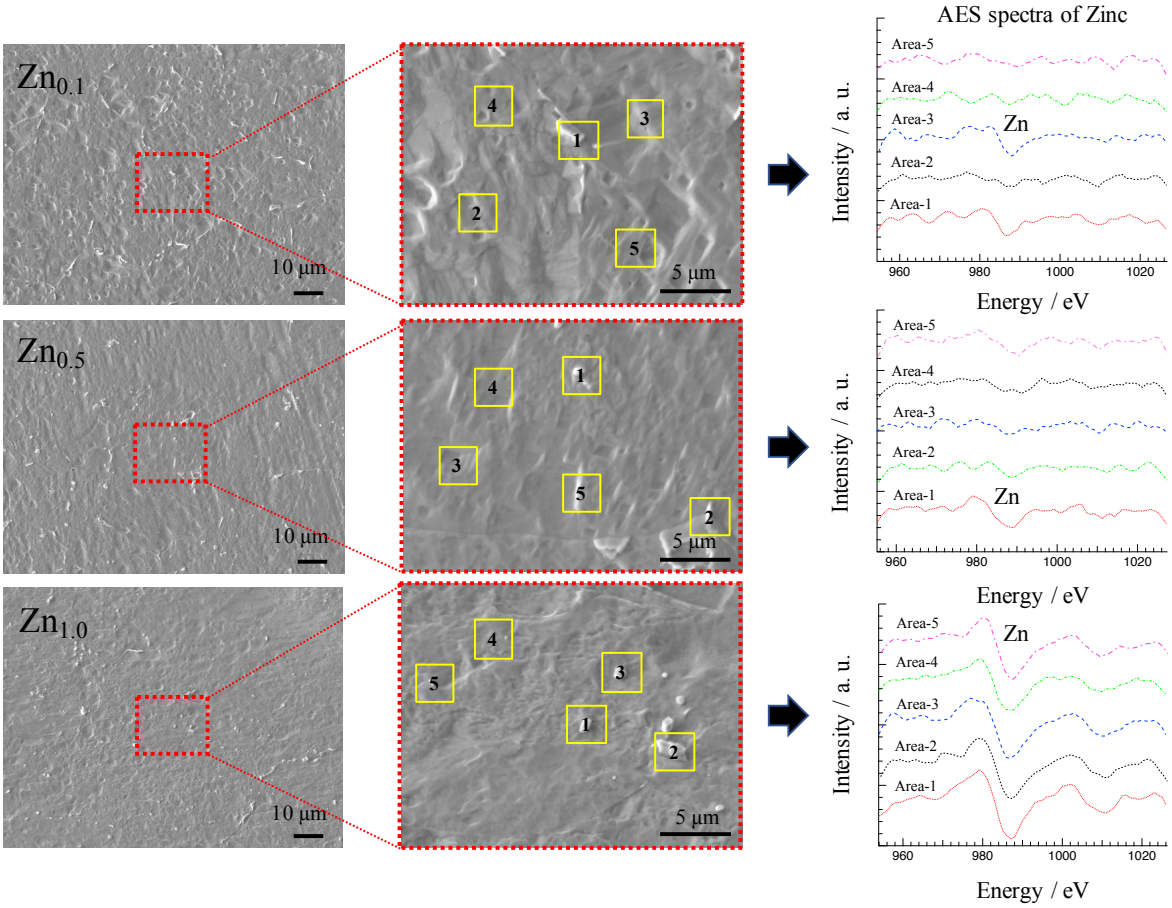

Fig. 6.8 Results of the AES analysis of specimens after immersion in the solutions for 3 d at 25°C.

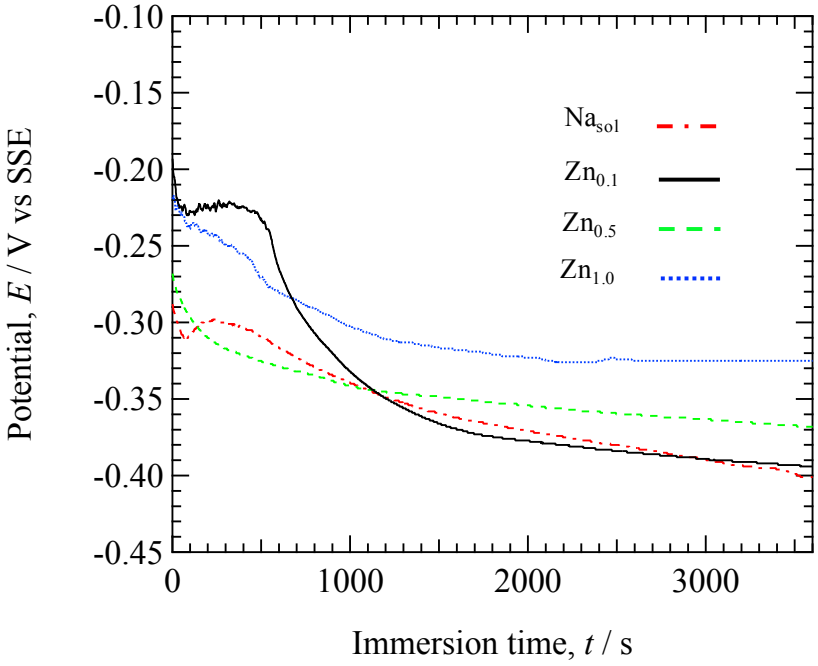

Fig. 6.9 Immersion potential of specimens after immersion in the solutions for 1 h at room temperature.

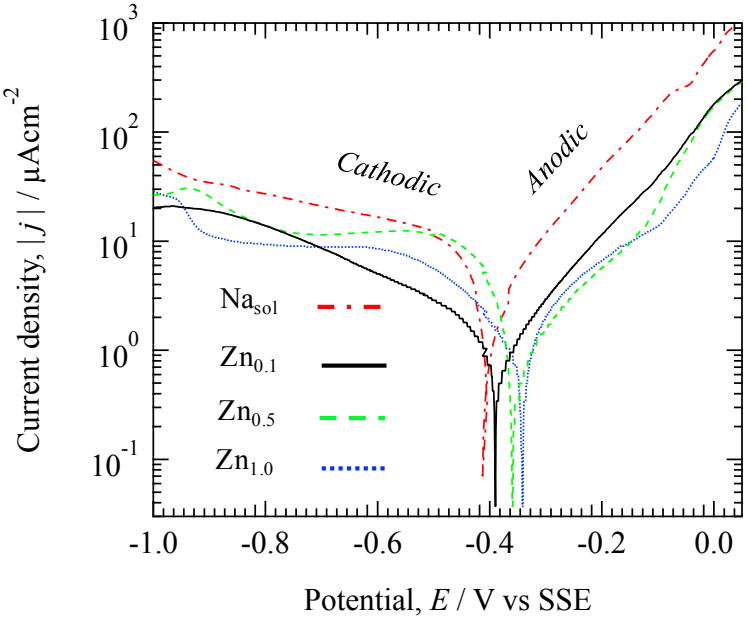

Fig. 6.10 Potentiodynamic a) cathodic and b) anodic polarization curves after immersion in the solutions for 1 h at room temperature.

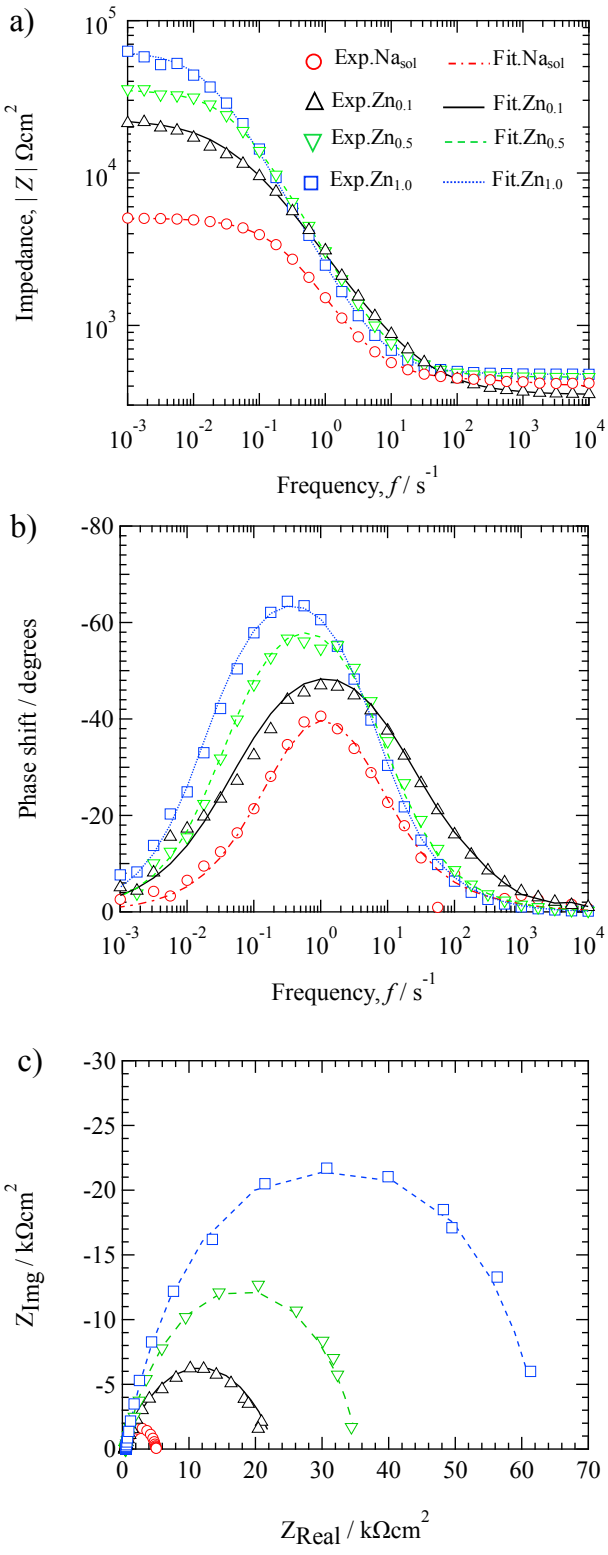

Fig. 6.11 Bode diagram of a) impedance, b) phase shift plot and c) Nyquist plot of specimen immersed in the solutions for 1 h at room temperature.

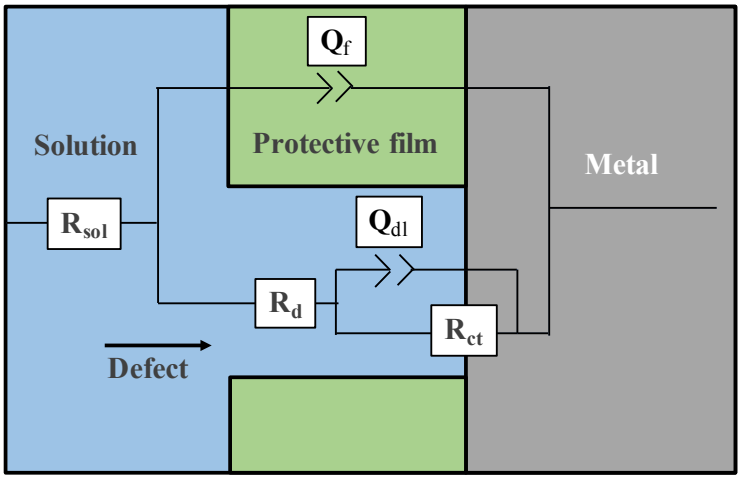

Fig. 6.12 Equivalent circuit of mild steel electrode with a protective film having defect to fit the EIS data.

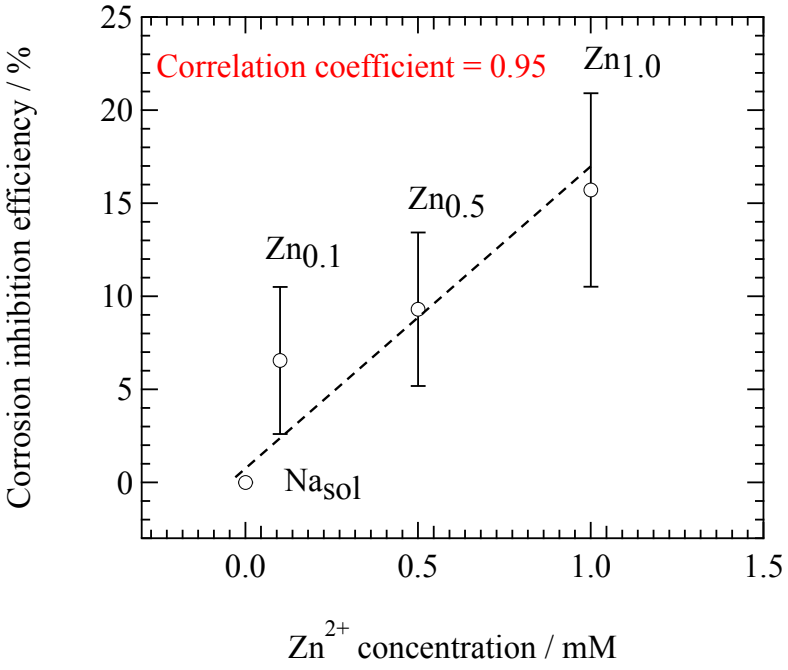

Fig. 6.13 Corrosion inhibition efficiency in the solutions with different concentrations of Zn^{2+}.

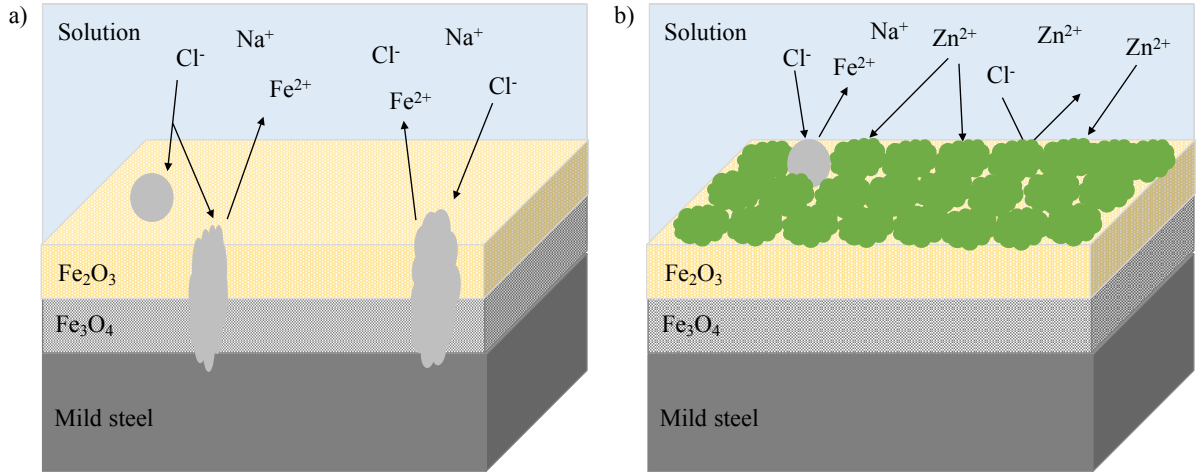

Fig. 6.14 Corrosion inhibition mechanism of Zn^{2+} in the solutions, a) acceleration of metal dissolution by Cl^- attack without Zn^{2+} in the solution, b) surface coverage by the Zn-layer formation and protection from Cl^- attack and metal dissolution.

References

1. E. Schindelholz, B. E. Risteen, and R. G. kelly, J. Electrochem. Soc., 161 (2014) C460-C470.
2. A. Soliz and L. Caceres, J. Electrochem. Soc., 162 (2015) C385-C395.
3. S. Li and L. H. Hihara, J. Electrochem. Soc., 162 (2015) C495-C502.
4. I. Santana, A. Pepe, E. Jimenez-Pique, S. pellice, I. Milosev, and S. Cere, Surf. Coat. Technol., 265 (2015) 106-116.
5. M. Morcillo, B. Chico, J. Alcantara, I. Diaz, R. Wolthuis, and D. Fuente, J. Electrochem. Soc., 163 (2016) C426-C439.
6. S. Khara, S. Choudhary, S. Sangal, and K. Mondal, Surf. Coat. Technol., 296 (2016) 203-210.
7. C. P. Gardiner and R. E. Melchers, Corros. Sci., 44 (2002) 2665-2673.
8. R. E. Melchers, Corros. Sci., 48 (2006) 4174-4201.
9. G. A. Rassoul and D. R. Rzaige, Iraqi J. Chem. Petroleum Eng., 9 (2007) 37-41.
10. A. C. Uzorh, Int. J. Eng. Sci., 2 (2013) 18-24.
11. H. Xian-jun, Z. Bi-ming, C. Shao-hui, F. Feng, and J. Jian-qing, J. Iron Steel Res. Int., 20 (2013) 47-52.
12. G. S. Vasyliev, Corros. Sci., 98 (2015) 33-39.
13. S. Cao, D. Liu, P. Zhang, L. Yang, P. Yang, H. Lu, and J. Gui, Scientific reports, 7, (2017).
14. X. Zheng, M. Gong, Q. Li, and L. Guo, Scientific reports, 8, (2018).
15. R. T. Foley, Corrosion, 26 (1970) 58-70.
16. D. D. Macdonald, J. Electrochem. Soc., 139 (1992) 3434-3449.
17. E. McCafferty, Introduction to Corrosion Science, Springer, New York (2010) 283-286.
18. M. A. Deyab, Electrochim. Acta, 202 (2016) 262-268.
19. Y. Song, G. Jiang, Y. Chen, P. Zhao, and Y. Tian, Scientific reports, 7, (2017).
20. D. M. Drazic and L. Z. Vorkapic, Corros. Sci., 18 (1978) 907-910.
21. M. G. A. Khedr and A. M. S. Lashien, J. Electrochem. Soc., 136 (1989) 968-972.
22. M. G. A. Khedr and A. M. S. Lashien, Corros. Sci., 33 (1992) 137-151.
23. J. N. Esposito, G. Economy, W. A. Byers, J. B. Esposito, F. W. Pement, R. J. Jacko, and C. A. Bergmann, in: Proc. 5th Int. Sympo. Environmental degradation of materials in nuclear power systems-water reactors, American Nuclear Society, (1992) 495-503.
24. S. Zhang, T. Shibata, and T. Haruna, Corros. Sci., 47 (2005) 1049-1061.

25. K. Otani, M. Sakairi, R. Sasaki, A. Kaneko, Y. Seki, and D. Nagasawa, J. Solid State Electrochem., 18 (2014) 325-332.
26. K. Otani and M. Sakairi, Corros. Sci., 111 (2016) 302-312.
27. Md. S. Islam, K. Otani, and M. Sakairi, Corros. Sci., 131 (2018) 17-27.
28. Md. S. Islam, K. Otani, and M. Sakairi, ISIJ International, 58 (2018) 1616-1622.
29. Md. S. Islam, K. Otani, and M. Sakairi, Corros. Sci., 140 (2018) 8-17.
30. I. Felhosi, Zs. Keresztes, F. H. Karman, M. Mohai, I. Bertoti, and E. Kalman, J. Electrochem. Soc., 146 (1999) 961-969.
31. J. Telegdi, M. M. Shaglouf, A. Shaban, F. H. Karman, I. Betroti, M. Mohai, and E. Kalman, Electrochim. Acta. 46 (2001) 3791-3799.
32. S. Sathiyanarayanan, C. Jeyaprabha, S. Muralidharan, and G. Venkatachari, App. Surf. Sci., 252 (2006) 8107-8112.
33. D. Q. Zhang, Q. R. Cai, X. M. He, L. X. Gao, and G. S. Kim, Mater. Chem. Phys., 114 (2009) 612-617.
34. M. Prabakaran, M. Venkatesh, S. Ramesh, and V. Periasamy, App. Surf. Sci., 276 (2013) 592-603.
35. K. Otani, Md. S. Islam, and M. Sakairi, J. Electrochem. Soci., 164 (2017) C498-C504.
36. T. Prosek, A. Nazarov, A. Le Gac, and D. Thierry, Prog. Org. Coat. 83 (2015) 26-35.
37. F. Thebault, B. Vuillemin, R. Oltra, C. Allely, K. Ogle, and O. Heintz, Corros. Sci., 97 (2015) 100-106.
38. F. Thebault, B. Vuillemin, R. Oltra, C. Allely, and K. Ogle, Corros. Sci., 56 (2011) 8347-8357.
39. E. Tada, S. Satoh, and H. Kaneko, Electrochim. Acta, 49 (2004) 2279-2285.
40. K. Ogle, V. Baudu, L. Garrigues, and X. Philippe, J. Electrochem. Soc., 147 (2000) 3654-3660.
41. K. Ogle, S. Morel, and D. Jacquet, J. Electrochem. Soc., 153 (2006) (1) B1-B5.
42. M. Sakairi, Y. Uchida, and H. Takahashi, ISIJ International, 46 (2006) 1218-1222.
43. M. Sakairi, Y. Uchida, T. Kikuchi, and H. Takahashi, ISIJ International, 48 (2008) 988-993.
44. M. Sakairi, M. Uchida, and T. Kikuchi, Zairyo-to-Kankyo, 59 (2010) 379-381.
45. T. Hirasaki, A. Nishikata, and T. Tsuru, J. Japan Inst. Metals, 6 (2002) 643-648.
46. A. K. Satapathy, G. Gunasekaran, S. C. Sahoo, K. Amit, and P. V. Rodrigues, Corros. Sci., 51 (2009) 2848-2856.

47. R. R. L. De Oliveira, D. A. C. Albuquerque, T. G. S. Cruz, F. M. Yamaji, and F. L. Leite, Federal University of São Carlos, Campus Sorocaba, Brazil, (2011) 147-174.
48. J. Han, B. N. Brown, D. Young and S. Nesic, J. Appl. Electrochem., 40 (2010) 683-690.
49. M. Pourbaix, Atlas of electrochemical equilibria in aqueous solutions, National Association of Corrosion Engineers, Huston, Texas (1974).
50. R. Al-Gaashani, S. Radiman, A. R. Daud, N. Tabet, and Y. Al-Douri, Ceramics Int., 39 (2013) 2283-2292.
51. C. Leygraf, and T. Graedel, Atmospheric Corrosion, Wiley Interscience, 131 (2001) 24-30.
52. J. Winiarski, W. Tylus, K. Winiarska, I. Szczygiel, and B. Szczygiel, J. Spectroscopy, 2018 (2018) 1-14.
53. X. G. Zhang, Corrosion and Electrochemistry of Zinc, Springer, Boston, MA, (1996) 157-181.
54. F. Vacandio, Y. Massiani, P. Gergaud and O. Thomas, *Corros. Sci*. 359 (2000) 221-227.
55. M. Mahdavian and R. Naderi, *Corros. Sci*. 53 (2011) 1194-1200.

Chapter 6 has been oriented from the following article

[Md. S. Islam and M. Sakairi, Effects of Zn^{2+} concentration on the corrosion of mild steel in NaCl aqueous solutions, *J. Electrochem. Soci.*, 166 2 (2019) C83-C90.]

Chapter 7: Summary

In this paper, the effects of metal cations on the corrosion of different steels in chloride aqueous solutions were investigated. There are some metal cations (Zn^{2+}, Al^{3+}, Mg^{2+}, and Zr^{4+}) that showed significant corrosion inhibition effect in chloride aqueous solutions. Especially, Zn^{2+} showed the highest corrosion inhibition effect on mild steel corrosion in chloride aqueous solutions at room temperature, and even at the elevated temperatures under the consideration of pH. The Zn^{2+} can form a layer on the surface oxide films, and thus the metal cation layer inhibited the chloride attack and metal dissolution reactions as well. In the case of stainless steel, Al^{3+} showed the highest corrosion inhibition effect in chloride aqueous solutions at room temperature. Stainless steel contains chromium and chromium oxide is formed as a surface film, and Al^{3+} also formed an oxide layer. Both oxides of Cr and Al combined and formed a strong fence against chloride attack and metal dissolution reactions in the solutions.

In chapter 1, the corrosions of metals in chloride aqueous environment have been discussed regarding the oxide film structure. An equation has been introduced to calculate the corrosion rate of metals. Different factors of corrosion have been discussed together with the effect of metal cation hardness and types of corrosion inhibitors have been discussed. Present research trend and purpose of the research also have been discussed in this chapter.

In chapter 2, the effects of metal cations on mild steel corrosion in 10 mM Cl^- aqueous solution were investigated by immersion tests and electrochemical tests in which surface analyses were carried out by SEM, EDS, and XPS. The corrosion behavior of mild steel was changed with *X*. However, corrosion rate was not closely correlated with *X*. From the XPS results, it was suggested that only Zn^{2+} attached to the metal surface and formed a layer with the oxide films thus inhibited the electrochemical reactions, and consequently lowered the corrosion rate.

In chapter 3, the corrosion behavior of SUS304 in 0.5 M chloride aqueous solution was studied by immersion tests, EIS, SEM, AFM, and XPS. The corrosion inhibition mechanism of metal cations with the surface oxide films have been clarified. However, *X* was not correlated with the corrosion rate. XPS results revealed that Zn^{2+} and Al^{3+} were existed on the steel surface as hydroxides and formed a layer by incorporating in the oxide films through the de-hydroxylation

process, and the layer of metal cation protected the chloride attack and metal dissolution as well.

In chapter 4, the role of metal cations on corrosion of coated steel substrate in concentrated chloride aqueous solution was investigated by immersion tests and electrochemical tests. The mechanism of effect was clarified based on the XPS, AFM, and EIS results, and suggested that Zn^{2+} formed a layer on the metal surface and acted as a barrier for the corrosion reactions.

In chapter 5, the effects of metal cations on mild steel corrosion in chloride aqueous solutions were investigated at different temperatures (25, 50 and 80°C). The relation between mass change and temperatures have been explained. Corrosion inhibition mechanism of metal cations at different temperatures has been clarified based on the experimental results, and it was suggested that Zn^{2+} attached to the metal surface and formed a layer of zinc-related products (Zinc oxide: ZnO, Zinc hydroxide: $Zn(OH)_2$ and Hydrozincite: $Zn_5(CO_3)_2(OH)_6$) that protected the chloride attack and metal dissolution as well.

In chapter 6, the effects of Zn^{2+} concentration on the mild steel corrosion in chloride aqueous solutions were clarified based on the immersion tests and electrochemical tests. Surface investigations were clarified by SEM, AFM, XPS, and AES. Corrosion inhibition efficiencies were clearly elucidated regarding the Zn^{2+} concentration in the solutions.

In chapter 7, summary of the research.

List of Publications

(1st Author)

1. Md. S. Islam, K. Otani and M. Sakairi, Effects of metal cations on mild steel corrosion in 10 mM Cl^- aqueous solution, *Corros. Sci.*, 131 (2018) 17-27.
2. Md. S. Islam, K. Otani and M. Sakairi, Corrosion inhibition effects of metal cations on SUS304 in 0.5 M Cl^- aqueous solution, *Corros. Sci*., 140 (2018) 8-17.
3. Md. S. Islam, K. Otani and M. Sakairi, Role of metal cations on corrosion of coated steel substrate in model aqueous layer, *ISIJ International*, 58 (2018) 1616-1622.
4. Md. S. Islam, K. Otani and M. Sakairi, Investigation of the corrosion inhibition performance of metal cations for mild steel in simulated fresh water at high temperature, *Zairyo-to-Kankyo*, 67 (2018) 457-461.
5. Md. S. Islam and M. Sakairi, Effects of Zn^{2+} concentration on the corrosion of mild steel in NaCl aqueous solutions, *J. Electrochem. Soci.*, 166 (2019) C83-C90.
6. Md. S. Islam and M. Sakairi, Corrosion inhibition of mild steel by metal cations in high pH simulated fresh water at different temperatures, *Corros. Sci.*, 153 (2019) 100-108.

List of Publications

(Co-Author)

1. K. Otani, Md. S. Islam and M. Sakairi, Inhibition ability of gluconates for fresh water corrosion of mild steel enhanced by metal cations, *J. Electrochem. Soci.*, 164 (9) C498-C504 (2017).
2. K. Otani, M. Sakairi, Md. S. Islam, Influence of metal cations on inhibitor performance of gluconates in the corrosion of mild steel in fresh water, *Corros. Rev.*, 36 (2018) 105-113.
3. M. Sakairi, K. Azumi and Md. S. Islam, Corrosion inhibition of metal cation on steels in supplied water of boiler environments, *J. Japan Boiler Association*, 411 (2018) 10-17.
4. K. Otani, Md. S. Islam, M. Sakairi, and Akira Kaneko, Auger electron spectroscopic analysis of corrosion products formed on A3003 aluminum alloy in model fresh water with different Zn^{2+} concentration, *J. Surf. Interface Anal.,* (2019) 1-7.
5. M. Sakairi, Md. S. Islam and K. Otani, Corrosion inhibition of steels in freshwater by metal cations, Rust prev. & cont. Japan 63 (2019) 200-207.

List of Conferences
(1st Author)

1. Md. Saiful Islam, Kyohei Otani and Masatoshi Sakairi, Influence of Metal Cations on Corrosion of Mild Steel in 10 mM Cl^- Aqueous Solution. (Oral presentation), Materials and Environments 2017, Japan Society of Corrosion Engineering, National Museum of Emerging Science & Innovation, Miraikan, Tokyo, Japan, May 2017.
2. Md. Saiful Islam, Kyohei Otani and Masatoshi Sakairi, Corrosion behavior of Type-304 stainless steel influenced by metal cations in 0.5 M Cl^- aqueous solution. (Oral presentation), Japan Society of Corrosion Engineering, The 64th Japan Conference on Materials and Environments, Naha, Okinawa, Japan, November 2017.
3. Md. Saiful Islam, Kyohei Otani and Masatoshi Sakairi, Effects of Metal Cations on Stainless Steel Corrosion in High Concentration of Cl^- Aqueous Solution. (Oral presentation), Corrosion Dream 2017 Your Researcher Seminar, Osaka University, Osaka, Japan, November 2017.
4. Md. Saiful Islam, Kyohei Otani and Masatoshi Sakairi, Effects of metal cations on corrosion of mild steel in model seawater (Oral presentation), 2018 ISIJ and JIM Joint Winter Domestic Meeting, Sapporo Education and Culture Hall, Sapporo, Japan, January 2018.
5. Md. Saiful Islam, Kyohei Otani and Masatoshi Sakairi, Effects of metal cations on corrosion of mild steel in model fresh water at different temperatures. (Oral presentation), Materials and Environments 2018, Japan Society of Corrosion Engineering, National Museum of Emerging Science & Innovation, Miraikan, Tokyo, Japan, May 2018.
6. Md. Saiful Islam, Kyohei Otani and Masatoshi Sakairi, Surface film structure of mild steel influenced by metal cations at high temperature in model aqueous solution. (Oral presentation), Japanese Chemical Society Hokkaido Branch Summer Meeting, Kitami Institute of Technology, Kitami, Japan, July 2018.
7. Md. Saiful Islam, Kyohei Otani and Masatoshi Sakairi, Effect of zinc ion concentration on the surface film structure of mild steel in aqueous solution with chloride ion. (Oral presentation), 18th Asian Pacific Corrosion Control Conference (APCCC-18), Centara Grand Mirage Beach Resort Pattaya, Thailand, November 2018.
8. Md. Saiful Islam and Masatoshi Sakairi, Corrosion behavior of aluminum 6000 alloy in NaCl aqueous solutions with metal cations. (Oral presentation), Japan Foundry

Engineering Association Hokkaido Brach Meeting-2019, Obihiro City Lifelong Learning Center, Japan, April 2019.

9. Md. Saiful Islam and Masatoshi Sakairi, Studies on orrosion behavior of mild steel in NaCl aqueous solution with zinc ions. (Poster presentation), 235th Electrochemical Society (ECS) Meeting, Dallas, TX, USA, May 2019.
10. Md. Saiful Islam and Masatoshi Sakairi, Corrosion study of aluminum 7075 alloy in metal cations containing chloride solution by surface analysis, (Oral presentation), Japan Chemical Society Hokkaido Branch Summer Meeting, Industrial Collage of Technology, Tomakomai city, Japan, July 2019.

List of Conferences
(Co-Author)

1. 坂入正敏，大谷恭平, Md. Saiful Islam, 日本金属学会，溶液組成による鉄の淡水腐食挙動変化 (Oral presentation), 日本鉄鋼協会両支部合同冬季講演大会, 室蘭, December 2016.
2. 坂入正敏，大谷恭平, Md. Saiful Islam, カチオンによる金属材料の耐食性変化 (Oral presentation), 日本金属学会第 160 回講演大会, 八王子, March 2017.
3. 大谷恭平，Md. Saiful Islam，坂入正敏, 新規腐食指標による複数の金属カチオンを含む淡水中における鋼の腐食予測 (Oral presentation), 材料と環境 2017, 東京, May 2017.
4. 大谷恭平, Md. Saiful Islam，坂入正敏, 溶液中で金属表面に形成した異なる耐食性を示す酸化物皮膜の表面分析 (Oral presentation), 日本化学会北海道支部 2017 年夏季研究発表会, 旭川, July 2017.
5. 坂入正敏，大谷恭平, Md. Islam Saiful, 金属の水溶液腐食に及ぼす亜鉛イオンの影響 (Oral presentation), 日本金属学会 2018 年春期大会, 東京, March 2018.
6. Masatoshi Sakairi, Kyohei Otani and Md. Saiful Islam, Role of metal cations on corrosion of metallic materials in aqueous environments (Oral presentation), 9th International Symposium on Marine Corrosion and Control, Qingdao, China, April 2018.
7. Masatoshi Sakairi, Kyohei Otani, and Md. Saiful Islam, Role of zinc ion on corrosion of metals in aqueous solution (Oral presentation), Eurocorr2018, Krakow, September 2018.
8. 坂入正敏，Md. Saiful Islam, 大谷恭平, 塩化物イオンを含む環境における鉄の腐食に及ぼす亜鉛イオン濃度の影響 (Oral presentation), 材料と環境討論会 2018, 富山, October 2018.
9. 坂入正敏，Md. Saiful Islam，兼子　彬, 金属カチオンによる A6061 アルミニウム合金の腐食挙動変化 (Oral presentation), 日本金属学会 2019 年春期講演大会, 東京, March 2019.
10. 坂入正敏，Md. Saiful Islam，大谷恭平, 電気化学インピーダンスを用いるアルミニウム合金の腐食挙動解析 (Oral presentation), 軽金属学会第 136 回春期大会, 富山, May 2019.

11. 坂ノ上聡志，Md. Saiful Islam，坂入正敏, 各種金属カチオンを含む溶液中における鋼の電気化学挙動変化 (Oral presentation), 材料と環境 2019, Ohmiya, Saitama, Japan, May 2019.